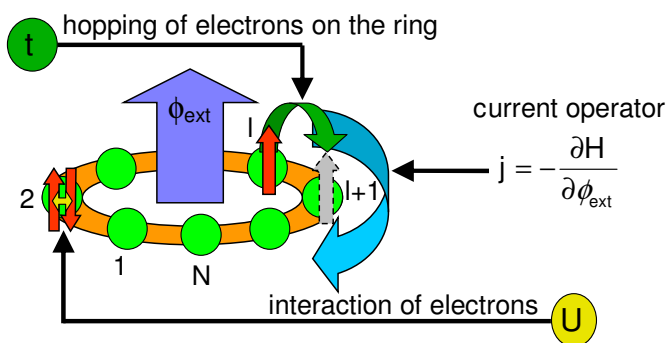

markus himmerich
persistent currents in quantum rings

dissertation
zur erlangung des grades
„doktor der naturwissenschaften“
am fachbereich physik der
johannes gutenbergs-universität
in mainz

von markus himmerich
geboren in hachenburg
mainz, den 15.02.2004



1. Berichtstatter: [REDACTED]*
2. Berichtstatter: [REDACTED]

Datum der mündlichen Prüfung: 30.04.2004

*Personal data has been removed from the online version of this thesis.

“Noli turbare circulos meos.”

— Legendary last words of Archimedes

To my parents

Abstract

In this thesis, three different types of quantum rings are studied. These are quantum rings with *diamagnetic*, *paramagnetic* or *spontaneous* persistent currents.

It turns out that the main observable to characterize quantum rings is the Drude weight. Playing a key role in this thesis, it will be used to distinguish between diamagnetic (positive Drude weight) and paramagnetic (negative Drude weight) ring currents. In most models, the Drude weight is positive. Especially in the thermodynamic limit, it is positive semi-definite. In certain models however, intuitively surprising, a negative Drude weight is found. This rare effect occurs, e.g., in one-dimensional models with a degenerate ground state in conjunction with the possibility of Umklapp scattering. One aim of this thesis is to examine one-dimensional quantum rings for the occurrence of a negative Drude weight. It is found, that the sign of the Drude weight can also be negative, if the band structure lacks particle-hole symmetry.

The second aim of this thesis is the modeling of quantum rings intrinsically showing a spontaneous persistent current. The construction of the model starts from the extended Hubbard model on a ring threaded by an Aharonov-Bohm flux. A feedback term through which the current in the ring can generate magnetic flux is added. Another extension of the Hamiltonian describes the energy stored in the internally generated field. This model is evaluated using exact diagonalization and an iterative scheme to find the minima of the free energy. The quantum rings must satisfy two conditions to exhibit a spontaneous orbital magnetic moment: a negative Drude weight and an inductivity above the critical level. The magnetic properties of cyclic conjugated hydrocarbons like benzene due to electron delocalization [magnetic anisotropy, magnetic susceptibility exaltation, nucleus-independent chemical shift (NICS)]—that have become important criteria for aromaticity—can be examined using this model.

Corrections to the presented calculations are discussed. The most substantial simplification made in this thesis is the neglect of the Zeeman interaction of the electron spins with the magnetic field. If a single flux tube threads a quantum ring, the Zeeman interaction is zero, but in most experiments, this situation is difficult to realize. In the more realistic situation of a homogeneous field, the Zeeman interaction has to be included, if the electrons have a total spin component in the direction of the magnetic field, or if the magnetic field is strong.

Zusammenfassung

In dieser Arbeit werden drei verschiedene Arten von Quantenringen beschrieben. Diese Quantenringe weisen *diamagnetische*, *paramagnetische* oder *spontane* Ringströme auf.

Eine wesentliche Größe, mit der man diese Quantenringe charakterisieren kann, ist das Drude-Gewicht. Es spielt eine wesentliche Rolle in dieser Arbeit und wird dazu genutzt, diamagnetische (positives Drude-Gewicht) und paramagnetische (negatives Drude-Gewicht) Ringströme zu unterscheiden. Für die meisten Modelle ist das Drude-Gewicht positiv. Überraschender Weise, tritt in manchen Ringen ein negatives Drude-Gewicht auf. Dieser seltene Effekt kann in eindimensionalen Ringen zum Beispiel auftreten, wenn der Grundzustand entartet ist, und Umklapp-Streuung möglich ist. Ein Ziel dieser Arbeit ist es, eindimensionale Ringe auf das Auftreten eines negativen Drude-Gewichts zu untersuchen.

Das zweite Ziel dieser Arbeit besteht darin, Quantenringe zu modellieren, die einen spontanen Ringstrom aufweisen. Die Konstruktion des Modells erfolgt auf der Grundlage des Hubbard-Modells auf einem Ring, der von einem Aharonov-Bohm-Fluss durchsetzt ist. Dieses Modell wird mit einem Rückkopplungsterm erweitert, der es dem Strom im Ring erlaubt, selbst einen magnetischen Fluss zu erzeugen. Dieses Modell wird mit Hilfe der Exakten Diagonalisierung und einem iterativen Schema ausgewertet, um die Minima der Freien Energie zu finden. Ein Quantenring muss zwei Bedingungen erfüllen um einen spontanen Ringstrom aufzuweisen: ein negatives Drude-Gewicht und eine Induktivität oberhalb des kritischen Niveaus. Die magnetischen Eigenschaften von zyklisch konjugierten Kohlenwasserstoffen wie Benzol, die durch die Elektronendelokalisierung in diesen Systemen entstehen, können mit diesem Modell untersucht werden. Dies sind die magnetische Anisotropie, die “magnetic susceptibility exaltation” und der “nucleus-independent chemical shift” (NICS), die wichtige Kriterien für die Aromatizität einer Verbindung sind.

Korrekturen für die vorgestellten Rechnungen werden diskutiert. Die grundlegendste Vereinfachung in dieser Arbeit ist die Vernachlässigung der Zeeman-Wechselwirkung der Spins der Elektronen mit dem magnetischen Feld. Wenn ein einzelner Flussschlauch einen Ring durchdringt, liefert die Zeeman-Wechselwirkung keinen Beitrag. In den meisten Experimenten kann diese Situation nicht hergestellt werden. Ein realistischerer Fall wäre ein Ring in einem homogenen Feld. In diesem Fall müsste die Zeeman-Wechselwirkung berücksichtigt werden, wenn die Elektronen eine resultierende Spin-Komponente in Richtung des magnetischen Felds aufweisen, oder wenn das magnetische Feld stark ist.

Contents

Abstract	1
Zusammenfassung	3
1 Introduction	7
1.1 Quantum rings	7
1.2 Aromaticity, ring currents and molecular electronics	8
1.3 Fabrication and short history of quantum rings	11
1.4 Theoretical description of quantum rings	13
1.5 Structure of this thesis	15
2 Transition to one-dimensional models	17
2.1 Two-dimensional continuum model	18
2.2 A ring threaded by a flux tube	20
2.2.1 The radial wave function of the ground state	22
2.2.2 The azimuthal wave function	24
2.2.3 Discussion of results	27
2.3 A ring in a homogeneous magnetic field	31
2.3.1 Perturbation of the ground-state wave function	32
2.3.2 Interpretation of the result	35
2.4 Corrections	36
2.4.1 Zeeman interaction	36
2.4.2 Relativistic corrections	37
3 Persistent currents and the Drude weight	41
3.1 Transport quantities	41
3.1.1 The Drude weight and the Meissner fraction	41
3.1.2 The electrical conductivity	44
3.1.3 The paramagnetic current	47
3.2 Example: The periodic Anderson model	49
3.2.1 Hamiltonian and band structure	50
3.2.2 The paramagnetic current	57
3.2.3 Drude weight	62
3.3 Systems with negative Drude weight	66
3.3.1 Asymmetric band structure	68

3.3.2	Open shells	70
4	A second-quantized model for quantum rings	73
4.1	Motivation through SQUIDs	74
4.1.1	Minimization of the free energy	74
4.1.2	Iterative scheme	74
4.2	The model and its analytic properties	76
4.2.1	The model Hamiltonian	78
4.2.2	Fourier transform of the many-particle states	81
4.2.3	Iterative scheme	82
4.2.4	Minimization of the free energy	82
4.2.5	The critical inductivity	85
4.2.6	Modification for large inductivities	87
4.2.7	Asymptotic expansion for large inductivities	89
4.2.8	Examination of the diagonality of the current operator	91
4.3	Numerical examination and physical consequences	96
4.3.1	Realistic parameters	96
4.3.2	Benzene	96
4.3.3	Systems with negative Drude weight	99
5	Conclusion	105
5.1	What has been achieved?	105
5.2	What remains to be investigated?	108
A	Units	109
B	Continuum model for quantum rings	111
B.1	Asymptotic expansion of a two-dimensional ring	111
B.2	Perturbation theory	114
C	The periodic Anderson model	117
C.1	Overview: Operators of the noninteracting PAM	118
C.2	Particle-hole symmetry in the PAM	119
C.3	Hartree-Fock study of the PAM	121
	Bibliography	127
	Acknowledgments	135
	Curriculum Vitae	137

1 Introduction

1.1 Quantum rings

Quantum rings are small conducting rings with only a few electrons. The size of the ring structure is of the order of the phase-coherence length of the electrons. We consider quantum rings to possess a discrete spectrum of electronic states and a coherent motion of electrons in the sense that electrons can propagate around the whole ring without inelastic scattering, maintaining a definite phase of their wave function. This condition allows the electrons to exhibit interesting interference phenomena in analogy to superconducting quantum interference devices (SQUIDs). These effects are Aharonov-Bohm oscillations (AB59) in the energy and magnetoresistance, and persistent currents (BIL83). It has to be noted that a clear separation between the momentum-relaxation length scales and the phase-randomization length scales exists. The latter can be essentially infinite at very low temperatures while the former are typically dependent upon the disorder and can vary from a length scale on the order of atomic dimensions to quite large values in nearly perfect crystals (WW92). This leads to interference phenomena even in rather large disordered samples described as mesoscopic that are found between the microscopic and macroscopic structures according to size. They are at the crossover from the quantum mechanical to the classical regime.

The phase-coherence length of the electrons can be measured. At a given temperature, in a given material, the phase-coherence length of the electrons is the circumference of the largest ring that shows Aharonov-Bohm oscillations in its physical quantities. The phase-coherence length can be about a micron in normal metal rings at liquid helium temperature. At room temperature, the phase-coherence length, which is roughly proportional to the inverse temperature, exceeds the circumference of a benzene molecule. A discussion of the effects of temperature and electron-phonon scattering on the phase-coherence length of an electron is found in chapter 3 of Ref. (Imr97). At low temperatures, the phonon degrees of freedom freeze out, therefore other mechanisms of dephasing should be taken into account. The electron-electron interaction is the dominant mechanism at low temperatures. Studies of the influence of the electron-electron interaction on electron dephasing have been conducted recently. It is a well known result that a ring pierced by a flux of half a flux quantum, which shifts the phase of an electron traveling through one arm of the ring by π in comparison to an electron traveling through the other arm of the ring, should exhibit vanishing electron transmission.

However, Žitko and Bonča recently found that the electron-electron interaction in the ring area leads to a finite transmission of electrons through the ring, thus dephasing the many-electron wave function (ŽB03). Therefore, the importance of the electron-electron interaction cannot be overestimated and the aim of this thesis is to arrive at a second-quantized model including the strong Coulomb repulsion in Chap. 4. The first few chapters deal with noninteracting electrons to bridge the gap between the initial work being done on quantum rings, which was for weakly interacting electrons, and the strongly correlated models that are applied to the topic at present.

This thesis is concerned with rings that behave purely quantum mechanically. These rings are found at the lower end of the nanoscopic scale. For example, the benzene molecule is a quantum ring. The π -electrons of benzene can move phase coherently through the molecule. This example indicates a link between the physical chemistry of aromatic and antiaromatic compounds and the topic of quantum rings. The ring currents (Laz00; GM01) that are calculated by theoretical chemists in order to explain nuclear magnetic resonance (NMR) spectroscopy of ring-shaped molecules are the persistent currents of quantum rings.

1.2 Aromaticity, ring currents and molecular electronics

Organic semiconductors have gained a lot of interest during recent years. Organic thin film transistors with the highest mobilities of electrons can be built from pentacene (DM01), an aromatic molecule that consists of five benzene rings. Also, for the development of molecular electronics (AR98), molecules with delocalized π -systems seem most promising (VPL02).

The term “molecular electronics” describes two different things. Electronic components consisting of a film or a liquid crystalline array of organic molecules are referred to as molecular electronics. Other authors have preferred to reserve the term for single molecule tasks such as single molecule-based devices or single molecular wires. It would be better to follow the suggestion of Petty *et al.* (PBB95) by using two subcategories, namely “molecular materials for electronics” for bulk applications and “molecular scale electronics” for single molecule applications.

In 1974, Aviram and Ratner suggested to plug a single molecule between two current leads which should show the current-voltage characteristic of a diode. It took some twenty years to carry out this challenging experiment. In the experiments, organic molecules with conjugated π -electrons are connected via sulphur atoms to gold surfaces at both sides of the molecule. A schematic of one of the most famous experiments by Reed *et al.* (RZM⁺97) is shown in Fig. 1.1. The current-voltage characteristic and the conductance was measured. With almost the same technique and a third electrode controlling the electrostatic potential at the place of the molecule, Park *et al.* succeeded in fabricating the first molecular field effect transistor (PPG⁺02).

The objective of part of this thesis is to investigate the static magnetic properties

1.2 Aromaticity, ring currents and molecular electronics

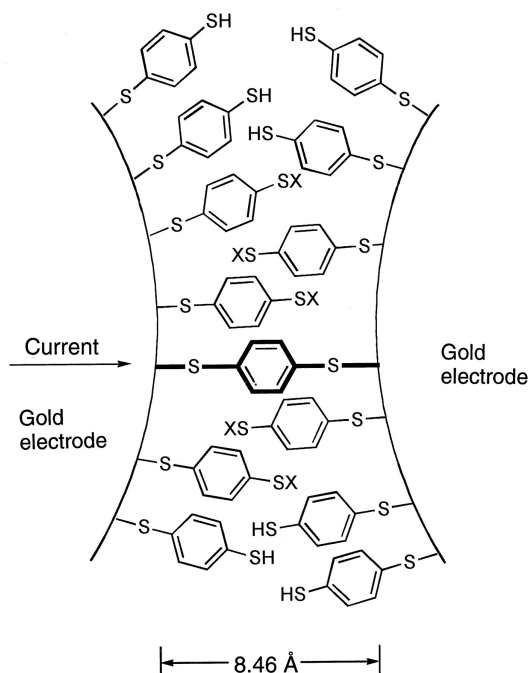


Figure 1.1: Schematic of a conducting molecular junction taken from Ref. (RZM⁺97). The benzene-1,4-thiolate self-assembled monolayer between the gold electrodes was formed in a mechanically controllable break junction.

of single aromatic molecules, specifically those properties originating from ring currents. Consequently, we do not connect the molecules to external wires nor do we look at the interaction with static electric fields, but these would be natural extensions of the work presented in this thesis.

There is no unique definition of the term aromaticity. Several physical, geometrical and chemical criteria (e.g., magnetic properties, equality of bond lengths, a particularly pleasant smell, a predisposition to nitration and sulphonation and a strong delocalization of spin) have been used to classify molecules as aromatic at different times. Therefore, there has been much confusion over the precise meaning and definition. For a review on aromaticity and its relation to ring currents see the recent articles of Lazzeretti (Laz00), Gomes, and Mallion (GM01).

The ring-current model was proposed in 1936 by Pauling (Pau36) to explain the experimental fact, that the magnetic “susceptibility ellipsoids of the aromatic molecules are found to be approximately prolate ellipsoids of revolution, with the long axis normal to the plane of the molecule”. In 1961, the effect of the ring current on the chemical shift of proton resonance spectra (Pop56) lead to the suggestion that these effects should be a criterion for aromaticity (EJ61). The magnetic field that the ring current in an aromatic ring generates enhances the magnetic field at the proton locations outside the ring and diminishes the field inside the ring (see Fig. 1.2). These substances are called diatropic in contrast to

paratropic rings that enhance the magnetic field in their interior (MGS94). There is a clear correlation between diatropic and aromatic substances on one hand and between paratropic and antiaromatic substances on the other hand.

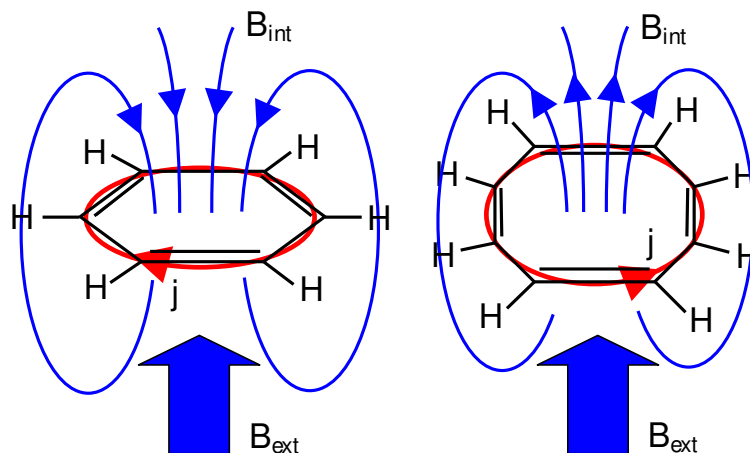


Figure 1.2: The diatropic aromatic benzene molecule is shown with its ring current on the left in contrast to the paratropic antiaromatic cyclooctatetraene molecule on the right.

Today, there is overwhelming evidence that aromaticity can be uniquely defined by magnetic properties. For example the magnetic anisotropy (Fly74) and the magnetic susceptibility exaltation (DWL68; DWL69) [defined as the difference between the magnetic susceptibility for the observed compound and the value estimated for the hypothetical system without cyclic electron delocalization] are used as a criterion next to the nucleus-independent chemical shift [NICS] (vRSMD⁺96) that has been proposed as the major criterion for aromaticity (WAT⁺02). However, the NICS is a theoretical criterion that is not observable by definition.

There are a lot of ab-initio methods for calculating chemical shifts for NMR spectroscopy. For a review see, e.g., Ref. (HJR99). All these methods are linear approximations for small fields. Of course, a linear response current cannot describe the system's behavior in arbitrarily high external magnetic fields. The response current should show a periodicity with respect to the number of flux quanta threading the ring. This periodicity will be destroyed due to Zeeman splitting of the electronic energies and spin flipping. Therefore, a highly nonlinear dependence of the current with respect to large enough external fields is expected. To force a flux quantum inside a benzene molecule—a hexagon with a side length of 140 pm—one would need an extremely high magnetic field of 8×10^4 T. It is not intended to reach such high values of magnetic field within the approximation scheme discussed in this thesis. The Zeeman interaction of the electron spins with the magnetic field is neglected. We are just interested in the orbital magnetic effects of quantum rings.

The topic of quantum rings is not restricted to molecular rings as is shown in the next section.

1.3 Fabrication and short history of quantum rings

Since the mid-eighties, there has been an impressive experimental development towards smaller and smaller quantum rings; with the most recent techniques the true quantum limit of nanoscopic rings containing only a few electrons was reached. At the same time, many experiments still study mesoscopic rings with hundreds of electrons. Early experiments in the eighties and nineties reported observations of Aharonov-Bohm oscillations and persistent currents in metallic gold or copper rings. The first observation of h/e flux-periodic oscillations in the magnetoresistance of a normal metal ring was made in 1985 by Webb *et al.* (WWUL85). They were using rings drawn with a scanning electron transmission microscope to a polycrystalline gold film. The rings were connected symmetrically to two current leads to measure the resistivity. The diameter was several hundred nanometers.

The oscillations were correctly predicted by several theoretical papers (BIL83; GI84; BIA84). Büttiker, Imry, and Landauer were the first to consider a normal metallic one-dimensional ring threaded by a magnetic field. They predicted, following earlier work of Byers, Yang (BY61), and Bloch (Blo70) concerning quantized flux in superconducting rings, that because of the modification of the boundary conditions by the magnetic flux, the electron wave function and then any physical property of the ring is a periodic function of the magnetic flux with a fundamental period of h/e . In superconducting cylinders and rings, these oscillations had been observed with a period of $h/2e$ because of electron pairing.

In 1990, Lévy *et al.* found $h/2e$ periodic oscillations in the magnetization response of 10^7 isolated copper rings with a diameter of approximately five hundred nanometers (LDDB90). These rings were fabricated by electron-beam techniques. Although the explanation of the phenomenon was incomplete, it was another proof of the existence of persistent currents in mesoscopic rings. It was found later that the h/e oscillations were washed out because the effect had randomly distributed signs in the different rings that were averaged over in the experiment. The amplitude and the sign of the persistent current depends on the number of electrons on the ring. Only the even harmonics of the effect survive the ensemble averaging (AGI91).

The next observation of h/e periodic oscillations in the magnetization of a single gold loop followed in 1991 (CWB⁺91). The production of the ring with a diameter of several thousand nanometers was done with standard electron-beam lithographic techniques.

In parallel, rings were fabricated in GaAs/AlGaAs heterojunctions by electron-beam lithographic techniques. The same h/e periodic oscillations in the magnetoresistance were observed (TCC⁺87). Oxidizing a ring structure with the tip of an atomic force microscope into a AlGaAs-GaAs heterostructure, Fuhrer *et al.* built a ring with diameter of 132 nm (FLI⁺01), containing a few hundred electrons (see Fig. 1.3). Their measurements showed an Aharonov-Bohm effect and allowed to deduce the energy spectra of their device (see Fig. 1.4). It turned out that their system can be well described within a single-particle picture because of an

effective screening of the electron-electron interaction by a metallic top gate, in which the electron density is some orders of magnitude higher than in the thin heterojunction.

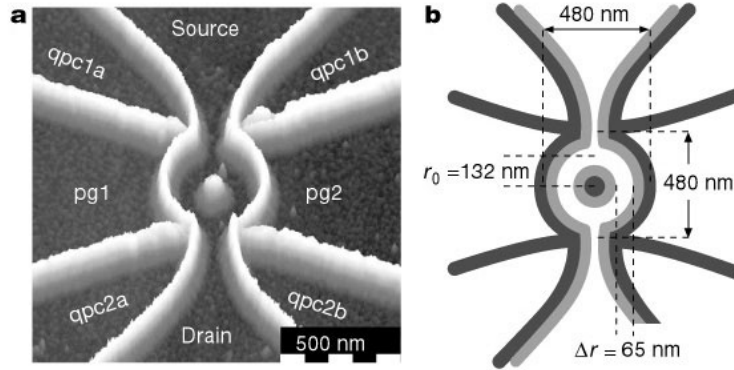


Figure 1.3: Sample layout. a, Micrograph of the quantum ring taken with the unbiased AFM-tip after writing the structure. The oxide lines (bright regions) deplete the 2DEG 34 nm below the surface separating the sample into several conductive (dark) regions. The current is passed from source to drain. The in-plane gates (qpc1a, qpc1b, qpc2a, qpc2b, pg1 and pg2) are used to tune the point contacts and two arms of the ring. b, Schematic sketch of the ring. The dark curves represent the oxide lines. From transmission measurements of the point contacts at source and drain we estimate the depletion length to be about 50 nm, which results in an estimated channel width of $r = 65$ nm. The average radius of the ring is $r_0 = 132$ nm. (FLI⁺01)

Experiments without a screening top gate, in the regime of strong electron-electron interaction, showed a reduced Aharonov-Bohm period (KFBH03). Indications for this so-called “fractional Aharonov-Bohm effect” were found in solutions of the Hubbard and Luttinger models. It was predicted for quantum rings in Ref. (NPHC96).

Even smaller nanoscopic rings have been fabricated by self-assembly of InAs dots on GaAs, using suitable heat treatment (WSH⁺00; LLG⁺00). A wide range of electronic and magnetic properties was investigated in these experiments.

Another hallmark in the research on mesoscopic rings was the prediction of a persistent current due to the Berry phase that arises in the presence of an inhomogeneous magnetic field by Loss *et al.* The Zeeman interaction couples the electron spin and the orbital motion, and results in a Berry phase (LGB90). Evidence for this effect was experimentally found in 1998 by Morpurgo *et al.* (MHK⁺98). They interpreted the splitting of certain peaks in the Fourier spectrum of the Aharonov-Bohm conductance oscillations as being due to this effect. An even more exotic effect in mesoscopic rings was proposed very recently by Kane. He describes a method for observing fractional statistics (Kan03). A coverage of these

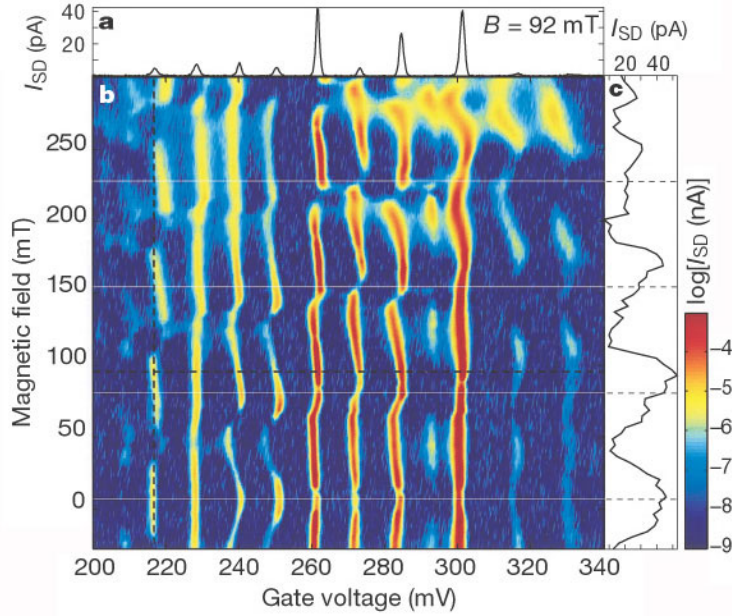


Figure 1.4: The addition spectrum. a, Measurement of Coulomb blockade resonances at fixed magnetic field. The current is measured as a function of a voltage applied to both plunger gates (pg1 and 2) simultaneously. b, The evolution of such sweeps with magnetic field results in the addition spectrum shown in color. The regions of high current (yellow/red) mark configurations in which a bound state in the ring aligns with the Fermi level in source and drain. The Aharonov-Bohm period expected from the ring geometry is indicated by the thin white horizontal lines. c, Magnetic field sweep for constant plunger gate voltage $V_{pg} = 218$ mV (dashed line in the color plot). This peak shows a maximum in amplitude for $B = 0$, whereas other peaks ($V_{pg} = 270$ mV) display a minimum. (FLI⁺01)

interesting effects in this thesis will have to be sacrificed for the sake of brevity.

1.4 Theoretical description of quantum rings

For quantum rings, two theoretical approaches have been developed. *Discrete* models describe the rings as consisting of N lattice sites with n electrons, which can hop from site to site. The electron-electron interaction is approximated to be an effective on-site interaction (see Fig. 1.5). The Hamiltonian is then a Hubbard model (Hub63; Gut63) or one of its extensions. By exact diagonalization or Bethe-ansatz techniques, this approximated Hamiltonian can be exactly solved. Another possibility is to assume a *continuum* model. The ring is modeled by an external confinement potential where the electrons move. The electron-electron interaction

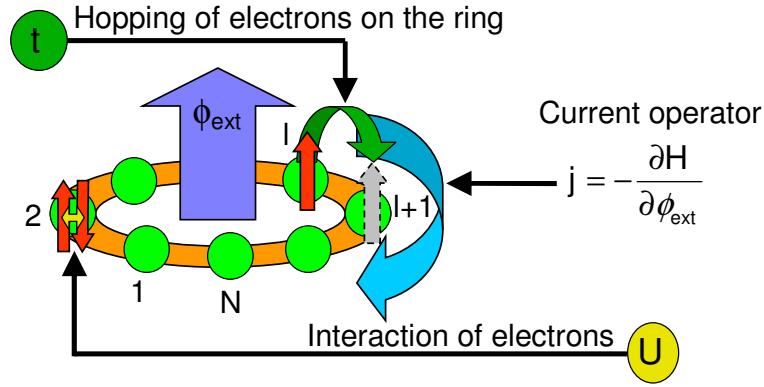


Figure 1.5: The Hubbard model on a ring is used to model quantum rings like, e.g., a benzene molecule. The amount of energy paid if two electrons are on the same site is U . The hopping amplitude is t . The current in the ring is needed to calculate the orbital magnetic moment of the ring.

is the normal Coulomb interaction. The exact Schrödinger equation is then approximately solved with quantum-Monte-Carlo methods, density-functional methods, or numerical diagonalization techniques for a desired number of lowest energy states (VKDM03).

Studying persistent currents in a ring of finite width and thus going beyond the one-dimensional picture of mesoscopic and nanoscopic rings is one of the most important goals. It is difficult to deal with the real spatial geometry of a ring, therefore rings of finite width have been approximated by simpler models, such as two-dimensional or three-dimensional straight wires with periodic boundary conditions. The homogeneous magnetic field was replaced by a magnetic flux tube confined to the hole region of the ring.

Within such models a varying magnetic field strength just changes the phases of the electrons, resulting in the periodic Aharonov-Bohm oscillations in the physical properties and the persistent currents j described above. In conclusion, the Aharonov-Bohm oscillations are caused by the magnetic flux that is enclosed by the ring. The vector potential describing the magnetic field can be eliminated from the Schrödinger equation by introducing a gauge transformation. The result is that the boundary condition is modified as $\psi(\varphi + 2\pi) = \exp(2\pi i\phi/\phi_0)\psi(\varphi)$, thus leading to the periodicity of the physical quantities in the magnetic flux ϕ with a period of the flux quantum $\phi_0 = h/e$. The magnetic moment M of a ring is simply related by $M = Aj$, where A is the area of the ring. These models have provided convenient tools for studying more complicated problems such as the effects of electron-electron interaction and disorder scattering on persistent currents. In this thesis, an effective one-dimensional model is also used to study the effect of feedback of the persistent current on the magnetic field. An inductivity assigned to the quantum ring will enable the persistent current to generate an in-

ternal magnetic field influencing the persistent current in turn. However, to gain a complete understanding of the persistent currents and their relation to a realistic 2D or 3D ring over the whole range of magnetic-field strength, the effect of penetration of magnetic field into the conducting region should be considered. This penetration can result in the breakdown of the simple linear relation between the magnetic moment and the persistent current in the ring or potentially in aperiodic Aharonov-Bohm oscillations, even if the spins of the electrons are neglected.

The magnetism of quantum rings is due either to *orbital currents* of electrons, or to their *spins*. We are predominantly concerned with the orbital magnetism in this thesis. This can be justified by looking at quantum rings that are threaded by a magnetic flux tube. In this case the spin magnetism of the electron is negligible. However, for quantum rings in a homogeneous field, spin magnetism is at least for open-shell configurations—where there is a nonvanishing total spin—very important. The model for quantum rings presented in the last chapter of this thesis can easily be extended by a Zeeman interaction term. No alteration of the solution scheme of the model is needed to evaluate the effects of the Zeeman interaction with the spin, except for the evaluation of the Hamiltonian in all different total-spin subspaces. Not to obscure the novel effects of the proposed model, we neglect the Zeeman interaction at all.

1.5 Structure of this thesis

In the next chapter, we examine noninteracting electrons in static external fields, neglecting the Zeeman interaction between spins and magnetic field. Insight is gained how the width of a two-dimensional quantum ring influences the energy levels of the ring. It is found out that the simple approximation of a phase shift in the wave function due to the flux in a ring is not valid for broad rings in homogeneous fields any more. However the one-dimensional approximation is useful and leading-order finite-width corrections can be included by a simple averaging process. The third dimension of a quantum ring is neglected in the calculations, because the wave function parallel to the magnetic field is not influenced by the field.

Afterwards, we return to one-dimensional rings and examine what properties paramagnetic rings in contrast to the normal diamagnetic rings have to fulfill. In paramagnetic rings, the ring currents amplify the magnetic field inside of the ring. In diamagnetic rings the ring current counteracts the magnetic field in the interior. The Drude weight—which is the sensitivity of the energy levels to twisted boundary conditions—is a tool to estimate the sign of the orbital magnetism of quantum rings. In the thermodynamic limit the Drude weight describes the *dc* conductivity of a wire. For small rings it was found to be negative for paramagnetic rings and positive for diamagnetic rings.

Taking a look at the mechanism underlying the self-interaction of currents flowing in superconducting rings through the generation of magnetic fields, a model for

quantum rings including an inductivity is developed. This model also includes the strong electron-electron interaction. After introducing an iterative scheme to solve the proposed model, the consequences for two systems are discussed. States with spontaneous persistent current can be found in quantum rings if the inductivity is above a critical value. It is not yet clear whether such high values of inductivity can occur in nature. Quantum rings with states of spontaneous persistent currents could be used as tiny storage devices if they existed.

2 Transition to one-dimensional models

In this chapter, the aim is to find out how the energy levels of a ring of noninteracting electrons with vanishing width (one-dimensional*) and a *thin flux tube* threading the ring are transformed if the width of the ring is broadened. The Schrödinger equation for the electrons on such a ring is separable into a radial and an azimuthal part. The energy of the one-dimensional (1D) ring diverges due to the confinement of the radial wave function to an infinitesimal space. If the divergence is subtracted—so that the energies are measured relatively to the ground-state energy, the energy levels of the 2D ring are the same as the energy levels of the 1D ring scaled by a simple factor depending on the ring width. It is an interesting fact that the azimuthal motion of the electrons influences the radial wave function of the electrons. If the group velocity of the azimuthal waves is different from zero, the radial states are pushed to the outer half of the ring.

The energy levels and wave functions of a 2D ring in a *homogeneous magnetic field* are then expanded in terms of the 2D ring threaded by a flux tube. The leading order corrections with respect to the ring width for the 2D ring in a homogeneous magnetic field can be captured systematically by a perturbation expansion. The Peierls substitution, which multiplies a phase factor depending on the magnetic flux in the ring to the wave function, is not valid any more. In a classical picture, the electrons moving on circles with different radii enclose different values of flux and interfere with each other, due to their different Peierls phase factors. This effect leads to the breakdown of the Peierls substitution in a 2D ring in a homogeneous magnetic field in the framework of this simplistic picture. The result of this nonsystematic approximation is used for comparison with the exact result only.

The phase factor is, besides relatively small relativistic corrections, the only effect that a magnetic vector potential has on the electrons, if the magnetic field does not pierce the space where the electrons are moving. In a weak homogeneous field, the phase factor is the most important effect, if there is no resulting spin component of the electrons in the direction of the magnetic field. In strong homogeneous fields and for electronic systems with a resulting spin component in the direction of the magnetic field, the Zeeman interaction has to be included. These facts will be briefly discussed in the last section of this chapter.

*A ring of finite width is called two-dimensional whereas a ring of vanishing width is called one-dimensional. Accordingly, a three-dimensional ring would be a ring with a two-dimensional intersection area when cut by a plane through its center of mass.

We neglect the third dimension of quantum rings in this chapter. Most experiments on quantum rings were carried out in semiconductor heterojunctions, building a ring structure in the essentially two-dimensional electron gas. The extent of a quantum ring parallel to the magnetic field is of minor importance. The wave function parallel to the magnetic field is to a lesser extent influenced by the magnetic field. It yields a constant contribution to the total energy of the system.

Having gained a clearer understanding of the similarities between 1D and 2D continuum ring models in magnetic fields, it is possible to restrict the research described in the following chapters to discrete 1D models. It is easy to include the strong effects of the Coulomb repulsion between electrons via the Hubbard interaction in discrete 1D models. The crossover from continuum to discrete models is justified by adding delta-peak shaped potentials to the continuum model. These peaks model the sites of the atoms in a ring molecule. The resulting 1D model is, consequently, a tight-binding model with a Peierls phase factor. This factor is split into parts describing the amount of phase that the electronic wave function collects as the electrons hop from site to site.

2.1 Two-dimensional continuum model

In this section, the effect that a magnetic field has on a 2D ring is examined. Noninteracting electrons of mass m and charge e are moving on a ring of width ϵ around the origin. The electrons on the ring in the x - y -plane are confined by a hard-wall potential. The sites of the atom cores on the ring are modeled by simple delta peaks in the potential that the electrons feel in the azimuthal direction (Kronig-Penney model). The magnetic field points in the direction of the z -axis (see Fig. 2.1).

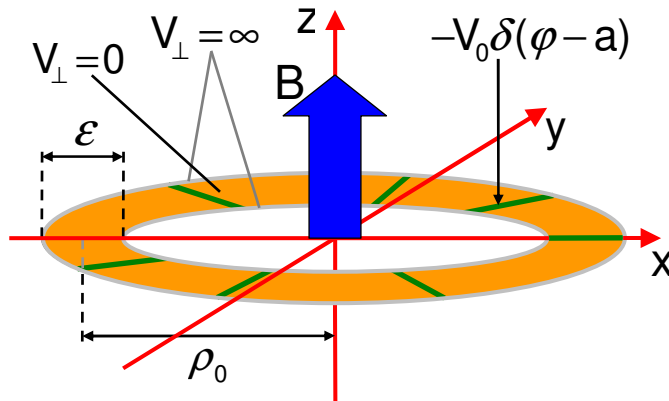


Figure 2.1: Ring with infinite potential walls, threaded by a magnetic field.

The starting point is the nonrelativistic Schrödinger equation. The Hamiltonian

2.1 Two-dimensional continuum model

for an electron in a magnetic field is ($e < 0$):

$$\begin{aligned}
 H &= \frac{1}{2m} (\mathbf{p} - e\mathbf{A})^2 + V \\
 &= \frac{1}{2m} \mathbf{p}^2 - \frac{e}{2m} (\mathbf{p} \cdot \mathbf{A} + \mathbf{A} \cdot \mathbf{p}) + \frac{e^2}{2m} \mathbf{A}^2 + V \\
 &= \frac{1}{2m} \mathbf{p}^2 - \frac{e}{m} \mathbf{A} \cdot \mathbf{p} + \frac{e^2}{2m} \mathbf{A}^2 + V \\
 &= -\frac{\hbar^2}{2m} \Delta + \frac{i\hbar e}{m} \mathbf{A} \cdot \nabla + \frac{e^2}{2m} \mathbf{A}^2 + V,
 \end{aligned} \tag{2.1}$$

with the penultimate equality coming from the Coulomb gauge ($\nabla \cdot \mathbf{A} = 0$). The cylindrically symmetric situation is best described in cylindric coordinates. The magnetic field is supposed to have an axially symmetric profile with respect to the z -axis. Therefore, the vector potential has only a φ -component. The Hamiltonian in cylindric coordinates is:

$$H = -\frac{\hbar^2}{2m} \left(\frac{\partial^2}{\partial \rho^2} + \frac{1}{\rho} \frac{\partial}{\partial \rho} + \frac{1}{\rho^2} \frac{\partial^2}{\partial \varphi^2} \right) + V(\rho, \varphi) + \frac{i\hbar e}{m} A_\varphi \frac{1}{\rho} \frac{\partial}{\partial \varphi} + \frac{e^2}{2m} A_\varphi^2. \tag{2.2}$$

The term before the last is the contribution of the angular momentum to the orbital magnetism. The last one is a diamagnetic contribution. Any expectation value of the last term is positive. As the vector potential increases linearly with the magnetic induction, the energy increases quadratically. The contribution to the magnetization in the ground state, which is the negative of the first derivative of the expectation value of the last term in the ground state with respect to the magnetic induction, is negative and directed opposite to the magnetic induction.

We separate the radial coordinate ρ into the average radius of the ring ρ_0 and the deviation from the average $\bar{\rho}$,

$$\rho = \rho_0 + \epsilon \bar{\rho}, \quad \bar{\rho} \in \left[-\frac{1}{2}; \frac{1}{2} \right]. \tag{2.3}$$

We assume that the potential has the form:

$$V(\rho, \varphi) = V_\perp(\rho) + \frac{\rho_0^2}{\rho^2} V_\parallel(\varphi). \tag{2.4}$$

The prefactor ρ_0^2/ρ^2 makes the resulting differential equation for the electron on the ring separable. The potential $V_\perp(\rho)$ describes the hard-wall confinement,

$$V_\perp(\rho) = \begin{cases} 0, & |\rho - \rho_0| < \frac{\epsilon}{2}, \\ \infty, & |\rho - \rho_0| \geq \frac{\epsilon}{2}, \end{cases} \tag{2.5}$$

leading to a boundary condition for the wave function

$$\Psi(\rho_0 + \epsilon \bar{\rho}, \varphi) = 0 \quad \forall \varphi, \quad \bar{\rho} = \pm \frac{1}{2}. \tag{2.6}$$

The potential $V_{\parallel}(\varphi)$ is the periodic Kronig-Penney potential:

$$V_{\parallel}(\varphi) = -V_0 \sum_{n=0}^{N-1} \delta(\varphi - an), \quad V_0 \geq 0, \quad (2.7)$$

where

$$a = \frac{2\pi}{N} \quad (2.8)$$

is the lattice constant and N is the number of atoms that constitute the ring. Due to the periodicity of the potential, we are later able to apply the Bloch theorem.

2.2 A ring threaded by a flux tube

In the framework of the above Kronig-Penney model on a ring threaded by a single flux tube, the validity of the Peierls substitution will be checked in this section. For any width of the ring, the model can be separated into a radial and an azimuthal part. In the Peierls substitution, the azimuthal wave function is assumed to be given by the azimuthal wave function of the model without magnetic flux, multiplied by a phase factor depending on the value of the magnetic flux in the ring.

If there is a magnetic flux tube $\mathbf{B} = \phi\delta(\mathbf{r})\mathbf{e}_z$ through the origin, the magnetic vector potential is

$$\mathbf{A} = \frac{\phi}{2\pi\rho}\mathbf{e}_{\varphi}. \quad (2.9)$$

Let β be the magnetic flux threading the ring in units of the flux quantum,

$$\beta = \frac{|e|\phi}{2\pi\hbar}. \quad (2.10)$$

The dimensionless potential and the dimensionless energy are

$$v(\varphi) = \frac{2m\rho_0^2 V_{\parallel}(\varphi)}{\hbar^2},$$

$$\eta = \frac{2m\rho_0^2 E}{\hbar^2}.$$

The time-independent Schrödinger equation is

$$0 = \left(H^{(0)} - E_{\nu}^{(0)} \right) \Psi_{\nu}^{(0)}$$

$$= -\frac{\hbar^2}{2m} \left(\frac{\partial^2}{\partial \rho^2} + \frac{1}{\rho} \frac{\partial}{\partial \rho} + \frac{1}{\rho^2} \frac{\partial^2}{\partial \varphi^2} + \frac{2i\beta}{\rho^2} \frac{\partial}{\partial \varphi} - \frac{\beta^2}{\rho^2} - \frac{1}{\rho^2} v(\varphi) + \frac{\eta_{\nu}^{(0)}}{\rho_0^2} \right) \Psi_{\nu}^{(0)}. \quad (2.11)$$

We denote quantities relating to the ring threaded by a flux tube with a bracketed zero as superscript, because the wave functions obtained in this section are shown

2.2 A ring threaded by a flux tube

to be the same as the ones of the ring with vanishing width in a homogeneous field. The ring with vanishing width is the unperturbed problem of the perturbation expansion in powers of the ring width, which is sought in the next section.

With the dimensionless length,

$$r = \frac{\rho}{\rho_0} = 1 + \frac{\epsilon}{\rho_0} \bar{\rho}, \quad (2.12)$$

the Schrödinger equation becomes

$$0 = \left[\frac{\partial^2}{\partial r^2} + \frac{1}{r} \frac{\partial}{\partial r} + \frac{1}{r^2} \left(\frac{\partial}{\partial \varphi} + i\beta \right)^2 - \frac{1}{r^2} v(\varphi) + \eta_\nu^{(0)} \right] \Psi_\nu^{(0)}. \quad (2.13)$$

We define the dimensionless Hamiltonian of the system by

$$D^{(0)} = \frac{\partial^2}{\partial r^2} + \frac{1}{r} \frac{\partial}{\partial r} + \frac{1}{r^2} \left(\frac{\partial}{\partial \varphi} + i\beta \right)^2 - \frac{1}{r^2} v(\varphi). \quad (2.14)$$

The Schrödinger equation can be separated into radial and azimuthal parts using a separation of variables. The result is (ν is a set of all quantum numbers):

$$\left(D^{(0)} + \eta_\nu^{(0)} \right) P_\nu(r) \chi_\nu(\varphi) = 0, \quad (2.15)$$

yielding

$$\begin{aligned} \frac{1}{P_\nu(r)} \left[r^2 \frac{\partial^2}{\partial r^2} + r \frac{\partial}{\partial r} + \eta_\nu^{(0)} r^2 \right] P_\nu(r) \\ + \frac{1}{\chi_\nu(\varphi)} \left[\left(\frac{\partial}{\partial \varphi} + i\beta \right)^2 - v(\varphi) \right] \chi_\nu(\varphi) = 0. \end{aligned} \quad (2.16)$$

Setting both parts equal to a constant $\pm \xi_\nu^2$ then gives

$$\begin{aligned} \left[r^2 \frac{\partial^2}{\partial r^2} + r \frac{\partial}{\partial r} + \eta_\nu^{(0)} r^2 - \xi_\nu^2 \right] P_\nu(r) = 0, \\ \left[\left(\frac{\partial}{\partial \varphi} + i\beta \right)^2 + \xi_\nu^2 - v(\varphi) \right] \chi_\nu(\varphi) = 0. \end{aligned} \quad (2.17)$$

These two differential equations are solved in the next sections. The aim is to study the interplay between the radial and azimuthal motion of electrons in quantum rings. The coupling between both directions of motion is a feature which is not present in one-dimensional models. It is interesting to know the differences between 1D and 2D quantum rings.

2.2.1 The radial wave function of the ground state

As in an infinite square potential well, the energy levels for the eigenfunctions in the radial direction are spaced like the squared radial quantum number. The energy levels diverge like ϵ^{-2} in the limit of vanishing ring width. For narrow rings, in which we are especially interested, the energy levels stemming from the different radial eigenfunctions are far apart. The energy bands stemming from the azimuthal structure of the ring do not depend (to leading order) on the ring width. We are interested in the low-temperature behavior of the system, hence we only determine the ground-state radial wave function in this section. The states built from the first excited radial wave function are considered energetically too high. Consequently, in the course of this section, the set of quantum numbers ν will be reduced to a set of quantum numbers for the azimuthal eigenstates.

The radial part of the Schrödinger equation is solved by Bessel functions of the first and second kind:

$$P_\nu(r) = AJ_{\xi_\nu} \left(\sqrt{\eta_\nu^{(0)}} r \right) + BY_{\xi_\nu} \left(\sqrt{\eta_\nu^{(0)}} r \right). \quad (2.18)$$

The boundary conditions are

$$P_\nu \left(1 \pm \frac{1}{2} \frac{\epsilon}{\rho_0} \right) = 0. \quad (2.19)$$

One condition sets the factor A in the linear combination of Bessel functions to a certain value. It involves finding the zeros of the function

$$\begin{aligned} J_{\xi_\nu} \left[\sqrt{\eta_\nu^{(0)}} \left(1 - \frac{1}{2} \frac{\epsilon}{\rho_0} \right) \right] Y_{\xi_\nu} \left[\sqrt{\eta_\nu^{(0)}} \left(1 + \frac{1}{2} \frac{\epsilon}{\rho_0} \right) \right] \\ - J_{\xi_\nu} \left[\sqrt{\eta_\nu^{(0)}} \left(1 + \frac{1}{2} \frac{\epsilon}{\rho_0} \right) \right] Y_{\xi_\nu} \left[\sqrt{\eta_\nu^{(0)}} \left(1 - \frac{1}{2} \frac{\epsilon}{\rho_0} \right) \right] \end{aligned} \quad (2.20)$$

to determine B . These zeros are not analytically known. Consequently, it is not possible to write down the exact solution of this problem in terms of a linear combination of Bessel functions. We could use the asymptotic expansion of the Bessel functions to determine the ground-state solution P_0 fulfilling the boundary conditions in the limit of vanishing ring width, but the author chose to expand the differential equation itself asymptotically in orders of ϵ , because this method allowed for an easier implementation in MATHEMATICA (see appendix B.1). The solution should depend on the variable $\bar{\rho}$. Taking a look at the scalar product for

2.2 A ring threaded by a flux tube

the radial wave functions,

$$\begin{aligned}
 (P_\mu, P_\nu) &= 2\pi \int_{\rho_0 - \epsilon/2}^{\rho_0 + \epsilon/2} \rho P_\mu^* P_\nu d\rho \\
 &= 2\pi\epsilon \int_{-\frac{1}{2}}^{\frac{1}{2}} \rho_0 P_\nu^* P_\mu d\bar{\rho} + 2\pi\epsilon^2 \int_{-\frac{1}{2}}^{\frac{1}{2}} \bar{\rho} P_\nu^* P_\mu d\bar{\rho} \\
 &= \epsilon (P_\mu, P_\nu)_s + \epsilon^2 (P_\mu, P_\nu)_a,
 \end{aligned} \tag{2.21}$$

it becomes clear that the lowest order in ϵ of the normalized radial wave functions is $1/\sqrt{\epsilon}$. We have split the scalar product into two parts. One contains a constant, which is a symmetric function, and the other contains the asymmetric function $\bar{\rho}$. Therefore, the indices s and a were chosen. The lowest order of the Hamiltonian and hence the energy is ϵ^{-2} . Using this information, the radial wave functions and the energy levels are expanded in the following way

$$\begin{aligned}
 P_\nu &= \frac{1}{\sqrt{\epsilon}} \sum_{n=0}^{\infty} \epsilon^n P_{n\nu}, \\
 \eta_\nu^{(0)} &= \frac{\rho_0^2}{\epsilon^2} \sum_{n=0}^{\infty} \epsilon^n \eta_{(n-2)\nu}^{(0)}.
 \end{aligned} \tag{2.22}$$

The Schrödinger equation for the radial wave function,

$$\begin{aligned}
 &\left[\frac{\rho_0^2}{\epsilon^2} \frac{\partial^2}{\partial \bar{\rho}^2} + \frac{2\rho_0\bar{\rho}}{\epsilon} \frac{\partial^2}{\partial \bar{\rho}^2} + \frac{\rho_0}{\epsilon} \frac{\partial}{\partial \bar{\rho}} + \bar{\rho}^2 \frac{\partial^2}{\partial \bar{\rho}^2} + \bar{\rho} \frac{\partial}{\partial \bar{\rho}} + \right. \\
 &\quad \left. + \left(1 + 2\bar{\rho} \frac{\epsilon}{\rho_0} + \bar{\rho}^2 \frac{\epsilon^2}{\rho_0^2} \right) \left(\frac{1}{\epsilon^2} \eta_{-2\nu}^{(0)} + \frac{1}{\epsilon} \eta_{-1\nu}^{(0)} + \eta_{0\nu}^{(0)} + \dots \right) - \xi_\nu^2 \right] \times \\
 &\quad \times \left(\frac{1}{\sqrt{\epsilon}} P_{0\nu} + \sqrt{\epsilon} P_{1\nu} + \epsilon^{\frac{3}{2}} P_{2\nu} + \dots \right) = 0,
 \end{aligned} \tag{2.23}$$

separated into different orders of ϵ is

$$\begin{aligned}
 0 &= \epsilon^{-\frac{5}{2}} \left(\rho_0^2 P_{0\nu} + \eta_{-2\nu}^{(0)} P_{0\nu}'' \right) \\
 &\quad + \epsilon^{-\frac{3}{2}} \left[2\rho_0\bar{\rho} P_{0\nu}'' + \rho_0 P_{0\nu}' + \rho_0^2 P_{1\nu}'' + \left(2\frac{\bar{\rho}}{\rho_0} \eta_{-2\nu}^{(0)} + \eta_{-1\nu}^{(0)} \right) P_{0\nu} + \eta_{-2\nu}^{(0)} P_{1\nu} \right] \\
 &\quad + \mathcal{O}\left(\epsilon^{-\frac{1}{2}}\right).
 \end{aligned} \tag{2.24}$$

The normalization condition,

$$\begin{aligned}
 1 &= \|\Psi_\nu\|^2 \\
 &= \sum_{m,n} \epsilon^{m+n+1} (P_{m\nu}, P_{n\nu}) \\
 &= (P_{0\nu}, P_{0\nu})_s + \epsilon (P_{0\nu}, P_{0\nu})_a + 2\epsilon (P_{0\nu}, P_{1\nu})_s + \mathcal{O}(\epsilon^2),
 \end{aligned} \tag{2.25}$$

has to be checked for every order separately. Solving the differential equations for the different orders, applying the boundary condition and normalization conditions leads to the radial ground-state wave function,

$$\begin{aligned}
 P_\nu(\bar{\rho}) &= \frac{\cos \pi \bar{\rho}}{\sqrt{\pi \rho_0 \epsilon}} - \frac{\sqrt{\epsilon \bar{\rho}}}{2\sqrt{\pi} \rho_0^{\frac{3}{2}}} \cos \pi \bar{\rho} + \frac{3\epsilon^{\frac{3}{2}} \bar{\rho}^2}{8\sqrt{\pi} \rho_0^{\frac{5}{2}}} \cos \pi \bar{\rho} \\
 &\quad - \epsilon^{\frac{5}{2}} \left[\frac{5\bar{\rho}^3 \cos \pi \bar{\rho}}{16\sqrt{\pi} \rho_0^{\frac{7}{2}}} + \frac{(\xi_\nu^2 - \frac{1}{4}) [\bar{\rho} \cos \pi \bar{\rho} + \pi(\xi_\nu^2 - \frac{1}{4}) \sin \pi \bar{\rho}]}{4\pi^{\frac{5}{2}} \rho_0^{\frac{7}{2}}} \right] + \mathcal{O}\left(\epsilon^{\frac{7}{2}}\right) \\
 &= \frac{\cos \pi \bar{\rho}}{\sqrt{\pi(\rho_0 + \epsilon \bar{\rho})\epsilon}} - \epsilon^{\frac{5}{2}} \frac{(\xi_\nu^2 - \frac{1}{4}) [\bar{\rho} \cos \pi \bar{\rho} + \pi(\xi_\nu^2 - \frac{1}{4}) \sin \pi \bar{\rho}]}{4\pi^{\frac{5}{2}} \rho_0^{\frac{7}{2}}} + \mathcal{O}\left(\epsilon^{\frac{7}{2}}\right),
 \end{aligned} \tag{2.26}$$

which still depends on the azimuthal state ν . The wave functions of a ring in a homogeneous magnetic field are expanded in a power series of the ring width in the next section. For very thin rings, the solution of the two systems is identical. We take a look at the deviations for finite ring width in the next section. For the perturbation theory, which is carried out to second order, it is sufficient to use the following approximation to the radial ground-state wave function:

$$P_0 = \frac{\cos \pi \bar{\rho}}{\sqrt{\pi(\rho_0 + \epsilon \bar{\rho})\epsilon}} + \mathcal{O}\left(\epsilon^{\frac{5}{2}}\right), \tag{2.27}$$

which does not depend on the azimuthal state.

The energy levels of the eigenstates that are realized by a product of the radial ground-state wave function and the available spectrum of azimuthal wave functions are

$$\eta_\nu^{(0)} = \pi^2 \left(\frac{\rho_0}{\epsilon}\right)^2 + \left[1 + \frac{\pi^2 - 6}{4\pi^2} \left(\frac{\epsilon}{\rho_0}\right)^2\right] \left(\xi_\nu^2 - \frac{1}{4}\right) + \mathcal{O}\left(\epsilon^4\right). \tag{2.28}$$

For further details on the calculation see the MATHEMATICA notebook included in appendix B.1. Obviously, the problem is symmetric in the ring width ϵ . Therefore, only even powers of ϵ can be present in the energy. The energy levels or bands of the 1D Kronig-Penney ring are ξ_ν^2 . We calculate this quantity in the next section.

2.2.2 The azimuthal wave function

The azimuthal wave function is determined in this section. If a magnetic flux tube is present in the ring, the wave function is altered by a phase factor independent of the ring width. This is an important result, because it proves the validity of the Peierls substitution for finite ring widths.

The azimuthal part of the Schrödinger equation,

$$\left[\left(\frac{\partial}{\partial \varphi} + i\beta \right)^2 + \xi_\nu^2 - v(\varphi) \right] \chi_\nu(\varphi) = 0, \tag{2.29}$$

2.2 A ring threaded by a flux tube

is solved by a wave function that includes a Peierls phase factor:

$$\chi_\nu = e^{-i\beta\varphi}\gamma_\nu. \quad (2.30)$$

Inserting this into Eq. (2.29) yields

$$\gamma_\nu'' + (\xi_\nu^2 - v)\gamma_\nu = 0. \quad (2.31)$$

Because the wave function χ_ν is single valued, we have

$$\chi_\nu(2\pi) = e^{-2\pi i\beta}\gamma_\nu(2\pi) = \gamma_\nu(0) = \chi_\nu(0). \quad (2.32)$$

Therefore, the new wave function γ_ν changes by a factor

$$\gamma_\nu(2\pi) = e^{2\pi i\beta}\gamma_\nu(0) \quad (2.33)$$

if the coordinate is moved around the ring.

The solution between the delta functions of the potential v is

$$\gamma_\nu(\varphi) = A_n e^{i\xi_\nu(\varphi-na)} + B_n e^{-i\xi_\nu(\varphi-na)}, \text{ for } a(n-1) \leq \varphi < an. \quad (2.34)$$

Integrating over the wave function γ at the places of the delta functions results in conditions how the first derivative of the wave function has to be connected going from one sector to another. The continuity of the wave function results in another set of equations:

$$\begin{aligned} \gamma_\nu(na + \epsilon) - \gamma_\nu(na - \epsilon) &= 0, \\ \gamma_\nu'(na + \epsilon) - \gamma_\nu'(na - \epsilon) &= -\frac{2m\rho_0^2 V_0}{\hbar^2} \gamma_\nu(na), \quad n \in \{0, 1, \dots, N-1\}. \end{aligned} \quad (2.35)$$

These conditions can be written in the form of a transfer matrix T_1 that connects the coefficients in one sector of the ring (A_n, B_n) to the coefficients in the next sector of the ring (A_{n+1}, B_{n+1}) :

$$\begin{aligned} \begin{pmatrix} A_{n+1} \\ B_{n+1} \end{pmatrix} &= T_1 \begin{pmatrix} A_n \\ B_n \end{pmatrix} \\ &= \begin{pmatrix} \left(1 + \frac{im\rho_0^2 V_0}{\hbar^2 \xi_\nu}\right) e^{i\xi_\nu a} & \frac{im\rho_0^2 V_0}{\hbar^2 \xi_\nu} e^{-i\xi_\nu a} \\ -\frac{im\rho_0^2 V_0}{\hbar^2 \xi_\nu} e^{i\xi_\nu a} & \left(1 - \frac{im\rho_0^2 V_0}{\hbar^2 \xi_\nu}\right) e^{-i\xi_\nu a} \end{pmatrix} \begin{pmatrix} A_n \\ B_n \end{pmatrix}. \end{aligned} \quad (2.36)$$

On the other hand, the Hamiltonian D commutes with every translation operator,

$$T_n \Psi(\rho, \varphi) = \Psi(\rho, \varphi + an), \quad (2.37)$$

due to the periodicity of the potential v . It can be easily shown, that the eigenvalues of the translation operators are phase factors e^{ilan} , $l \in \mathbb{Z}$. This is a part of

the Bloch theorem. The single-valuedness of the wave function χ_ν in combination with the Peierls phase factor

$$\begin{aligned} T_N \chi_\nu(\varphi) &= \chi_\nu(\varphi + 2\pi) \\ &= e^{i(k-\beta)2\pi} e^{-i\beta\varphi} \gamma_\nu(\varphi) \\ &\stackrel{!}{=} e^{-i\beta\varphi} \gamma_\nu(\varphi). \end{aligned} \quad (2.38)$$

leads to the condition

$$e^{i(k-\beta)2\pi} = 1. \quad (2.39)$$

Therefore, the Bloch momenta k are

$$k = \nu + \beta, \quad \nu \in \mathbb{Z}. \quad (2.40)$$

The possible Bloch momenta of the azimuthal wave function are thus shifted by the magnetic field. The total phase factor that can be extracted from the wave function and contains the magnetic field and the Bloch momentum explicitly does not change as the magnetic field varies. The change of the magnetic field is compensated by the change of the Bloch momenta. The rest of the wave function changes, because of a change in the conditions that determine ξ_ν , A_0 and B_0 . The eigenvalues of T_1 are $e^{\pm ika}$. This leads to a condition for the trace of the transfer matrix:

$$\begin{aligned} e^{ika} + e^{-ika} &= \text{Tr } T_1 = \left(1 + \frac{im\rho_0^2 V_0}{\hbar^2 \xi_\nu}\right) e^{i\xi_\nu a} + \left(1 - \frac{im\rho_0^2 V_0}{\hbar^2 \xi_\nu}\right) e^{-i\xi_\nu a}, \\ \cos ka &= \cos \xi_\nu a - \frac{mV_0\rho_0^2}{\hbar^2 \xi_\nu} \sin \xi_\nu a. \end{aligned} \quad (2.41)$$

This relation can be inverted numerically to give $\xi_\nu(k)$ [see Fig. 2.2]. The relation between the coefficients A_0 and B_0 is determined by the eigenvectors of T_1 . The normalization determines the coefficients up to a global phase factor. The normalization condition for A_0 and B_0 is

$$\begin{aligned} \int_0^{2\pi} \chi_\nu^* \chi_\nu d\varphi &= N \int_0^{2\pi/N} (A_0 A_0^* e^{-2\text{Im } \xi_\nu \varphi} + B_0 B_0^* e^{2\text{Im } \xi_\nu \varphi} \\ &\quad + A_0 B_0^* e^{2i \text{Re } \xi_\nu \varphi} + B_0 A_0^* e^{-2i \text{Re } \xi_\nu \varphi}) d\varphi \\ &= 2\pi. \end{aligned} \quad (2.42)$$

The complete wave function is

$$\begin{aligned} \chi_\nu(\varphi) &= e^{-i\beta\varphi} e^{ikna} (A_0 e^{i\xi_\nu(\varphi-na)} + B_0 e^{-i\xi_\nu(\varphi-na)}), \text{ for } a(n-1) \leq \varphi < an \\ &= e^{-i\beta\varphi} e^{iks(\varphi)} (A_0 e^{i\xi_\nu(\varphi-s(\varphi))} + B_0 e^{-i\xi_\nu(\varphi-s(\varphi))}). \end{aligned} \quad (2.43)$$

Here $s(\varphi) = a[\varphi/a]$, where $[x]$ denotes the function that gives the integer part of a rational number x .

The azimuthal wave function is exact for all ring widths. Consequently, the Peierls substitution is exact for all rings threaded by a flux tube in the above described way.

2.2 A ring threaded by a flux tube

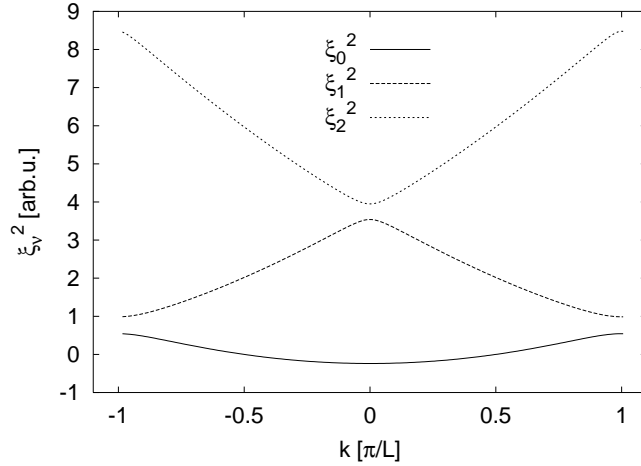


Figure 2.2: The band structure of the Kronig-Penney model.

2.2.3 Discussion of results

The energy levels are determined by the equation (2.31), which does not depend on the magnetic flux, and the boundary condition (2.33). It is obvious that the energy levels are periodic in the magnetic flux β with a period 1, i.e., a period of h/e for the flux that is not scaled by the flux quantum. By taking the complex conjugate of (2.31) and (2.33) we obtain: The energy levels are even functions of β . These are, except for a factor of $1/2$ in the period with respect to the flux, the theorems derived by Byers and Yang in 1961 (BY61) for superconducting rings in magnetic fields. A superconducting ring in a homogeneous field corresponds in many respects to a flux tube in a normal conducting ring with phase coherent motion of electrons, as, due to the Meissner effect, the magnetic field in the ring is compensated by surface currents. Byers and Yang further state that the periodicity and evenness of the energy levels remains valid if the spin of the electrons is introduced. The operation of complex conjugation in the proof of the evenness of the energy levels had to be replaced by the time reversal operation and the proof depended on the time reversal invariance of the interaction, they write.

The same theorems were derived in 1970 by Bloch (Blo70) for a superconducting ring with a barrier, looking not at the total magnetic flux in the ring, but the flux of the external magnetic field. He also pointed out that the current in the ring, which is the derivative of the free energy of the ring with respect to the flux is an odd function with respect to the magnetic flux of the external magnetic field.

In 1983, Büttiker, Imry and Landauer (BIL83) proved the same theorems for one-dimensional metal rings, neglecting the Zeeman effect. Up to now we looked at a two-dimensional ring, threaded by a flux tube. In the next chapter, we will look at a two-dimensional ring in a homogeneous magnetic field. One expects that the simple periodic dependence of all physical quantities in the ring on the flux will not survive.

Adding the proper prefactors to the dimensionless quantities we derived, the momentum of the ν th stationary state is

$$p_\nu = \hbar \frac{2\pi}{L} k_\nu = \frac{\hbar}{\rho_0} \left(\nu + \frac{\phi}{\phi_0} \right). \quad (2.44)$$

The momentum thus increases linearly with the flux. The group velocity in the circular motion of the ν th state can be approximated as

$$V_\nu^g = \frac{\partial E_\nu}{\partial p} = \frac{\rho_0 \phi_0}{\hbar} \frac{\partial E_\nu}{\partial \phi} = \frac{2\pi \rho_0}{|e|} \frac{\partial E_\nu}{\partial \phi}. \quad (2.45)$$

An electron occupying the ν th energy level contributes

$$j_\nu = \frac{e V_\nu^g}{2\pi \rho_0} = - \frac{\partial E_\nu}{\partial \phi} \quad (2.46)$$

to a current which is itself periodic. This current, carried by an electron in the ν th level induces a magnetic moment $M = j_\nu A$, which has been observed, e.g., in the experiments of Lévy (Lév00).

On the other hand, the quantum number ν is the quantum number of the canonical angular momentum $\mathbf{L} = \mathbf{r} \times \mathbf{p}$, whereas

$$\lambda = \nu + \phi/\phi_0 \quad (2.47)$$

is the eigenvalue of the kinetic angular momentum $\mathbf{\Lambda} = \mathbf{r} \times \boldsymbol{\pi}$, which can take every real value.

The energy levels of the 2D ring threaded by a flux have been derived as

$$E_\nu^{(0)} = \frac{\hbar^2}{2m\rho_0^2} \left\{ \pi^2 \left(\frac{\rho_0}{\epsilon} \right)^2 + \left[1 + \frac{\pi^2 - 6}{4\pi^2} \left(\frac{\epsilon}{\rho_0} \right)^2 \right] \left(\xi_\nu^2 - \frac{1}{4} \right) \right\} + \mathcal{O}(\epsilon^4) \quad (2.48)$$

to sub-sub-leading order in the ring width. If we subtract the divergence and constants ($\epsilon \rightarrow 0$), this equation simplifies to the well known energy levels of a 1D ring,

$$E_\nu = \frac{\hbar^2 \xi_\nu^2}{2m\rho_0^2}. \quad (2.49)$$

In the limit of vanishing potential V_0 , the familiar result (CP94) for the energy levels for a 1D free-electron ring is recovered (see Fig. 2.3),

$$E_\nu = \frac{\hbar^2}{2m\rho_0^2} \lambda^2. \quad (2.50)$$

The effect of the ring width ϵ in Eq. 2.48 is completely contained within a prefactor to the one-dimensional energy levels ξ_ν . Hence, the structure of the energy levels of a 2D ring threaded by a flux tube can be quantitatively described by a 1D ring that captures the azimuthal structure with effective parameters. In chapter

2.2 A ring threaded by a flux tube

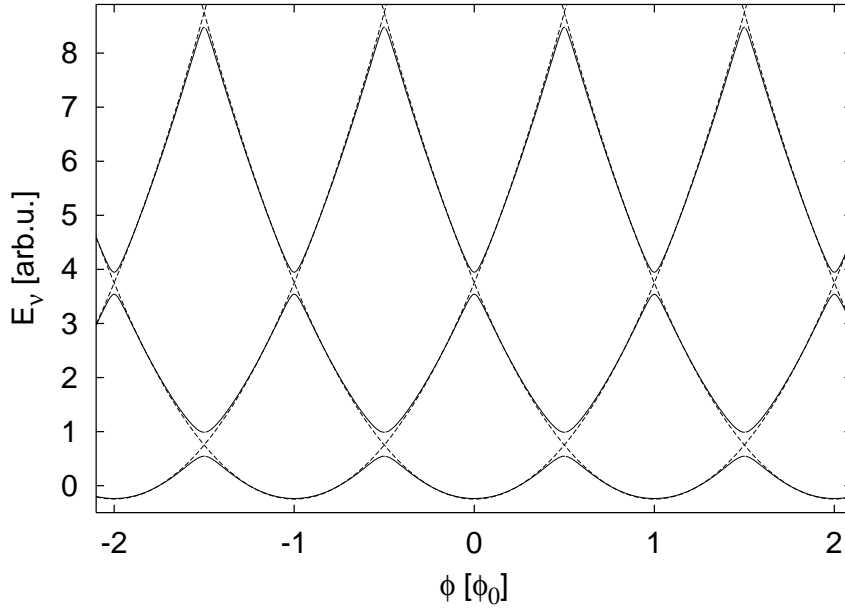


Figure 2.3: The electronic spectrum of the 1D ring threaded by a flux tube is periodic in the number of flux quanta threading the ring. The periodic Kronig-Penney potential opens gaps at the wave vectors which are multiples of π/L and correspond to fluxes which are multiples of half a flux quantum.

4.3.2, we describe the azimuthal structure of the π -electrons in the ring-shaped benzene molecule by a Hubbard model with empirically determined parameters. This would be pointless, if it was not possible to describe a thick ring by an effective one-dimensional one.

Without magnetic flux in the ring, the minima of the energy bands are at $\nu = 0$ and the energy bands are symmetric about $\nu = 0$, a natural consequence of time-reversal symmetry. If flux penetrates the ring, the minima of the bands are shifted to $\nu = -\phi/\phi_0$.

The probability density to find an electron in the ν th state at a specific distance from the origin within the ring is

$$d_\nu(\bar{\rho}) = 2\pi\epsilon(\rho_0 + \epsilon\bar{\rho})|P_\nu(\bar{\rho})|^2. \quad (2.51)$$

Taking a glance at Eq. (2.26), we notice that the probability density is shaped like a squared cosine and reaches its maximum at the middle of the ring, independent of the strength of the flux tube threading the ring, if only the first three orders in ϵ are considered. The contribution to the order of $\epsilon^{\frac{5}{2}}$ reveals two things: The approximation is trustworthy only for moderately large values of the azimuthal energy ξ_ν^2 and the average radius of the radial wave function is enlarged by the velocity of the electrons. This effect is graphically shown in Fig. 2.4. It is interesting to note that for a 2D ring, even without the potential ($V_0 = 0$), the azimuthal motion

is not decoupled from the radial motion. For a 2D straight wire, the longitudinal state does not influence the transversal state. Here, the situation is different. Every different azimuthal state has a different radial eigenfunction. Thus, it is not surprising that a deviation from the parabolic behavior of the azimuthal bands was found by Tan and Inkson for another radial confinement potential (TI96).

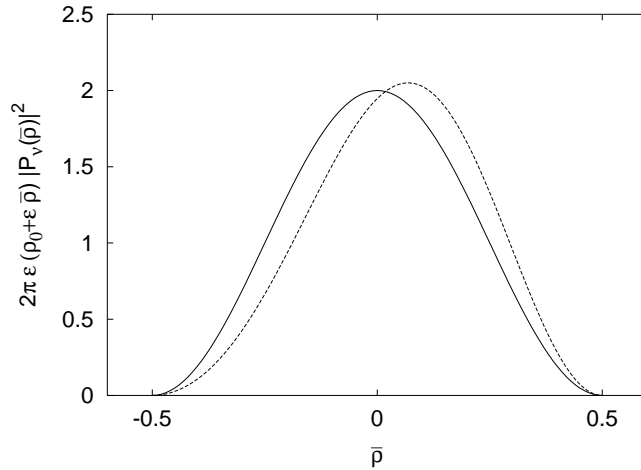


Figure 2.4: The probability density to find an electron at a specific radius is plotted for two different values of flux in the ring for the stationary ground state. The solid curve is for zero flux, whence the probability density is centered at the middle of the ring. The dashed curve is for a flux tube of 100 flux quanta in the ring, or equivalently for an kinetic angular momentum of $100\hbar$. The velocity of the electrons forces the electrons more to the outer bound of the ring. The radius and the width ($\rho_0 = 200\text{nm}$, $\epsilon = 20\text{nm}$) are chosen to be of the same order of magnitude as the ones used in experiments on quantum rings in heterostructures.

The numerical value of the averaged radius in the ν th level of a ring without azimuthal potential,

$$\langle \bar{\rho} \rangle_\nu = \int_{-0.5}^{0.5} \bar{\rho} d_\nu(\bar{\rho}) d\bar{\rho}, \quad (2.52)$$

has been evaluated and plotted against the kinetic angular momentum, which is proportional to the group velocity of the azimuthal wave packet as shown above (see Fig. 2.5). The shift of the radius to the outer half of the ring ($\bar{\rho} > 0$) is symmetric about $\lambda = 0$ which corresponds to zero velocity of the electrons. It does not matter whether the electrons move right or left around the ring. This effect has nothing to do with the Lorentz force. The magnetic induction is zero in the space where the electrons are moving. Hence, also the Lorentz force is zero. This effect is related to the centrifugal force that a particle undergoing a circular motion experiences.

2.3 A ring in a homogeneous magnetic field

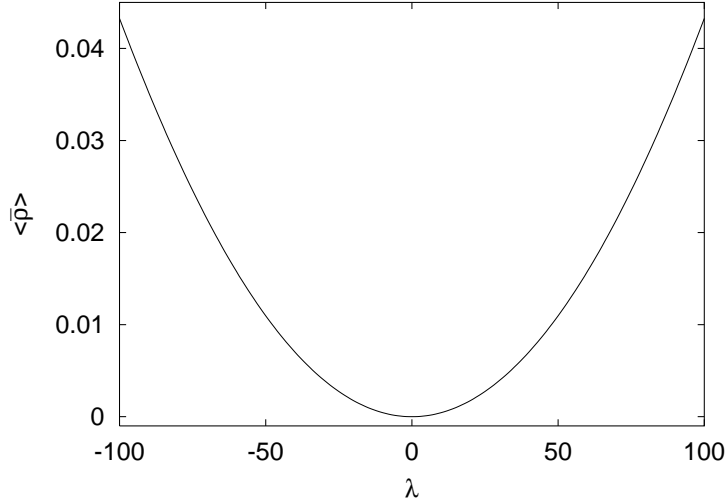


Figure 2.5: The shift of the average value of the radius of the radial wave function as a function of the kinetic angular momentum for a ring with a radius of $\rho_0 = 200\text{nm}$ and a width of $\epsilon = 20\text{nm}$. There is no azimuthal potential on the ring. The positive values of the averaged radius indicate a shift of the probability density from the center to the outer half of the ring.

2.3 A ring in a homogeneous magnetic field

The ring of vanishing ring width and the Peierls substitution are approximations for the two-dimensional ring in a homogeneous field. We calculate the first-order corrections with respect to the ring width. Therefore, we apply perturbation theory and expand the wave functions and eigenenergies in terms of the ring threaded by a flux tube.

The homogeneous magnetic field,

$$\mathbf{B} = B\hat{e}_z,$$

is represented by the vector potential,

$$\mathbf{A} = \frac{1}{2}\mathbf{B} \times \mathbf{r}.$$

The terms in the Hamiltonian (2.1) depending on the vector potential become

$$\begin{aligned} \frac{i\hbar e}{m}\mathbf{A} \cdot \nabla &= \frac{i\hbar e}{2m}(\mathbf{B} \times \mathbf{r}) \cdot \nabla \\ &= \frac{i\hbar e}{2m}\mathbf{B} \cdot (\mathbf{r} \times \nabla) \\ &= -\frac{e}{2m}\mathbf{B} \cdot \mathbf{L} \\ &= \frac{i\hbar e}{2m}B\frac{\partial}{\partial\varphi} \end{aligned} \tag{2.53}$$

and

$$\begin{aligned}
 \frac{e^2}{2m} \mathbf{A}^2 &= \frac{e^2}{8m} (\mathbf{B} \times \mathbf{r})^2 \\
 &= \frac{e^2}{8m} [B^2 r^2 - (\mathbf{B} \cdot \mathbf{r})^2] \\
 &= \frac{e^2}{8m} B^2 \rho^2.
 \end{aligned} \tag{2.54}$$

The Schrödinger equation is

$$\begin{aligned}
 0 &= (\mathbf{H} - E_\nu) \Psi_\nu \\
 &= -\frac{\hbar^2}{2m} \left(\frac{\partial^2}{\partial \rho^2} + \frac{1}{\rho} \frac{\partial}{\partial \rho} + \frac{1}{\rho^2} \frac{\partial^2}{\partial \varphi^2} - \frac{ieB}{\hbar} \frac{\partial}{\partial \varphi} \right. \\
 &\quad \left. - \frac{e^2 B^2}{4\hbar^2} \rho^2 - \frac{1}{\rho^2} v(\varphi) + \frac{\eta_\nu}{\rho_0^2} \right) \Psi_\nu.
 \end{aligned} \tag{2.55}$$

If we again call the dimensionless flux in the ring

$$\beta = \pi \rho_0^2 B \frac{|e|}{2\pi \hbar} = \frac{|e| B \rho_0^2}{2\hbar}, \tag{2.56}$$

the dimensionless Schrödinger equation becomes (with the definitions from the last section):

$$\begin{aligned}
 0 &= (\mathbf{D} + \eta_\nu) \Psi_\nu \\
 &= \left[\frac{\partial^2}{\partial r^2} + \frac{1}{r} \frac{\partial}{\partial r} + \frac{1}{r^2} \frac{\partial^2}{\partial \varphi^2} + 2i\beta \frac{\partial}{\partial \varphi} - \beta^2 r^2 - \frac{v(\varphi)}{r^2} + \eta_\nu \right] \Psi_\nu \\
 &= \left[\mathbf{D}^{(0)} + 2i\beta \left(1 - \frac{1}{r^2} \right) \frac{\partial}{\partial \varphi} + \beta^2 \left(\frac{1}{r^2} - r^2 \right) + \eta_\nu \right] \Psi_\nu.
 \end{aligned} \tag{2.57}$$

2.3.1 Perturbation of the ground-state wave function

The operator \mathbf{D} can be expanded in terms of ϵ ,

$$\mathbf{D} = \sum_{n=0}^{\infty} \epsilon^n \mathbf{D}^{(n)}. \tag{2.58}$$

The first orders (-2 to 0) of the expansion are contained in $\mathbf{D}^{(0)}$. We expect the deviation from the Peierls factor in the wave function to appear in second-order perturbation theory. The first- and second-order perturbations are

$$\begin{aligned}
 \mathbf{D}^{(1)} &= \frac{4\beta\bar{\rho}}{\rho_0} \left(-\beta + i \frac{\partial}{\partial \varphi} \right), \\
 \mathbf{D}^{(2)} &= \frac{2\beta\bar{\rho}^2}{\rho_0^2} \left(\beta - 3i \frac{\partial}{\partial \varphi} \right).
 \end{aligned} \tag{2.59}$$

2.3 A ring in a homogeneous magnetic field

Also the wave function and the eigenvalues of D can be expanded in terms of ϵ :

$$\begin{aligned}\Psi_\nu &= \frac{1}{\sqrt{\epsilon}} \sum_{n=0}^{\infty} \epsilon^n \Psi_\nu^{(n)}, \\ \eta_\nu &= \sum_{n=0}^{\infty} \epsilon^n \eta_\nu^{(n)}.\end{aligned}\tag{2.60}$$

The correction to the eigenstates is expanded in terms of the unperturbed eigenstates:

$$\begin{aligned}\Psi_\nu^{(1)} &= \sum_l a_{l\nu}^{(1)} \Psi_l^{(0)}, \\ \Psi_\nu^{(2)} &= \sum_l a_{l\nu}^{(2)} \Psi_l^{(0)}.\end{aligned}\tag{2.61}$$

The corrections to both, energy and eigenstates, are now calculated explicitly. In the unperturbed model containing only a flux tube through the ring, the levels of the radial wave function are to lowest order of ϵ spaced like n^2/ϵ^2 . Thus, there is a large energy gap between the lowest band and the following one for narrow rings. We are only interested in the first- and second-order corrections to the ground-state wave function and energy. They are not influenced by excited radial states. The energy levels of the unperturbed problem contribute to the second-order perturbation expansion coefficient of the energy eigenvalues and to the first-order expansion coefficient of the eigenstates through a fraction,

$$\begin{aligned}\frac{1}{\eta_l^{(0)} - \eta_\nu^{(0)}} &= \frac{1}{\left(\frac{c_1}{\epsilon^2} + c_2 + c_3\epsilon^2\right) - \left(\frac{c_4}{\epsilon^2} + c_5 + c_6\epsilon^2\right)} \\ &= \begin{cases} \mathcal{O}(\epsilon^2), & c_1 \neq c_4, \\ \mathcal{O}(\epsilon^0), & c_1 = c_4. \end{cases}\end{aligned}\tag{2.62}$$

This energy fraction is multiplied with the expectation value of the perturbing operator. The constants c_i do not depend on the ring width. This expectation value is of the order ϵ^0 . Hence, the excited radial states lead to a fourth-order contribution to the eigenenergies and to a third-order contribution to the eigenstates. This is the reason why we restrict the unperturbed states to the products of the azimuthal states with the radial ground-state wave function [see Eq. (2.27)]:

$$\Psi_\nu^{(0)} = P_0 \chi_\nu.\tag{2.63}$$

The set of quantum numbers ν simplifies to one quantum number purely describing the azimuthal dependency of the wave function. We apply the usual formulas of perturbation theory to obtain the corrections to the energy and the states. The

first-order energy correction correction yields:

$$\begin{aligned}
 \eta_\nu^{(1)} &= - \left\langle \Psi_\nu^{(0)}, D^{(1)} \Psi_\nu^{(0)} \right\rangle \\
 &= - \int_{-\frac{1}{2}}^{\frac{1}{2}} d\bar{\rho} \epsilon(\rho_0 + \epsilon\bar{\rho}) \frac{\cos^2(\pi\bar{\rho})}{\pi(\rho_0 + \epsilon\bar{\rho})\epsilon} \bar{\rho} \int_0^{2\pi} d\varphi \chi_\nu^* \frac{D^{(1)}}{\bar{\rho}} \chi_\nu \\
 &= 0.
 \end{aligned} \tag{2.64}$$

The second-order energy corrections are:

$$\begin{aligned}
 \eta_\nu^{(2)} &= 0 - \left\langle \Psi_\nu^{(0)}, D^{(2)} \Psi_\nu^{(0)} \right\rangle \\
 &= - \int_{-\frac{1}{2}}^{\frac{1}{2}} d\bar{\rho} \epsilon(\rho_0 + \epsilon\bar{\rho}) \frac{\bar{\rho}^2}{\pi} \cos^2(\pi\bar{\rho}) \int_0^{2\pi} d\varphi \chi_\nu^* \frac{D^{(2)}}{\bar{\rho}^2} \chi_\nu \\
 &= - \frac{\pi^2 - 6}{12\pi^3} \frac{\beta}{\rho_0^2} \int_0^{2\pi} d\varphi \chi_\nu^* \left(\beta - 3i \frac{\partial}{\partial\varphi} \right) \chi_\nu \\
 &= - \frac{\pi^2 - 6}{12\pi^3} \frac{\beta}{\rho_0^2} [2\pi\beta - 3i(-2\pi i\beta + 2\pi ik |A_0^* + B_0|^2)] \\
 &= - \frac{\pi^2 - 6}{6\pi^2} \frac{\beta}{\rho_0^2} (-2\beta + 3k |A_0^* + B_0|^2).
 \end{aligned} \tag{2.65}$$

The result of equation (B.2) was used in the penultimate identity. Adding the correction to the unperturbed energy levels, we obtain the energy levels of a two-dimensional quantum ring in a homogeneous magnetic field to sub-sub-leading order:

$$\begin{aligned}
 \eta_\nu &= \eta_\nu^{(0)} + \left(\frac{\epsilon}{\rho_0} \right)^2 \frac{\pi^2 - 6}{6\pi^2} (2\beta^2 - 3\beta k |A_0^* + B_0|^2) + \mathcal{O}(\epsilon^4) \\
 &= \pi^2 \left(\frac{\rho_0}{\epsilon} \right)^2 + \xi_\nu^2 - \frac{1}{4} + \frac{\pi^2 - 6}{4\pi^2} \left(\frac{\epsilon}{\rho_0} \right)^2 \left[\xi_\nu^2 - \frac{1}{4} \right. \\
 &\quad \left. + \frac{4}{3}\beta^2 - 2\beta k |A_0^* + B_0|^2 \right] + \mathcal{O}(\epsilon^4).
 \end{aligned} \tag{2.66}$$

For the eigenstates, there is also only a second-order contribution. The first-order expansion coefficients are zero:

$$\begin{aligned}
 a_{l\nu}^{(1)} &= \frac{\left\langle \Psi_l^{(0)}, D^{(1)} \Psi_\nu^{(0)} \right\rangle}{\eta_l^{(0)} - \eta_\nu^{(0)}} = 0 \quad \text{for } l \neq \nu, \\
 a_{\nu\nu}^{(1)} &= 0.
 \end{aligned} \tag{2.67}$$

The second-order coefficients are:

$$\begin{aligned}
 a_{l\nu}^{(2)} &= 0 + \frac{\langle \Psi_l^{(0)}, D^{(2)} \Psi_\nu^{(0)} \rangle}{\eta_l^{(0)} - \eta_\nu^{(0)}} \\
 &= \left(\frac{\pi^2 - 6}{6\pi^2 \rho_0^2} \right) \frac{-2\beta^2 + 3k\beta |A_0^* + B_0|^2}{\xi_l^2 - \xi_\nu^2} \quad \text{for } l \neq \nu, \\
 a_{\nu\nu}^{(2)} &= 0.
 \end{aligned} \tag{2.68}$$

The physical meaning of these results is discussed in the next section.

2.3.2 Interpretation of the result

If the Kronig-Penney potential on the ring is switched off ($V_0 = 0$), the resulting energy levels are:

$$\eta_\nu = \eta_\nu^{(0)} + \frac{\pi^2 - 6}{4\pi^2} \left(\frac{\epsilon}{\rho_0} \right)^2 \left[-\frac{2}{3}\beta^2 - 2\beta\nu \right] + \mathcal{O}(\epsilon^4). \tag{2.69}$$

The azimuthal energy ξ_ν^2 was replaced by $[\nu + \beta(\bar{\rho})]^2$.

A result with almost the same analytical structure can be obtained in an easier but nonsystematic way. This result is just used for comparison with the exact perturbation theory. In a classical picture, we can imagine the electrons moving at different radii of the ring. Circles with different radii enclose different values of magnetic flux in a homogeneous magnetic field. The electrons prefer to move at the radii where their probability density $d_\nu(\bar{\rho})$ is high. Thus, it should be possible to describe the energy levels for the two-dimensional ring in a homogeneous magnetic field by averaging the following energy levels of a ring threaded by a flux tube:

$$\eta_\nu^{(0)}(\bar{\rho}) = \pi^2 \left(\frac{\rho_0}{\epsilon} \right)^2 + \left[1 + \frac{\pi^2 - 6}{4\pi^2} \left(\frac{\epsilon}{\rho_0} \right)^2 \right] \left[(\nu + \beta(\bar{\rho}))^2 - \frac{1}{4} \right] + \mathcal{O}(\epsilon^4). \tag{2.70}$$

The magnetic flux is now depending on the radius:

$$\beta(\bar{\rho}) = \beta \left[1 + 2\frac{\epsilon}{\rho_0} \bar{\rho} + \left(\frac{\epsilon}{\rho_0} \right)^2 \bar{\rho}^2 \right]. \tag{2.71}$$

By averaging the energies,

$$\begin{aligned}
 \bar{\eta}_\nu^{(0)} &= \int_{-\frac{1}{2}}^{\frac{1}{2}} d\bar{\rho} d_\nu(\bar{\rho}) \eta_\nu^{(0)}(\bar{\rho}) \\
 &= \eta_\nu^{(0)} + (2\nu\beta + 6\beta^2) \left[\frac{\epsilon}{\rho_0} \right]^2 \int_{-\frac{1}{2}}^{\frac{1}{2}} 2 \cos^2(\pi\bar{\rho}) \bar{\rho}^2 d\bar{\rho} + \mathcal{O}(\epsilon^4) \\
 &= \eta_\nu^{(0)} + \frac{\pi^2 - 6}{4\pi^2} \left(\frac{\epsilon}{\rho_0} \right)^2 \left[2\beta^2 + \frac{2}{3}\nu\beta \right] + \mathcal{O}(\epsilon^4),
 \end{aligned} \tag{2.72}$$

a result similar to Eq. (2.69) is obtained, if terms of order higher than ϵ^2/ρ_0^2 are neglected. Prefactors are different from those resulting from the systematic perturbation expansion.

The expansion coefficients of the perturbed states of the ring in the homogeneous field [see Eq. (2.68)] depend explicitly on the magnetic field. Therefore, it is not possible any more to describe the effect of the magnetic field completely by the Peierls phase factor. In the classical picture introduced above, the electrons moving on circles with different radii acquire different phases. Thus, the electrons on different circles are able to interfere with each other, and although the classical approximation seems to be simplistic and the result is not the exact result obtained from perturbation theory, it also underlines the breakdown of the Peierls substitution. The correction to the Peierls substitution can be systematically derived with the perturbation expansion shown above.

2.4 Corrections

We have studied quantum rings containing noninteracting electrons. The effect of the electron-electron interaction is very important. It will be considered in the following chapters. The electron-electron interaction can influence the direction in which the persistent current is flowing in a quantum ring (see Sec. 3.3). It is also very important for the occurrence of spontaneous persistent currents (see Sec. 4).

In systems threaded by a flux tube, the Zeeman interaction of the spins of the electrons with the magnetic field is zero. However in homogeneous magnetic fields, in which most experiments are carried out, the Zeeman interaction results in an important contribution to the energy of the quantum rings. In addition, in high magnetic fields, relativistic corrections gain importance. These effects will be discussed in the next sections.

2.4.1 Zeeman interaction

In comparison to the above applied Schrödinger theory, the Pauli equation, being the nonrelativistic limit of the Dirac equation, includes the Zeeman interaction between the magnetic field and the intrinsic magnetic moment of the electron due to its spin. This interaction energy is

$$-g_S \frac{e}{2m} \mathbf{S} \cdot \mathbf{B}. \quad (2.73)$$

This term can be written in terms of the flux, if the field points in the z -direction:

$$-g_S \frac{\hbar}{2m\rho_0^2} S_z \frac{\phi}{\phi_0}. \quad (2.74)$$

A discussion of the effects of this term is found in Ref. (KKM).

Spin magnetism is a large contribution to the magnetism of quantum rings in strong magnetic fields. However, it is neglected in this thesis. It is a linear contribution for quantum rings in homogeneous magnetic fields. If a quantum ring is threaded by a flux tube, the magnetic field \mathbf{B} does not penetrate the region where the electrons move. Therefore, the interaction energy with the spins of the electrons is zero. Experimentally, however, it might be difficult to produce a situation where the magnetic field is zero in the space of the quantum ring where the electrons are moving. Thus, the Zeeman interaction is very important for comparison with experiments in homogeneous magnetic fields. If, however, the total spin of the electrons on the quantum ring is zero, the Zeeman interaction is also zero in the limit of weak fields. The behavior in weak homogeneous fields can be extracted from calculations excluding the Zeeman interaction for systems without a resulting spin component in the direction of the magnetic field. This is what we will do in one of the last chapters, extracting the part of the magnetic susceptibility of benzene that stems from persistent currents. The total spin of the π -electrons in benzene is zero, therefore our calculations are valid in weak homogeneous fields. In increasingly strong homogeneous fields, the Zeeman interaction induces an increasing number of spin flips and eventually dominates the energy of the system completely.

2.4.2 Relativistic corrections

The speed of electrons in mesoscopic rings is of the order of the speed of electrons in the underlying solids ($v/c \approx 10^{-2}$) (Lév00). The relativistic corrections are of the order v^2/c^2 . These corrections are important at high magnetic field strengths. The future work on the topic should focus on the relativistic corrections, in order to put the following arguments on a sufficiently solid base and to measure the importance of the corrections quantitatively.

The stronger the magnetic fields are, the more important the relativistic corrections become. In extremely strong magnetic fields, the usual chemical bonds between atoms and therefore quantum rings cease to exist. In a magnetic field, the transverse motion of an electron is quantized into Landau levels. The cyclotron radius (the characteristic size of the wave packets) becomes as small as the Bohr radius at a magnetic field strength of $B = 2.56 \times 10^5$ T. The radius of the wave packets is then below the bond length of the material that forms the quantum rings and the bonds are broken (Lai01). Magnetic fields of this strength are not producible in present day laboratories, they are typically found on surfaces of neutron stars. The highest fields obtained on the earth are approximately 1000 T with flux compression by explosives. The typical pulse duration of such a strong magnetic field is several microseconds.

In the section treating the benzene quantum rings, we show a plot of the persistent currents up to one flux quantum in the benzene ring. It is not sure whether the molecule would still exist in a homogeneous field of 8×10^4 T, which is needed to force one flux quantum inside of the benzene ring. The purpose of these calcu-

lations is to show the principal physical phenomena that could exist in quantum rings. The calculations are only valid in the low field limit or for thin flux tubes in the ring. However, for larger rings it is possible to force one quantum of magnetic flux inside of a ring at weaker fields (the flux increases with the squared radius in a homogeneous field). With the method of exact diagonalization it was not possible to do the calculations for a larger number of electrons. With future nano technology it should be possible to tailor coupled quantum dots to form a quantum ring with a larger radius but the same number of relevant electrons and the same hopping amplitude between the dots.

Spin-orbit coupling

Relativistic corrections include the spin-orbit coupling. For an arbitrary real-valued central potential, $V(\rho)$, the spin-orbit coupling contribution to the Hamiltonian is

$$\frac{1}{m^2 c^2} \frac{1}{\rho} \frac{dV}{d\rho} \mathbf{L} \cdot \mathbf{S}. \quad (2.75)$$

The potential that was used to describe the confinement of the electrons on the quantum ring is constant on the actual ring. Although the first derivative of the potential diverges at the edges of the ring, the probability to find an electron vanishes at these edges. The limiting process should be applied rigorously to reach a conclusion whether there is a spin-orbit coupling in the above described model or not.

For more realistic potentials there surely is a spin-orbit coupling effect. For the π -electrons of benzene, e.g., the spin-orbit coupling should be less important than for a hydrogen atom. The radius of the circular path of the π -electrons is large (140 pm) compared to the radius of the low-lying energy eigenstates of the hydrogen electron (50 pm). The $1/\rho$ -dependence of the spin-orbit coupling thus leads to an approximately three times lower spin-orbit coupling effect than in the lowest lying states of the hydrogen electron. The inner electrons of the carbon atoms in the benzene molecule screen the Coulomb potentials of the carbon nuclei. This diminishes the $\frac{dV}{d\rho}$ factor in the spin-orbit coupling.

Most importantly the factor $1/c^2$ diminishes the magnitude of the spin-orbit coupling for weak magnetic fields. In strong fields, the velocity of the electrons increases, thus increasing the angular momentum.

Darwin term

The Darwin term is

$$\frac{\hbar^2}{8m^2 c^2} \Delta V(\rho). \quad (2.76)$$

In the hydrogen atom, the Darwin term only contributes to the states without angular momentum, because the Coulomb potential in combination with the Laplacian leads to a delta function, which only influences the states whose wave

functions penetrate the origin. In a quantum ring, the Laplacian of the central confining potential is not singular. Therefore, it should influence all states, no matter what their angular momentum is. However, the factor $1/c^2$ reduces the importance once again.

Kinetic energy and relativistic mass increase

The relativistic correction to the kinetic energy is

$$-\frac{p^4}{8m^3c^2}. \quad (2.77)$$

This correction and the relativistic mass increase are present in quantum rings. However, these corrections do not lead to any new physical phenomena. The physical effects being present in the model should only be displaced to other values of the magnetic field by the relativistic mass increase.

In conclusion, the spin-orbit coupling seems to be the most interesting relativistic correction to the energy of quantum rings. Due to its dependence on the angular momentum and the electron spin, significant new physical phenomena can be expected by the inclusion of this term, whereas the other terms seem to merely renormalize the parameters of the model.

3 Persistent currents and the Drude weight

In this chapter, the Drude weight—a quantity measuring the strength of the persistent current in a quantum ring—is examined for different systems. With the help of the Drude weight, the direction in which the persistent current in a quantum ring flows can be determined. After deriving the Drude weight as the singular part of the electrical conductivity, the Drude weight is calculated for the periodic Anderson model. Within this model, a negative Drude weight appears for certain fillings and sizes of the ring. A negative Drude weight is a hint at a paramagnetic persistent current in a quantum ring, thus enhancing the external magnetic field. A paramagnetic ring current is totally unexpected if we look at classical conducting rings. Classical conducting rings obey Lenz’s law and therefore a current is induced that counteracts the external magnetic field. However, Lenz’s law applies to the induction of currents in varying magnetic fields, whereas we look at the persistent currents in quantum rings in static magnetic fields that stem from the Aharonov-Bohm effect. However, paramagnetic ring currents are not a very familiar effect. Therefore, in the following sections, the Drude weight is calculated at length making use of different definitions and thus consolidating the negative Drude weight for different finite systems. In the thermodynamic limit, the Drude weight, being related to the conductivity of a system, is of course positive semidefinite.

According to our calculations, a negative Drude weight either stems from an open-shell configuration of the ground state, where the states at the Fermi surface are not completely filled and Umklapp scattering can transfer electrons from one side of the Fermi surface to the other, or a band structure which is not particle-hole symmetric. The goal of this section is to elucidate these criteria, and to underline them by giving some examples of model systems that exhibit paramagnetic response.

3.1 Transport quantities

3.1.1 The Drude weight and the Meissner fraction

The easiest accessible experimentally measurable transport quantity is the *dc* resistivity $\rho = 1/\sigma(0)$, where $\sigma(\omega)$ denotes the dynamical electrical conductivity. The

conductivity has been derived within linear response theory by Kubo. In systems with correlated electrons one has to take into account besides the regular part of the conductivity σ_{reg} also a singular contribution,

$$\sigma(\omega) = 2\pi D\delta(\omega) + \sigma_{\text{reg}}(\omega), \quad (3.1)$$

where D represents the Drude weight. At zero temperature the Drude weight is the central quantity determining the *dc* charge transport. As formulated by Kohn, the Drude weight—which is also called the charge stiffness—can be expressed as the second derivative of the ground-state energy with respect to the applied magnetic flux,

$$D = \frac{N}{2} \left. \frac{\partial^2 E_0}{\partial \phi^2} \right|_{\phi=0}, \quad (3.2)$$

where N is the system size. A finite Drude weight is characteristic for a conductor or a metal. For an insulator, whether it be a band insulator (due to a filled band of electrons) or a Mott-Hubbard insulator (due to strong electron-electron repulsion), the Drude weight vanishes. At finite temperature, the Drude weight vanishes also for normal conductors. However, a finite Drude weight at finite temperature would be a signature of an ideal conductor, which does not show any energy dissipation. This case is realized by a number of nontrivial integrable many-fermion models. All integrable many-fermion models are one-dimensional (ZP03).

On the other hand, in a mesoscopic system, the persistent current is

$$j = -\frac{\partial F}{\partial \phi}. \quad (3.3)$$

Therefore, the charge stiffness D provides a measure for the persistent current for small flux since $j = -2D\phi/N$ at zero temperature. At finite temperature, the free energy F of the system is not the ground-state energy of the system and the Drude weight is not simply the first derivative of the persistent current for small flux. However, a quantity being the first derivative of the persistent current for small flux can be defined. This is the Meissner fraction,

$$\rho_S = \left. \frac{\partial^2 F}{\partial \phi^2} \right|_{\phi=0}. \quad (3.4)$$

Although both ρ_S and D are related to the current correlation function, which will we explained in the following sections, they correspond to different limits besides the different prefactor. The Meissner fraction ρ_S being a thermodynamic quantity corresponds to the limit $\omega \rightarrow 0$ first and then $q \rightarrow 0$, whereas D corresponds to the limit taken in the reverse order. For finite temperature the two quantities are distinct. For a macroscopic system ρ_S measures the superfluid density and will be zero for a non-superfluid system, whereas D can be nonzero if the system is perfectly conducting but not superconducting (e.g., free electrons in the absence of impurities). If one has a finite system, then ρ_S need not be zero, even if the system is not superconducting (GS95).

3.1 Transport quantities

The Meissner fraction estimates the ability of a system to exhibit the Meissner effect, which is related to the perfect diamagnetism of superconductors: If a normal metal in a magnetic field is cooled below its superconducting transition temperature, the magnetic flux is abruptly expelled. Thus the transition, when it occurs in a magnetic field, is accompanied by the appearance of whatever surface current is required to cancel the magnetic field in the interior of the specimen. This is not implied by perfect conductivity ($D > 0$) alone, even though perfect conductivity does imply a somewhat related property: If a perfect conductor, initially in zero magnetic field, is moved into a region of nonzero field, then Faraday's law of induction gives rise to eddy currents that cancel the magnetic field in the interior. If, however, a magnetic field were established in a perfect conductor, its expulsion would be equally resisted. Eddy currents would be induced to maintain the field if the sample were moved into a field free-region. Thus, perfect conductivity implies a time-independent magnetic field in the interior, but is noncommittal as to the value that field must have. In a superconductor, the field is not only independent of time, but also zero (AM76).

For a mesoscopic system, where the system size N is finite, ρ_s will be finite and gives the slope of the persistent current for small flux,

$$j = -\rho_s \phi. \quad (3.5)$$

Thus, mesoscopic systems show a Meissner effect. A persistent current flows only depending on the value of the magnetic field in the system. This current can be paramagnetic or diamagnetic, enhancing or diminishing the magnetic field in the sample interior. However, the persistent current does not depend on the history of the system.

In the view of this new insight—that the existence of the Meissner effect in a material does not depend on superconductivity (at least for mesoscopic samples of the material), but on the ability of a system to maintain a persistent current depending only on the value of the magnetic field in it, which is described by the Meissner fraction—we can try to give a new definition of the term phase-coherence length. The phase-coherence length of electrons in a material was earlier said to be measured by the circumference of the largest ring built from the material threaded by a magnetic flux, for which the electrons in the ring show Aharonov-Bohm oscillations, which could be visualized by measuring the magnetoresistance of the ring, for example. In a theoretical model at arbitrary temperature, for arbitrary scattering mechanisms, and arbitrary interaction mechanisms of the electrons, the phase-coherence length L_ϕ of the electrons might be defined as the largest circumference of a ring aN for which the absolute value of the Meissner fraction stays above a threshold b ,

$$L_\phi = \max_N \left\{ aN; \left| \frac{\partial^2 F(N, \phi)}{\partial \phi^2} \right|_{\phi=0} \right\}. \quad (3.6)$$

Thus, estimations of the influence of strong electron correlation on the phase-coherence length could be conducted without the construction chosen very recently

in (ŽB03). They calculated the reflectivity of a ring for one electron at half a flux quantum in the ring, which should be zero for total phase-coherence of the electrons in the ring. Moreover, the phase-coherence length L_ϕ of electrons could be rigorously defined without resorting to the one-particle picture and without the estimation of inelastic scattering times.

In the following sections, we resort to the Drude weight instead of the Meissner fraction, because we mainly focus on quantum rings at zero temperature. At zero temperature, the Drude weight and the Meissner fraction for a finite system are equally capable of indicating the sign of the persistent current in a quantum ring, but the use of the Drude weight is more widespread in the physics community.

3.1.2 The electrical conductivity

A system subjected to an external electric field responds by a redistribution of the charges in the system. For a small field, the currents in the system are proportional to the electric field. The conductivity of a system is defined as the proportionality between the current and the total electric field in the system, which is the sum of the external field and the electric field induced by the currents in the system. In a time-invariant system which is homogeneous above a certain length scale (e.g., the lattice spacing) the total current density is

$$\langle \mathbf{j} \rangle(\mathbf{r}, t) = \int d\mathbf{r}' \int_{-\infty}^t dt' \underline{\sigma}(\mathbf{r} - \mathbf{r}', t - t') \mathbf{E}(\mathbf{r}', t'). \quad (3.7)$$

This equation can be Fourier transformed to yield

$$\langle \mathbf{j} \rangle(\mathbf{q}, \omega) = \underline{\sigma}(\mathbf{q}, \omega) \mathbf{E}(\mathbf{q}, \omega). \quad (3.8)$$

Since photons have a much steeper (linear) energy dispersion than electrons within the Brillouin zone, the transmitted momentum is essentially zero for not too high energies. Thus, in the optical frequency regime and below we can take the long-wavelength limit $\mathbf{q} \rightarrow 0$ (Blü03):

$$\langle \mathbf{j} \rangle(\omega) = \underline{\sigma}(\omega) \mathbf{E}(\omega). \quad (3.9)$$

Due to the neglect of disorder in this thesis, the only relevant processes that influence the electrical conductivity are electron-phonon scattering and electron-electron repulsion. The latter can influence the transport quantities fundamentally if it becomes strong, transforming a conductor into a Mott-Hubbard insulator. In the absence of electron-phonon scattering, the relevant Hamiltonian includes the kinetic energy, the periodic potential and the electron-electron interaction. The electron-electron scattering sparks current relaxation and dissipation. Therefore, the current density is not conserved, i.e.,

$$[\mathbf{H}, \mathbf{j}] \neq 0. \quad (3.10)$$

3.1 Transport quantities

Leaving the continuous models of the last chapter behind, discrete tight-binding models, including a hopping term (representing the effect of the periodic lattice potential and the kinetic energy) as well as the electron-electron interaction,

$$H = - \sum_{lm\sigma} t_{lm} c_{m\sigma}^\dagger c_{l\sigma} + H_{\text{int}}, \quad (3.11)$$

are considered predominantly in this chapter. To gain insight into the electrical conductivity $\sigma(\omega)$, we follow the approach of Kohn (Koh64). A fictitious magnetic flux $\phi = aNA$ is introduced through a torus (of circumference aN) representing the lattice (lattice constant a) with periodic boundary conditions. The flux tube leads to a vector potential \mathbf{A} considered equal on all lattice sites. The vector potential can be included in the model by the Peierls substitution,

$$c_{l\sigma}^\dagger \rightarrow c_{l\sigma}^\dagger \exp\left(-i\frac{e}{\hbar}\mathbf{A} \cdot \mathbf{x}_l\right), \quad (3.12)$$

which stems from a gauge transform and effectively modifies the hopping matrix elements t_{lm} . The interaction term H_{int} remains unchanged by the gauge transform due to its dependence on local particle densities only. Expanding the Hamiltonian into a power series of the magnetic flux per lattice site ($\phi/N = a\mathbf{A}$), we obtain

$$\begin{aligned} H(a\mathbf{A}) &= - \sum_{lm\sigma} t_{lm} e^{i\frac{e}{\hbar}\mathbf{A} \cdot \mathbf{x}_{lm}} c_{m\sigma}^\dagger c_{l\sigma} + H_{\text{int}} \\ &= H(0) + (-a\mathbf{A}) \cdot \mathbf{j}_p - \frac{e^2}{2\hbar^2} a^2 \mathbf{A} \cdot \underline{\tau} \mathbf{A} \\ &= H(0) + H', \end{aligned} \quad (3.13)$$

where the vector $\mathbf{x}_{lm} = \mathbf{x}_j - \mathbf{x}_i$. \mathbf{j}_p and $\underline{\tau}$ are the paramagnetic current operator and the stress tensor operator (which is directly related to the kinetic energy) respectively:

$$\begin{aligned} \mathbf{j}_p &= -i\frac{e}{\hbar} \sum_{lm\sigma} t_{lm} \frac{\mathbf{x}_{lm}}{a} c_{m\sigma}^\dagger c_{l\sigma}, \\ \underline{\tau} &= - \sum_{lm\sigma} t_{lm} \frac{\mathbf{x}_{lm} \otimes \mathbf{x}_{lm}}{a^2} c_{m\sigma}^\dagger c_{l\sigma}. \end{aligned} \quad (3.14)$$

The electrical current, being the negative first derivative of the Hamiltonian with respect to the total flux in the ring, is therefore a sum,

$$\mathbf{j} = -\frac{\partial H}{aN\partial\mathbf{A}} = \frac{1}{N}\mathbf{j}_p + \frac{e^2}{N\hbar^2}a\underline{\tau}\mathbf{A}. \quad (3.15)$$

The measured value of the current $\langle \mathbf{j} \rangle$ is the average of the velocity of the particles times their charge. The paramagnetic current is proportional to the momentum operator. The above analysis applies also to an oscillating vector potential $\mathbf{A}(t) =$

3 Persistent currents and the Drude weight

$\mathbf{A}(\omega) \exp(-i\omega^+t)$ with $\omega^+ = \omega + i\delta$ with $\delta \rightarrow 0$. This induces an electric field in the system,

$$\mathbf{E}(t) = i\omega^+ \mathbf{A}(\omega) \exp(-i\omega^+t), \quad (3.16)$$

yielding

$$\mathbf{j} = \frac{1}{N} \mathbf{j}_p - \frac{iae^2}{N\omega^+\hbar^2} \mathcal{I} \mathbf{E}(t). \quad (3.17)$$

Now, the Kubo formula for electrical conductivity can be derived evaluating $\langle \mathbf{j}_p \rangle$ as a linear response to H' . In the absence of spontaneous persistent currents in the material under consideration, the time dependence of the expectation value of the current operator can be expressed as a commutator if terms nonlinear in the electric field are neglected:

$$\begin{aligned} \langle \psi | \mathbf{j}_p | \psi \rangle (t) &= -\frac{i}{\hbar} \int_{-\infty}^t dt' \langle \psi | [\mathbf{j}_p(t), H'(t')] | \psi \rangle \\ &= \frac{a}{\omega^+\hbar} \int_{-\infty}^t dt' \langle \psi | [\mathbf{j}_p(t), \mathbf{j}_p(t') \cdot \mathbf{E}(t)] | \psi \rangle e^{i\omega^+(t-t')} \\ &= \sum_{\beta} \frac{a}{\omega^+\hbar} E_{\beta}(t) \int_{-\infty}^t dt' e^{i\omega^+(t-t')} \langle \psi | [j_{p\alpha}(t), j_{p\beta}(t')] | \psi \rangle, \end{aligned} \quad (3.18)$$

where α and β denote spatial indices. If we extract the complex conductivity $\tilde{\sigma}$ from the equation (3.9), the result is the Kubo formula,

$$\begin{aligned} \tilde{\sigma}_{\alpha\beta}(\omega) &= \frac{a}{N} \left[\frac{1}{\omega^+\hbar} \int_{-\infty}^t dt' e^{i\omega^+(t-t')} \langle [j_{p\alpha}(t), j_{p\beta}(t')] \rangle - \frac{ie^2}{\omega^+\hbar^2} \langle \tau_{\alpha\beta} \rangle \right] \\ &= \frac{a}{N} \left[\frac{1}{\omega^+\hbar} \int_0^{\infty} dt e^{i\omega^+t} \langle [j_{p\alpha}(t), j_{p\beta}(0)] \rangle - \frac{ie^2}{\omega^+\hbar^2} \langle \tau_{\alpha\beta} \rangle \right] \\ &= \frac{ia}{N\omega^+} \left[\frac{e^2}{\hbar^2} \langle \tau_{\alpha\beta} \rangle - \chi_{\alpha\beta}(\omega) \right], \end{aligned} \quad (3.19)$$

where we defined

$$\chi_{\alpha\beta}(\omega) = \frac{i}{\hbar} \int_0^{\infty} dt e^{i\omega^+t} \langle [j_{p\alpha}(t), j_{p\beta}(0)] \rangle. \quad (3.20)$$

The real part of the complex conductivity $\tilde{\sigma}$ can be compared with Eq. (3.1), to obtain the Drude weight,

$$\begin{aligned} D_{\alpha\alpha} &= \frac{1}{2} \lim_{\omega \rightarrow 0} \omega \text{Im} \tilde{\sigma}_{\alpha\alpha}(\omega) \\ &= \frac{a}{2N} \left[\frac{e^2}{\hbar^2} \langle \tau_{\alpha\alpha} \rangle - \chi_{\alpha\alpha}(0) \right]. \end{aligned} \quad (3.21)$$

3.1 Transport quantities

In a finite one-dimensional system, the Drude weight at temperature $T = 0$ can be written in terms of the eigenstates $|n\rangle$ with corresponding energy E_n (CZP95), setting $\hbar = e = k_B = a = 1$:

$$D = \frac{\langle -\tau \rangle}{2N} - \frac{1}{N} \sum_{n \neq 0} \frac{|\langle n | j_p | 0 \rangle|^2}{E_n - E_0}. \quad (3.22)$$

This definition of the Drude weight can be easily extended to finite temperature:

$$D = \frac{1}{N} \left[\frac{1}{2} \langle -\tau \rangle - \sum_{m \neq n} p_n \frac{|\langle n | j_p | m \rangle|^2}{E_m - E_n} \right], \quad (3.23)$$

where p_n denotes the Boltzmann weight $e^{-E_n/T}/Z$ and $Z = \sum_n e^{-E_n/T}$. On the other hand (Koh64), we can evaluate, using second order perturbation theory for the flux per lattice site ($\phi_1 = \phi/N$) $\phi_1 \rightarrow 0$, a shift of the level $|n\rangle$:

$$E_n(\phi_1) = \langle n | H(\phi_1 = 0) | n \rangle - \phi_1 \langle n | j_p | n \rangle - \phi_1^2 \sum_{m \neq n} \frac{|\langle n | j_p | m \rangle|^2}{E_m - E_n} - \frac{1}{2} \phi_1^2 \langle n | \tau | n \rangle. \quad (3.24)$$

Extracting second order terms in ϕ_1 (the curvature of levels) we see that

$$D = \frac{1}{2N} \sum_n p_n \left. \frac{\partial^2 E_n}{\partial \phi_1^2} \right|_{\phi_1=0} = \frac{N}{2} \sum_n p_n \left. \frac{\partial^2 E_n}{\partial \phi^2} \right|_{\phi=0}. \quad (3.25)$$

Thus, the Drude weight is a sensitivity of the states to the applied flux.

3.1.3 The paramagnetic current

The paramagnetic current was derived in the last section by expanding the Hamiltonian with respect to a magnetic flux and taking the first order expansion coefficient. However, there is another simple way to obtain the paramagnetic current via the continuity equation,

$$\frac{\partial}{\partial t} \rho(\mathbf{x}, t) = -\nabla \cdot \mathbf{j}(\mathbf{x}, t). \quad (3.26)$$

This method is needed to calculate the paramagnetic current in the periodic Anderson model, as will be explained in the next sections.

From the polarization,

$$\mathbf{P} = \int d\mathbf{x} \mathbf{x} \rho(\mathbf{x}), \quad (3.27)$$

which simplifies to

$$\mathbf{P} = \sum_l \mathbf{x}_l n_l \quad (3.28)$$

in lattice models, the current can be calculated via the continuity equation (Mah90):

$$\begin{aligned} \frac{\partial}{\partial t} \mathbf{P} &= \int d\mathbf{x} \mathbf{x} \frac{\partial}{\partial t} \rho(\mathbf{x}, t) \\ &= - \int d\mathbf{x} \mathbf{x} \nabla \cdot \mathbf{j}_p(\mathbf{x}, t) \\ &= \int d\mathbf{x} \mathbf{j}_p(\mathbf{x}) \cdot \nabla(\mathbf{x}) \\ &= \int d\mathbf{x} \mathbf{j}_p(\mathbf{x}) \\ &= \mathbf{j}_p. \end{aligned} \quad (3.29)$$

With the use of the Heisenberg equation of motion, we obtain

$$\mathbf{j}_p = \frac{\partial \mathbf{P}}{\partial t} = i[\mathbf{H}, \mathbf{P}]. \quad (3.30)$$

We can now calculate the paramagnetic current for a model with nearest-neighbor hopping. If the vectors to the nearest-neighbor lattice sites are called $\boldsymbol{\delta}$, the hopping term of the electrons is

$$H_{\text{hop}} = -t \sum_{l\delta\sigma} d_{l+\delta,\sigma}^\dagger d_{l\sigma}. \quad (3.31)$$

Here, we called the creators and annihilators of the electrons $d_{l\sigma}^\dagger$ and $d_{l\sigma}$ respectively, to make a connection with the periodic Anderson model, with which the conduction electrons in d -orbitals are described. The current is therefore

$$\begin{aligned} \mathbf{j}_{\text{hop}} &= i[\mathbf{H}_{\text{hop}}, \mathbf{P}] \\ &= -it \sum_{l\delta\sigma m} [d_{l+\delta,\sigma}^\dagger d_{l\sigma}, \mathbf{x}_m n_m^d] \\ &= -it \sum_{l\delta\sigma m} \mathbf{x}_m d_{l+\delta,\sigma}^\dagger \delta_{lm} d_{m\sigma} - \mathbf{x}_m d_{m\sigma}^\dagger \delta_{m,l+\delta} d_{l\sigma} \\ &= -it \sum_{l\delta\sigma} (\mathbf{x}_l - \mathbf{x}_{l+\delta}) d_{l+\delta,\sigma}^\dagger d_{l\sigma} \\ &= it \sum_{l\delta\sigma} \boldsymbol{\delta} d_{l+\delta,\sigma}^\dagger d_{l\sigma}. \end{aligned} \quad (3.32)$$

This result is consistent with Eq. (3.14), if \hbar , the lattice constant a and the electron charge e are set to one.

3.2 Example: The periodic Anderson model

The periodic Anderson model is now used as an example system for the calculation of the Drude weight. The periodic Anderson model was initially formulated to explain the properties of the rare-earth and the actinide metallic compounds including the heavy fermion compounds. The superconducting and magnetic properties of heavy-fermion materials have attracted much attention because of their non-conventional character. These materials have very large specific heat coefficients, indicating very large effective quasi-particle masses, hence the designation heavy fermions. Some of these materials order antiferromagnetically at low temperatures (examples are UAgCu_4 , UCu_7 , U_2Zn_{17}) while others (such as UBe_{13} , CeCu_2Si_2 , UPt_3) order in a superconducting state and others show no ordering (such as CeAl_3 , UAuPt_4 , CeCu_6 , UAl_2). Some compounds exhibit phases where antiferromagnetic order coexists with unconventional superconductivity. Examples are: UPd_2Al_3 , CePd_2Si_2 and CeIn_3 . In the prototype heavy-fermion system $\text{Ce}_x\text{Cu}_2\text{Si}_2$ the coexistence of d -wave superconductivity and magnetic order was clearly identified in a narrow range of x values around ≈ 0.99 .

Systems that exhibit both superconductivity and antiferromagnetism at low temperatures have ratios between the Néel temperature T_N and the superconducting critical temperature T_c of the order of $T_N/T_c \approx 1 - 100$. The coexistence of both types of order can be tuned by external parameters such as external pressure or changes in the stoichiometry.

A description of the normal state properties of the heavy-fermion systems has been attempted assuming a generalization of the impurity Anderson model on a lattice. In the periodic Anderson model the energy of a single electron in an f -orbital (e.g., $4f^1$) is ϵ^f and the energy of two electrons in the same f -orbital ($4f^2$) is $2\epsilon^f + U^f$, where U^f is the on-site Coulomb repulsion. The energy of the $4f^2$ state is much larger than the energy of the $4f^1$ state. Thus, if the charge fluctuations at the f -orbital are small, the ($4f^1$) electron may behave as a local moment.

The complexity of heavy-fermion systems arises from the interplay between Kondo screening of local moments, the antiferromagnetic (RKKY) interaction between the moments and the superconducting correlations between the heavy quasi-particles. The local moments form in partially filled f -shells of Ce and U ions. The absence of magnetic order in some cases could perhaps be due to complete Kondo screening or to a spin liquid arrangement of the local moments. In the normal nonmagnetic state the periodic Anderson model predicts Fermi liquid like behavior and explains the main features at low temperatures, such as the large effective masses and the Kondo resonance near the Fermi level. But the main technical difficulty is the competition between Kondo compensation of the localized spins and the magnetic interaction between them. This interaction is mediated by the conduction electrons (RKKY-type). Related to this competition is the effectiveness of the compensating cloud around each f -site (PA02).

3.2.1 Hamiltonian and band structure

The basic ingredients of the periodic Anderson model are a narrow and correlated f -band hybridized with a dispersive d -band. The d - and f -orbitals of an atom are orthogonal. Therefore, the local hybridization of the d - and f -orbitals at the same lattice site should be small compared to the contributions to the hybridization from nearest-neighbor lattice sites [see, e.g., (vDMHZ01)]. Sketches of the periodic Anderson model with local and nearest-neighbor hybridization are shown in Fig. 3.1 and Fig. 3.2. It is clear, that the form of the current operator depends on

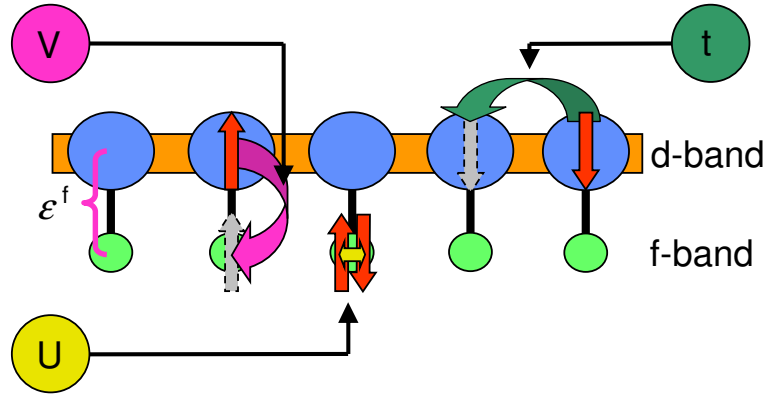


Figure 3.1: The one-dimensional periodic Anderson model with local hybridization contains a dispersive d -band (where the electrons can hop from site to site with a hopping amplitude t) and a correlated f -band (U is the strength of the Coulomb repulsion). The f -band is taken to be dispersionless ($\epsilon^f = 0$). The local hybridization enables the electrons to move from a d -orbital to an f -orbital with amplitude V at the same lattice site.

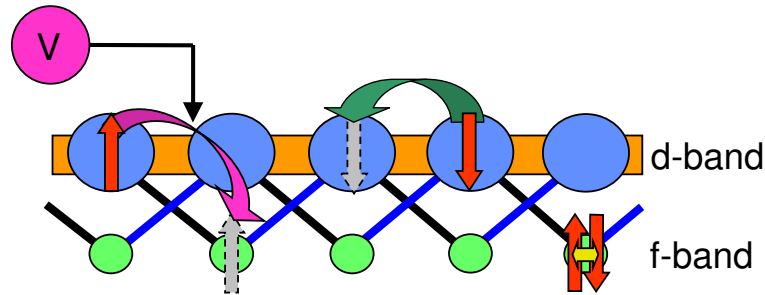


Figure 3.2: The one-dimensional periodic Anderson model with nearest-neighbor hybridization enables the electrons to move from the d -orbitals of one site to the f -orbitals of a nearest-neighbor site and back again.

the exact form of the hybridization. The hybridization of heavy-fermion materials will in general be a mixture of on-site and nearest-neighbor hybridizations and

3.2 Example: The periodic Anderson model

possibly contributions from further-neighbor sites. Thus, in order to determine the dependence of results on the hybridization, we perform most calculations for the on-site and nearest-neighbor version of the hybridizations.

The model is described by the following Hamiltonian:

$$\begin{aligned}
H_{\text{PAM}} = & -t \sum_{\langle lm \rangle, \sigma} (d_{l\sigma}^\dagger d_{m\sigma} + d_{m\sigma}^\dagger d_{l\sigma}) - \sum_{l, m, \sigma} V_{lm} (d_{l\sigma}^\dagger f_{m\sigma} + f_{m\sigma}^\dagger d_{l\sigma}) \\
& + \epsilon^f \sum_{l, \sigma} n_{l\sigma}^f + U^f \sum_l n_{l\uparrow}^f n_{l\downarrow}^f.
\end{aligned} \tag{3.33}$$

The operators $d_{l\sigma}^\dagger$ and $f_{l\sigma}^\dagger$ create electrons with spin σ in d - and f -orbitals respectively at the lattice site l of a hypercubic lattice. Although the lattice structure of real heavy-fermion materials is more complicated, we chose a hypercubic lattice in order to be able to compare our results with literature data. The hopping amplitude t describes the hopping of the d -electrons to a nearest-neighbor site. The sum $\sum_{\langle lm \rangle}$ is taken over nearest-neighbor pairs. Via the hopping amplitude V_{lm} , the hybridization of the d - and f -orbitals is taken into account. Letting $V_{lm} = V\delta_{lm}$, yields local hybridization. Nearest-neighbor hybridization is obtained by $V_{ll'} = V\delta_{|l-l'|, 1}$. The interaction between the d -electrons is weaker than the interaction between the f -electrons. Therefore, to a good approximation, only the interaction term containing U^f is present. The operator $n_{l\sigma}^f = f_{l\sigma}^\dagger f_{l\sigma}$ is the number operator of the electrons of spin σ at lattice site l . The potential of the f -electrons is ϵ^f . From Eq. (3.33) we define the noninteracting part of the Hamiltonian H_{PAM}^0 the resulting Hamiltonian when $U^f = 0$.

With the use of the following equations, the Hamiltonian H_{PAM}^0 will be transformed to momentum space for different hybridizations:

$$\begin{aligned}
c_{l\sigma} &= N^{-\frac{d}{2}} \sum_{\mathbf{k} \in B} e^{i\mathbf{k}\mathbf{x}_l} c_{\mathbf{k}\sigma} \\
c_{\mathbf{k}\sigma} &= N^{-\frac{d}{2}} \sum_l e^{-i\mathbf{k}\mathbf{x}_l} c_{l\sigma} \\
N^d \delta_{ll'} &= \sum_{\mathbf{k}} e^{i\mathbf{k}(\mathbf{x}_l - \mathbf{x}_{l'})} \\
N^d \delta_{\mathbf{k}\mathbf{k}'} &= \sum_l e^{-i(\mathbf{k} - \mathbf{k}')\mathbf{x}_l}.
\end{aligned} \tag{3.34}$$

These relations are valid for $c=d$ and $c=f$ as well. The first part of the Hamiltonian is transformed to momentum space by the following calculation. The sum $\sum_{\langle lm \rangle}$

is taken over all nearest-neighbor pairs in both orientations:

$$\begin{aligned}
 -t \sum_{(\ell'), \sigma} d_{l\sigma}^\dagger d_{l'\sigma} &= -t \sum_{(\ell'), \sigma} \left(N^{-\frac{d}{2}} \sum_{\mathbf{k} \in B} e^{i\mathbf{k}\mathbf{x}_l} d_{\mathbf{k}\sigma} \right)^\dagger \left(N^{-\frac{d}{2}} \sum_{\mathbf{k}' \in B} e^{i\mathbf{k}'\mathbf{x}_{l'}} d_{\mathbf{k}'\sigma} \right) \\
 &= -\frac{t}{N^d} \sum_{\mathbf{k}, \mathbf{k}', \sigma} \sum_{(\ell')} e^{-i(\mathbf{k}\mathbf{x}_l - \mathbf{k}'\mathbf{x}_{l'})} d_{\mathbf{k}\sigma}^\dagger d_{\mathbf{k}'\sigma} \\
 &= -\frac{t}{N^d} \sum_{\mathbf{k}, \mathbf{k}', \sigma} \sum_{(\ell')} e^{-i(\mathbf{k}-\mathbf{k}')\mathbf{x}_l} e^{i\mathbf{k}'(\mathbf{x}_{l'}-\mathbf{x}_l)} d_{\mathbf{k}\sigma}^\dagger d_{\mathbf{k}'\sigma} \\
 &= -\frac{t}{N^d} \sum_{\mathbf{k}, \mathbf{k}', \sigma} \left(\sum_l e^{-i(\mathbf{k}-\mathbf{k}')\mathbf{x}_l} \right) \sum_{\ell=1}^d \left(e^{ik'_\ell a} + e^{-ik'_\ell a} \right) d_{\mathbf{k}\sigma}^\dagger d_{\mathbf{k}'\sigma} \\
 &= \sum_{\mathbf{k}, \sigma} \epsilon_{\mathbf{k}} d_{\mathbf{k}\sigma}^\dagger d_{\mathbf{k}\sigma}, \quad \text{where } \epsilon_{\mathbf{k}} = -2t \sum_{\ell=1}^d \cos k_\ell a.
 \end{aligned} \tag{3.35}$$

The spatial components of vectors are counted with the index $\ell \in \{x, y, z\}$. This applies to a d -dimensional hypercubic lattice.

With the quasi-particles (TSU97), it is possible to diagonalize the noninteracting part of the Hamiltonian of the periodic Anderson model in momentum space:

$$\begin{aligned}
 a_{\mathbf{k}\sigma} &= u_{\mathbf{k}} d_{\mathbf{k}\sigma} + v_{\mathbf{k}} f_{\mathbf{k}\sigma} \\
 a_{\mathbf{k}\sigma}^\dagger &= u_{\mathbf{k}}^* d_{\mathbf{k}\sigma}^\dagger + v_{\mathbf{k}}^* f_{\mathbf{k}\sigma}^\dagger \\
 b_{\mathbf{k}\sigma} &= -v_{\mathbf{k}} d_{\mathbf{k}\sigma} + u_{\mathbf{k}} f_{\mathbf{k}\sigma} \\
 b_{\mathbf{k}\sigma}^\dagger &= -v_{\mathbf{k}}^* d_{\mathbf{k}\sigma}^\dagger + u_{\mathbf{k}}^* f_{\mathbf{k}\sigma}^\dagger.
 \end{aligned} \tag{3.36}$$

The quasi-particle operators fulfill the canonical anticommutator relations,

$$\begin{aligned}
 \{a_{\mathbf{k}\sigma}, a_{\mathbf{k}'\sigma'}\} &= 0 & \{b_{\mathbf{k}\sigma}, b_{\mathbf{k}'\sigma'}\} &= 0 & \{a_{\mathbf{k}\sigma}, b_{\mathbf{k}'\sigma'}\} &= 0 \\
 \{a_{\mathbf{k}\sigma}^\dagger, a_{\mathbf{k}'\sigma'}^\dagger\} &= 0 & \{b_{\mathbf{k}\sigma}^\dagger, b_{\mathbf{k}'\sigma'}^\dagger\} &= 0 & \{a_{\mathbf{k}\sigma}^\dagger, b_{\mathbf{k}'\sigma'}^\dagger\} &= 0 \\
 \{a_{\mathbf{k}\sigma}, a_{\mathbf{k}'\sigma'}^\dagger\} &= \delta_{\mathbf{k}\mathbf{k}'} \delta_{\sigma\sigma'} & \{b_{\mathbf{k}\sigma}, b_{\mathbf{k}'\sigma'}^\dagger\} &= \delta_{\mathbf{k}\mathbf{k}'} \delta_{\sigma\sigma'} & \{a_{\mathbf{k}\sigma}, b_{\mathbf{k}'\sigma'}^\dagger\} &= 0,
 \end{aligned} \tag{3.37}$$

under the condition that $|u_{\mathbf{k}}|^2 + |v_{\mathbf{k}}|^2 = 1$ is fulfilled (this follows from, e.g., $\{a_{\mathbf{k}\sigma}, a_{\mathbf{k}'\sigma'}^\dagger\} = \delta_{\mathbf{k}\mathbf{k}'} \delta_{\sigma\sigma'}$). The parameters $u_{\mathbf{k}}$ and $v_{\mathbf{k}}$ can be chosen to be real. The d - and f -electrons can be expressed through the quasi-particles,

$$\begin{aligned}
 f_{\mathbf{k}\sigma} &= v_{\mathbf{k}} a_{\mathbf{k}\sigma} + u_{\mathbf{k}} b_{\mathbf{k}\sigma} \\
 f_{\mathbf{k}\sigma}^\dagger &= v_{\mathbf{k}} a_{\mathbf{k}\sigma}^\dagger + u_{\mathbf{k}} b_{\mathbf{k}\sigma}^\dagger \\
 d_{\mathbf{k}\sigma} &= u_{\mathbf{k}} a_{\mathbf{k}\sigma} - v_{\mathbf{k}} b_{\mathbf{k}\sigma} \\
 d_{\mathbf{k}\sigma}^\dagger &= u_{\mathbf{k}} a_{\mathbf{k}\sigma}^\dagger - v_{\mathbf{k}} b_{\mathbf{k}\sigma}^\dagger.
 \end{aligned} \tag{3.38}$$

3.2 Example: The periodic Anderson model

Local hybridization

The second part of the Hamiltonian is transformed to momentum space for the local hybridization $V_{ll'} = V\delta_{ll'}$:

$$\begin{aligned}
H_{\text{LH}} &= - \sum_{l,l',\sigma} V\delta_{ll'} (d_{l\sigma}^\dagger f_{l'\sigma} + f_{l'\sigma}^\dagger d_{l\sigma}) \\
&= -V \sum_{l,\sigma} (d_{l\sigma}^\dagger f_{l\sigma} + f_{l\sigma}^\dagger d_{l\sigma}) \\
&= -\frac{V}{N^d} \sum_{\mathbf{k},\mathbf{k}',\sigma} \sum_l e^{-i(\mathbf{k}'-\mathbf{k})\cdot\mathbf{x}_l} (d_{\mathbf{k}\sigma}^\dagger f_{\mathbf{k}'\sigma} + f_{\mathbf{k}'\sigma}^\dagger d_{\mathbf{k}\sigma}) \\
&= -V \sum_{\mathbf{k},\sigma} (d_{\mathbf{k}\sigma}^\dagger f_{\mathbf{k}\sigma} + f_{\mathbf{k}\sigma}^\dagger d_{\mathbf{k}\sigma}).
\end{aligned} \tag{3.39}$$

The quasi-particle operators are inserted into the Hamiltonian H_{PAM}^0 in momentum space with local hybridization,

$$\begin{aligned}
H_{\text{PAM}}^0 &= \sum_{\mathbf{k},\sigma} [\epsilon_{\mathbf{k}} d_{\mathbf{k}\sigma}^\dagger d_{\mathbf{k}\sigma} - V (d_{\mathbf{k}\sigma}^\dagger f_{\mathbf{k}\sigma} + f_{\mathbf{k}\sigma}^\dagger d_{\mathbf{k}\sigma}) + \epsilon^f f_{\mathbf{k}\sigma}^\dagger f_{\mathbf{k}\sigma}] \\
&= \sum_{\mathbf{k},\sigma} [(\epsilon_{\mathbf{k}} u_{\mathbf{k}}^2 + \epsilon^f v_{\mathbf{k}}^2 - 2V u_{\mathbf{k}} v_{\mathbf{k}}) a_{\mathbf{k}\sigma}^\dagger a_{\mathbf{k}\sigma} \\
&\quad + (\epsilon_{\mathbf{k}} v_{\mathbf{k}}^2 + \epsilon^f u_{\mathbf{k}}^2 + 2V u_{\mathbf{k}} v_{\mathbf{k}}) b_{\mathbf{k}\sigma}^\dagger b_{\mathbf{k}\sigma} \\
&\quad + (V(v_{\mathbf{k}}^2 - u_{\mathbf{k}}^2) + (\epsilon^f - \epsilon_{\mathbf{k}})u_{\mathbf{k}}v_{\mathbf{k}}) a_{\mathbf{k}\sigma}^\dagger b_{\mathbf{k}\sigma} \\
&\quad + (V(v_{\mathbf{k}}^2 - u_{\mathbf{k}}^2) + (\epsilon^f - \epsilon_{\mathbf{k}})u_{\mathbf{k}}v_{\mathbf{k}}) b_{\mathbf{k}\sigma}^\dagger a_{\mathbf{k}\sigma}].
\end{aligned} \tag{3.40}$$

In order to obtain a diagonal Hamiltonian, the non-diagonal terms should vanish:

$$V(v_{\mathbf{k}}^2 - u_{\mathbf{k}}^2) + (\epsilon^f - \epsilon_{\mathbf{k}})u_{\mathbf{k}}v_{\mathbf{k}} = 0. \tag{3.41}$$

In connection with the condition,

$$|u_{\mathbf{k}}|^2 + |v_{\mathbf{k}}|^2 = 1, \tag{3.42}$$

solutions for $u_{\mathbf{k}}$ and $v_{\mathbf{k}}$ can be determined:

$$\begin{aligned}
u_{\mathbf{k}} &= \sqrt{\frac{1}{2} - \frac{\epsilon_{\mathbf{k}} - \epsilon^f}{2\sqrt{(\epsilon_{\mathbf{k}} - \epsilon^f)^2 + 4V^2}}} \\
v_{\mathbf{k}} &= \sqrt{\frac{1}{2} + \frac{\epsilon_{\mathbf{k}} - \epsilon^f}{2\sqrt{(\epsilon_{\mathbf{k}} - \epsilon^f)^2 + 4V^2}}}.
\end{aligned} \tag{3.43}$$

Inserting the solution into the Hamiltonian leads to two energy bands,

$$E_{\mathbf{k}}^\pm = \frac{1}{2} \left(\epsilon_{\mathbf{k}} + \epsilon^f \pm \sqrt{(\epsilon_{\mathbf{k}} - \epsilon^f)^2 + 4V^2} \right), \tag{3.44}$$

and a diagonal Hamiltonian:

$$H_{\text{PAM}}^0 = \sum_{\mathbf{k}, \sigma} E_{\mathbf{k}}^+ b_{\mathbf{k}\sigma}^\dagger b_{\mathbf{k}\sigma} + E_{\mathbf{k}}^- a_{\mathbf{k}\sigma}^\dagger a_{\mathbf{k}\sigma}. \quad (3.45)$$

At vanishing hybridization, $V = 0$, the tight-binding band of the d -electrons and the narrow band of the f -electrons are recovered (see Fig. 3.3).

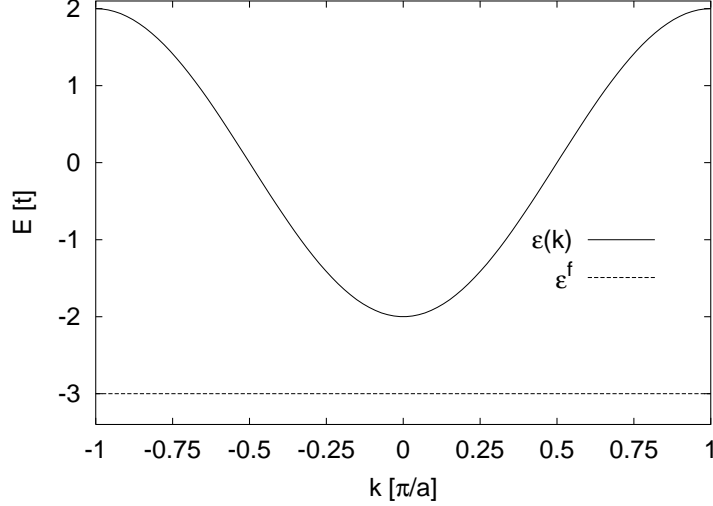


Figure 3.3: Band structure of the one-dimensional periodic Anderson model with vanishing hybridization and $\epsilon^f = -3t$.

If ϵ^f lies in the d -band and the hybridization is switched on, there are two hybridized bands which are separated by a gap. The width of the gap is

$$\begin{aligned} \Delta &= E_{(0,0,\dots)}^+ - E_{(\pi,\pi,\dots)}^- \\ &= -2dt + \frac{1}{2} \left[\sqrt{(2dt + \epsilon^f)^2 + 4V^2} + \sqrt{(2dt - \epsilon^f)^2 + 4V^2} \right], \end{aligned} \quad (3.46)$$

where d is the dimension of the hypercubic lattice. The bands for the one-dimensional periodic Anderson model with ϵ^f intersecting the d -band are shown in Fig. 3.4. The width of the gap between the two bands is shown for various parameters in Fig. 3.5.

The width of the bands is (BBG00)

$$\begin{aligned} W^\pm &= E_{(0,0,\dots)}^\pm - E_{(\pi,\pi,\dots)}^\pm \\ &= 2dt \pm \frac{1}{2} \left[\sqrt{(2dt - \epsilon^f)^2 + 4V^2} - \sqrt{(2dt + \epsilon^f)^2 + 4V^2} \right]. \end{aligned} \quad (3.47)$$

The more negative ϵ^f becomes, the narrower will the lower band be. ($W^- \rightarrow 0$). The bandwidth of the upper band goes to the bandwidth of the free electron gas ($W^+ \rightarrow 4dt$) in that case.

3.2 Example: The periodic Anderson model

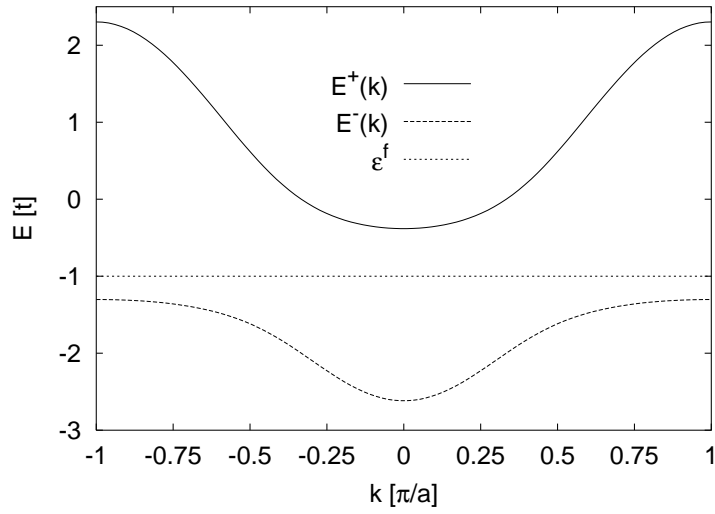


Figure 3.4: The bands of the one-dimensional periodic Anderson model at $V = t$, $\epsilon^f = -t$.

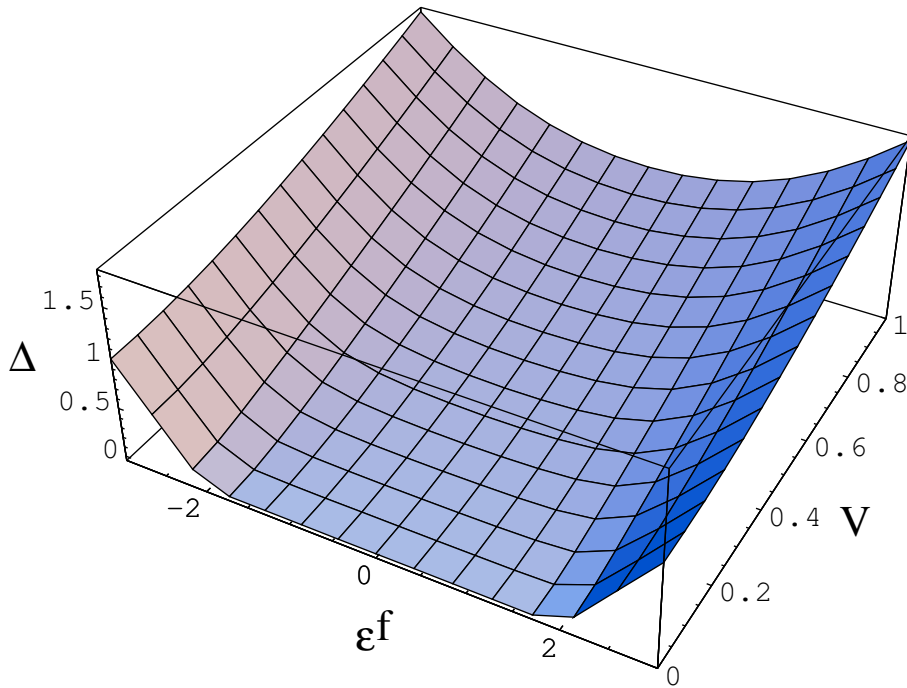


Figure 3.5: Gap of the one-dimensional periodic Anderson model with local hybridization at different values of ϵ^f and V in units of the hopping amplitude t .

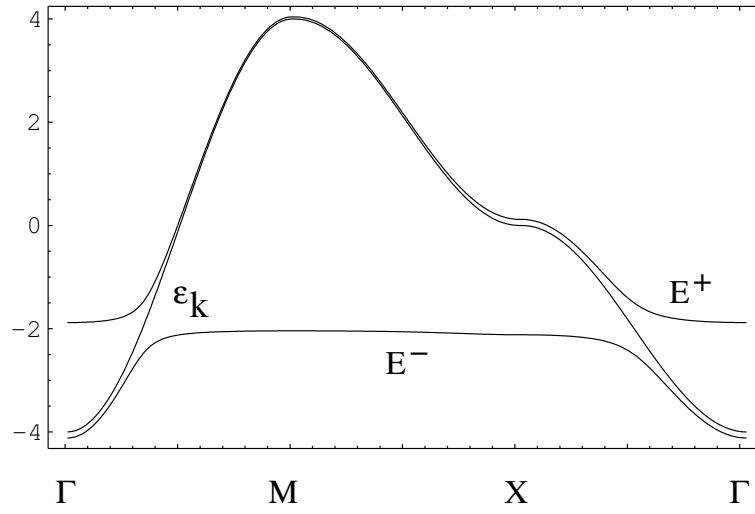


Figure 3.6: Band structure of the two-dimensional periodic Anderson model with local hybridization, $\epsilon^f = -2$, and $V = 0.5$, in comparison with the tight-binding band ($V = 0$, $\epsilon^f = 0$) in units of the hopping amplitude t (BG98).

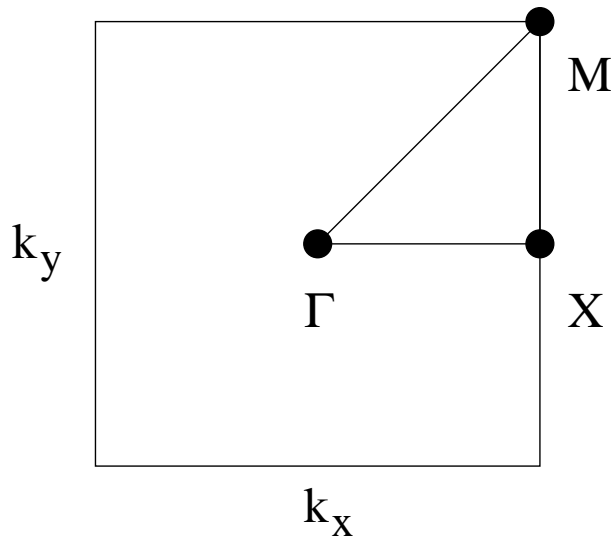


Figure 3.7: Brillouin zone of a square lattice (BG98).

Nearest-neighbor hybridization

With the nearest-neighbor hybridization $V_{lm} = V\delta_{|l-m|,1}$ (vDMHZ01; HMS99; HB00; HHSM00), the hybridization part of the Hamiltonian is derived in analogy to Eq. (3.35):

$$\begin{aligned} H_{\text{NNH}} &= - \sum_{l,l',\sigma} V\delta_{|l-l'|,1} (d_{l\sigma}^\dagger f_{l'\sigma} + f_{l'\sigma}^\dagger d_{l\sigma}) \\ &= -V \sum_{(l'),\sigma} (d_{l\sigma}^\dagger f_{l'\sigma} + f_{l'\sigma}^\dagger d_{l\sigma}) \\ &= \frac{V}{t} \sum_{\mathbf{k},\sigma} \epsilon_{\mathbf{k}} (d_{\mathbf{k}\sigma}^\dagger f_{\mathbf{k}\sigma} + f_{\mathbf{k}\sigma}^\dagger d_{\mathbf{k}\sigma}). \end{aligned} \quad (3.48)$$

The noninteracting Hamiltonian is thus

$$H_{\text{PAM}}^0 = \sum_{\mathbf{k},\sigma} \left[\epsilon_{\mathbf{k}} d_{\mathbf{k}\sigma}^\dagger d_{\mathbf{k}\sigma} + \frac{V}{t} \epsilon_{\mathbf{k}} (d_{\mathbf{k}\sigma}^\dagger f_{\mathbf{k}\sigma} + f_{\mathbf{k}\sigma}^\dagger d_{\mathbf{k}\sigma}) + \epsilon^f f_{\mathbf{k}\sigma}^\dagger f_{\mathbf{k}\sigma} \right]. \quad (3.49)$$

The energy bands are

$$E_{\mathbf{k}}^\pm = \frac{1}{2} \left(\epsilon_{\mathbf{k}} + \epsilon^f \pm \sqrt{(\epsilon_{\mathbf{k}} - \epsilon^f)^2 + 4 \left(\frac{V}{t} \epsilon_{\mathbf{k}} \right)^2} \right), \quad (3.50)$$

where we note that, in the formulas for the local hybridization, V can simply be replaced by $-\frac{V}{t}\epsilon_{\mathbf{k}}$. The band structure for the two-dimensional periodic Anderson model is shown in Fig. 3.8. The maxima and minima of the bands are not at the Γ - and M -point any more. For example, the minimum in E^+ is at $E_{(\frac{\pi}{2}, \frac{\pi}{2}, \dots)}^+$ if $\epsilon^f > 0$ and the minimum of E^- is found at $E_{(\frac{\pi}{2}, \frac{\pi}{2}, \dots)}^-$ if $\epsilon^f < 0$. Therefore, it is more difficult to calculate the gap between the bands analytically. A graph of the gap width is shown in Fig. 3.9. The periodic Anderson model with local hybridization has a nonvanishing energy gap where the band of the f -electrons intersects the band of the d -electrons (VCS⁺95). Thus, a band insulator is obtained. This is also true for the symmetric periodic Anderson model ($\epsilon^f = 0$). For nearest-neighbor hybridization, there is no gap for the symmetric model.

For further insight we appended a section about particle-hole transformations in the periodic Anderson model (see Sec. C.2).

3.2.2 The paramagnetic current

We calculate the paramagnetic current in the periodic Anderson model with the use of equation (3.30). This equation relates the paramagnetic current to the commutator of the Hamiltonian and the polarization. The part of the Hamiltonian that describes the interaction of the f -electrons commutes with the polarization. Therefore, we only need to consider the hopping and the hybridization terms. The paramagnetic current due to nearest-neighbor hopping was calculated before [see Eq. (3.32)].

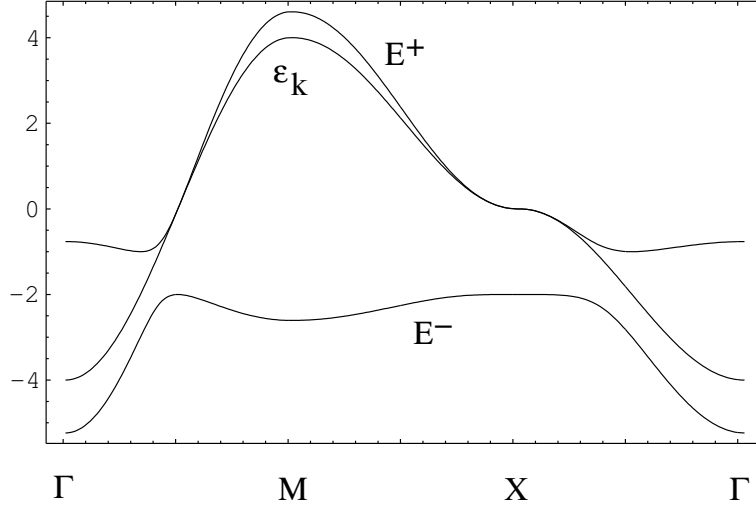


Figure 3.8: The band structure of the two-dimensional periodic Anderson model with nearest-neighbor hybridization, $\epsilon^f = -2$, and $V = 0.5$ in comparison with the tight-binding band ($V = 0$, $\epsilon^f = 0$) in units of the hopping amplitude t .

Local hybridization

The Hamiltonian of the local hybridization H_{LH} [see Eq. (3.39)] commutes with the polarization. The terms that contribute to the commutator,

$$\begin{aligned}
 [d_{l\sigma}^\dagger f_{l\sigma}, \mathbf{x}_l d_{l\sigma}^\dagger d_{l\sigma}] &= -\mathbf{x}_l d_{l\sigma}^\dagger f_{l\sigma}, \\
 [d_{l\sigma}^\dagger f_{l\sigma}, \mathbf{x}_l f_{l\sigma}^\dagger f_{l\sigma}] &= \mathbf{x}_l d_{l\sigma}^\dagger f_{l\sigma}, \\
 [f_{l\sigma}^\dagger d_{l\sigma}, \mathbf{x}_l d_{l\sigma}^\dagger d_{l\sigma}] &= \mathbf{x}_l f_{l\sigma}^\dagger d_{l\sigma}, \text{ and} \\
 [f_{l\sigma}^\dagger d_{l\sigma}, \mathbf{x}_l f_{l\sigma}^\dagger f_{l\sigma}] &= -\mathbf{x}_l f_{l\sigma}^\dagger d_{l\sigma},
 \end{aligned} \tag{3.51}$$

cancel each other. Since these terms do not contribute to the current, the paramagnetic current in the periodic Anderson model with local hybridization is

$$\mathbf{j}_{\text{LH}} = \mathbf{j}_{\text{hop}}, \tag{3.52}$$

which is simply the current of the hopping d -electrons.

To evaluate the impact of the paramagnetic current on the Drude weight, we transform the current operator to momentum space and to the quasi-particle space

3.2 Example: The periodic Anderson model

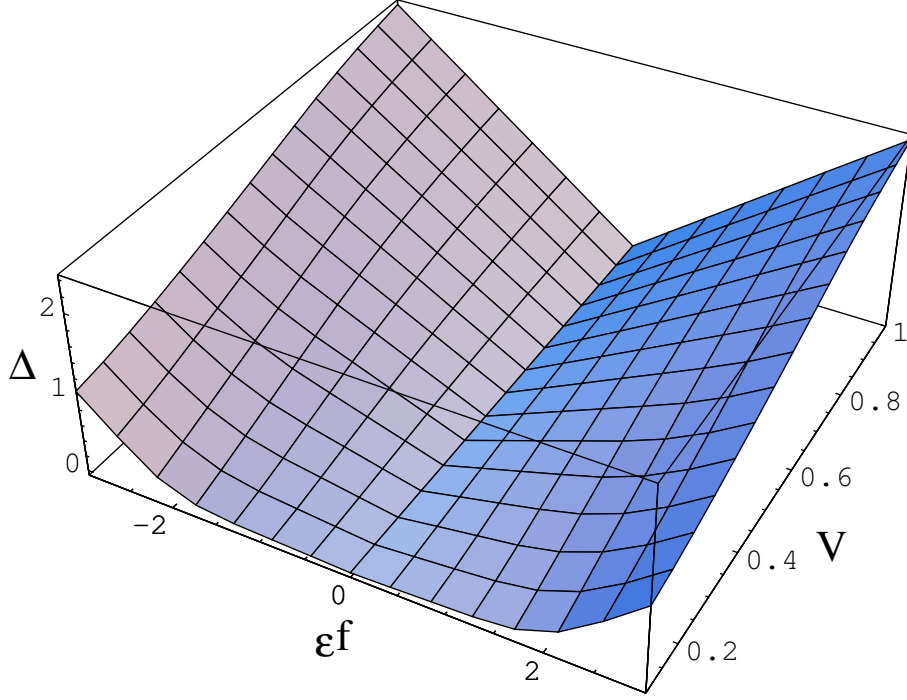


Figure 3.9: The width of the gap of the one-dimensional periodic Anderson model with nearest-neighbor hybridization is shown with respect to ϵ^f and V . All quantities are plotted in units of the hopping amplitude t .

afterwards. The paramagnetic current in momentum space is:

$$\begin{aligned}
 it \sum_{l\delta\sigma} \delta d_{l+\delta,\sigma}^\dagger d_{l\sigma} &= it \sum_{l\delta} \delta \sum_{\sigma} \left[\left(N^{-\frac{d}{2}} \sum_{\mathbf{k}} e^{i\mathbf{k}\mathbf{x}_{l+\delta}} d_{\mathbf{k}\sigma} \right)^\dagger \left(N^{-\frac{d}{2}} \sum_{\mathbf{k}'} e^{i\mathbf{k}'\mathbf{x}_l} d_{\mathbf{k}'\sigma} \right) \right] \\
 &= \frac{it}{N^d} \sum_{\mathbf{k}\mathbf{k}'\sigma} \sum_{l\delta} \delta e^{-i[\mathbf{k}\mathbf{x}_{l+\delta} - \mathbf{k}'\mathbf{x}_l]} d_{\mathbf{k}\sigma}^\dagger d_{\mathbf{k}'\sigma} \\
 &= \frac{it}{N^d} \sum_{\mathbf{k}\mathbf{k}'\sigma} \left(\sum_l e^{i[\mathbf{k}-\mathbf{k}']\mathbf{x}_l} \right) \left(\sum_{\delta} \delta e^{i\mathbf{k}\mathbf{x}_\delta} \right) d_{\mathbf{k}\sigma}^\dagger d_{\mathbf{k}'\sigma} \\
 &= \frac{it}{N^d} \sum_{\mathbf{k}\mathbf{k}'\sigma} N^d \delta_{\mathbf{k}\mathbf{k}'} \sum_{\ell=1}^d (e^{ik_\ell a} - e^{-ik_\ell a}) \\
 &= \sum_{\mathbf{k}\sigma} \eta_{\mathbf{k}} d_{\mathbf{k}\sigma}^\dagger d_{\mathbf{k}\sigma},
 \end{aligned} \tag{3.53}$$

where

$$\eta_{\mathbf{k}} = -2t \sum_{\ell=1}^d \sin k_\ell a. \tag{3.54}$$

The Bogoliubov transformation leads to

$$\begin{aligned}
 j &= \sum_{\mathbf{k}\sigma} \eta_{\mathbf{k}} (u_{\mathbf{k}} a_{\mathbf{k}\sigma}^\dagger - v_{\mathbf{k}} b_{\mathbf{k}\sigma}^\dagger) (u_{\mathbf{k}} a_{\mathbf{k}\sigma} - v_{\mathbf{k}} b_{\mathbf{k}\sigma}) \\
 &= \sum_{\mathbf{k}\sigma} \eta_{\mathbf{k}} [u^2 a_{\mathbf{k}\sigma}^\dagger a_{\mathbf{k}\sigma} + v^2 b_{\mathbf{k}\sigma}^\dagger b_{\mathbf{k}\sigma} - u_{\mathbf{k}} v_{\mathbf{k}} (a_{\mathbf{k}\sigma}^\dagger b_{\mathbf{k}\sigma} + b_{\mathbf{k}\sigma}^\dagger a_{\mathbf{k}\sigma})] \\
 &= \sum_{\mathbf{k}\sigma} \eta_{\mathbf{k}} \left[\left(\frac{1}{2} - \frac{\epsilon_{\mathbf{k}}}{2\sqrt{\epsilon_{\mathbf{k}}^2 + 4V^2}} \right) a_{\mathbf{k}\sigma}^\dagger a_{\mathbf{k}\sigma} + \left(\frac{1}{2} + \frac{\epsilon_{\mathbf{k}}}{2\sqrt{\epsilon_{\mathbf{k}}^2 + 4V^2}} \right) b_{\mathbf{k}\sigma}^\dagger b_{\mathbf{k}\sigma} \right. \\
 &\quad \left. - \frac{V}{\sqrt{\epsilon_{\mathbf{k}}^2 + 4V^2}} (a_{\mathbf{k}\sigma}^\dagger b_{\mathbf{k}\sigma} + b_{\mathbf{k}\sigma}^\dagger a_{\mathbf{k}\sigma}) \right]. \tag{3.55}
 \end{aligned}$$

This paramagnetic current operator is not diagonal. It can therefore lead to contributions to the Drude weight. In contrast, the paramagnetic current operator of the periodic Anderson model with nearest-neighbor hybridization is diagonal in the Bogoliubov space. Due to this fact, it does not contribute to the Drude weight.

Nearest-neighbor hybridization

With the nearest-neighbor hybridization, there are additional terms contributing to the paramagnetic current. The Hamiltonian for the nearest-neighbor hybridization is

$$\begin{aligned}
 H_{\text{NNH}} &= -V \sum_{(lm)\sigma} (d_{l\sigma}^\dagger f_{m\sigma} + f_{m\sigma}^\dagger d_{l\sigma}) \\
 &= -V \sum_{l\delta\sigma} (d_{l+\delta,\sigma}^\dagger f_{l\sigma} + f_{l+\delta,\sigma}^\dagger d_{l\sigma}). \tag{3.56}
 \end{aligned}$$

The nearest-neighbor hybridization allows the electrons to get from one lattice site to a nearest-neighbor lattice site (see Fig. 3.10) There are the following terms

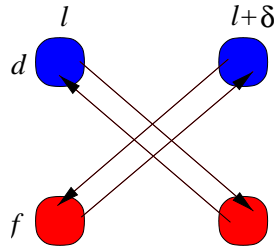


Figure 3.10: There are four possibilities how electrons can go from lattice site l to lattice site $l+\delta$ and back again through hybridization of the d -orbitals with the f -orbitals.

3.2 Example: The periodic Anderson model

in the commutator with the polarization:

$$[f_{l+\delta,\sigma}^\dagger d_{l\sigma}, \mathbf{x}_m n_m^d] = \delta_{ml} \mathbf{x}_m f_{l+\delta,\sigma}^\dagger d_{m\sigma} \quad (3.57a)$$

$$[f_{l+\delta,\sigma}^\dagger d_{l\sigma}, \mathbf{x}_m n_m^f] = -\delta_{m,l+\delta} \mathbf{x}_m f_{m\sigma}^\dagger d_{l\sigma} \quad (3.57b)$$

$$[d_{l+\delta,\sigma}^\dagger f_{l\sigma}, \mathbf{x}_m n_m^d] = -\delta_{m,l+\delta} \mathbf{x}_m d_{m\sigma}^\dagger f_{l\sigma} \quad (3.57c)$$

$$[d_{l+\delta,\sigma}^\dagger f_{l\sigma}, \mathbf{x}_m n_m^f] = \delta_{ml} \mathbf{x}_m d_{l+\delta,\sigma}^\dagger f_{m\sigma}. \quad (3.57d)$$

The paramagnetic current in the periodic Anderson model with nearest-neighbor hybridization is:

$$\begin{aligned} \mathbf{j}_{\text{NNH}} &= \mathbf{j}_{\text{hop}} + [\mathbf{H}_{\text{NNH}}, \mathbf{P}] \\ &= \mathbf{j}_{\text{hop}} + iV \sum_{l\delta\sigma} \boldsymbol{\delta} (d_{l+\delta,\sigma}^\dagger f_{l\sigma} + f_{l+\delta,\sigma}^\dagger d_{l\sigma}). \end{aligned} \quad (3.58)$$

In momentum space, we obtain

$$j = \sum_{k\sigma} \eta_k \left[d_{k\sigma}^\dagger d_{k\sigma} + \frac{V}{t} (d_{k\sigma}^\dagger f_{k\sigma} + f_{k\sigma}^\dagger d_{k\sigma}) \right]. \quad (3.59)$$

Transforming the current operator to the space of the quasi-particles, the current becomes

$$\begin{aligned} j &= \sum_{k\sigma} \eta_k \left\{ (u_k a_{k\sigma}^\dagger - v_k b_{k\sigma}^\dagger) (u_k a_{k\sigma} - v_k b_{k\sigma}) \right. \\ &\quad \left. + \frac{V}{t} [(u_k a_{k\sigma}^\dagger - v_k b_{k\sigma}^\dagger) (v_k a_{k\sigma} + u_k b_{k\sigma}) \right. \\ &\quad \left. + (v_k a_{k\sigma}^\dagger + u_k b_{k\sigma}^\dagger) (u_k a_{k\sigma} - v_k b_{k\sigma})] \right\} \\ &= \sum_{k\sigma} \left\{ \left(u_k^2 + 2\frac{V}{t} v_k u_k \right) a_{k\sigma}^\dagger a_{k\sigma} + \left(v_k^2 - 2\frac{V}{t} v_k u_k \right) b_{k\sigma}^\dagger b_{k\sigma} \right. \\ &\quad \left. + \left[\frac{V}{t} (u_k^2 - v_k^2) - u_k v_k \right] (a_{k\sigma}^\dagger b_{k\sigma} + b_{k\sigma}^\dagger a_{k\sigma}) \right\} \\ &= \sum_{k\sigma} \eta_k \left[\left(\frac{1}{2} - \frac{1}{2} \text{sgn}(\epsilon_k) \sqrt{1 + \frac{4V^2}{t^2}} \right) a_{k\sigma}^\dagger a_{k\sigma} \right. \\ &\quad \left. + \left(\frac{1}{2} + \frac{1}{2} \text{sgn}(\epsilon_k) \sqrt{1 + \frac{4V^2}{t^2}} \right) b_{k\sigma}^\dagger b_{k\sigma} \right]. \end{aligned} \quad (3.60)$$

This operator is diagonal. Therefore it does not contribute to the Drude weight and the Drude weight can be calculated in terms of the kinetic energy operator alone ($T=0$):

$$D_{\text{NNH}} = \frac{\langle \psi_0 | -\tau | \psi_0 \rangle}{2N}. \quad (3.61)$$

The nearest-neighbor hybridization also changes the operators of the total current and the kinetic energy, because the hybridization needs to be multiplied by a Peierls phase factor:

$$H = \sum_{l\delta\sigma} [-t d_{l+\delta,\sigma}^\dagger d_{l\sigma} - V (d_{l+\delta,\sigma}^\dagger f_{l\sigma} + f_{l+\delta,\sigma}^\dagger d_{l\sigma})] e^{i\delta\frac{\phi}{N}} + H_{\text{int}}. \quad (3.62)$$

An overview of all operators relevant for calculating the Drude weight of the noninteracting periodic Anderson model is found in appendix C.1.

3.2.3 Drude weight

The asymmetric band structure of the periodic Anderson model can lead to a negative Drude weight. The band structure of the one-dimensional periodic Anderson model with local hybridization is shown in Fig. 3.11. At the point k_1 , the gap between the two bands is minimal. For vanishing hybridizations, the gap goes to zero. Around k_1 , the curvature in the lower band is strongly negative for small hybridizations. This negative curvature leads to the negative Drude weight that we observed for systems where the lower band is filled at least to k_1 and the upper band is empty. Regarded separately, the two bands are not particle-hole symmetric, even for the so-called ‘symmetric’ periodic Anderson model ($\epsilon^f = 0$).

The thermodynamic limit

The Drude weight of the one-dimensional periodic Anderson model with local hybridization below half filling is calculated in the thermodynamic limit in this section. At first, we calculate the Drude weight with the use of Eq. (3.22). Afterwards, the Drude weight is calculated by determining the curvature of the ground-state energy.

The expectation value of the kinetic energy operator is (see appendix C.1 for the kinetic energy in terms of the quasi-particles):

$$\begin{aligned} \frac{\langle \psi_0 | -\tau | \psi_0 \rangle}{2N} &= -\frac{1}{N} \sum_{|k| < k_F} \epsilon_k \Xi_k^- \\ &= \frac{1}{N} \sum_{|k| < k_F} \frac{N}{2\pi} (2t \cos k) \left[\frac{1}{2} + \frac{t \cos k}{\sqrt{(2t \cos k)^2 + 4V^2}} \right] \frac{2\pi}{N} \\ &\stackrel{N \rightarrow \infty}{=} \frac{1}{2\pi} \int_{-k_F}^{k_F} t \cos k \left[1 + \frac{t \cos k}{\sqrt{(t \cos k)^2 + V^2}} \right] dk \\ &= \frac{t}{\pi} \sin k_F + \frac{1}{\pi} \sqrt{\frac{1}{h}} \left[hE \left(k_F \middle| \frac{t^2}{h} \right) - V^2 F \left(k_F \middle| \frac{t^2}{h} \right) \right], \end{aligned} \quad (3.63)$$

3.2 Example: The periodic Anderson model

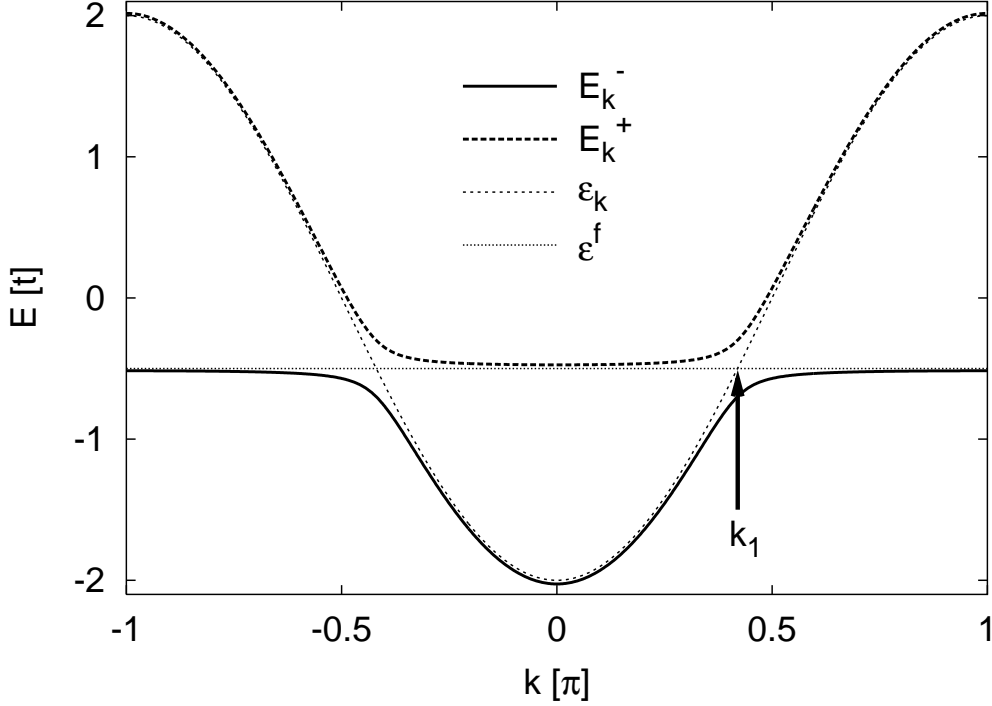


Figure 3.11: The two bands of the noninteracting periodic Anderson model are shown for $t = 1$, $V = 0.3$, $\epsilon^f = -0.5$ and $U^f = 0$. At the point k_1 the f -level intersects the tight-binding band.

where k_F is the Fermi momentum up to which the lower band is filled,

$$k_F = 2\pi n. \quad (3.64)$$

The filling n is 0.5 for the completely filled lower band. Thus, the equation (3.63) is valid for $0 \leq n \leq \frac{1}{2}$. F and E are the incomplete elliptic integrals of the first and second kind respectively. The parameters g and h are

$$\begin{aligned} g &= t^2 + 2V^2 + t^2 \cos(2k_F), \\ h &= t^2 + V^2. \end{aligned} \quad (3.65)$$

The expectation value of the paramagnetic current operator that also contributes to the Drude weight,

$$\begin{aligned} -\frac{1}{N} \sum_{n \neq 0} \frac{|\langle \psi_n | j_p | \psi_0 \rangle|^2}{E_n - E_0} = \\ -\frac{1}{N} \sum_{n \neq 0} \frac{|\langle \psi_n | \sum_{k\sigma} \eta_k \Upsilon_k (b_{k\sigma}^\dagger a_{k\sigma} + a_{k\sigma}^\dagger b_{k\sigma}) | \psi_0 \rangle|^2}{E_n - E_0}, \end{aligned} \quad (3.66)$$

can be evaluated. If only the lower band of quasi-particles is filled, the part of the current operator that annihilates electrons in the upper band is $a_{k\sigma}^\dagger b_{k\sigma} |\psi_0\rangle = 0$. The other part of the current operator excites quasi-particles from the lower band to the upper band. Spin and momentum of these quasi-particles are conserved. Thus, the expectation value of the current operator is

$$\begin{aligned}
 -\frac{1}{N} \sum_{n \neq 0} \frac{|\langle \psi_n | j_p | \psi_0 \rangle|^2}{E_n - E_0} &= -\frac{1}{N} \sum_{|k| < k_F, \sigma \in \{\uparrow, \downarrow\}} \frac{|\eta_k \Upsilon_k|^2 |\langle \psi_0 | a_{k\sigma}^\dagger b_{k\sigma} b_{k\sigma}^\dagger a_{k\sigma} | \psi_0 \rangle|^2}{E_k^+ - E_k^-} \\
 &= -\frac{2}{N} \sum_{|k| < k_F} \frac{|\eta_k \Upsilon_k|^2}{E_k^+ - E_k^-} \\
 &\stackrel{N \rightarrow \infty}{=} -\frac{1}{2\pi} \int_{-k_F}^{k_F} \frac{(tV \sin k)^2}{(V^2 + t^2 \cos^2 k)^{\frac{3}{2}}} dk \\
 &= \frac{\sqrt{2} t^2 \sin 2k_F}{2\pi \sqrt{g}} \\
 &\quad - \frac{1}{\pi} \sqrt{\frac{1}{h}} \left[hE \left(k_F \left| \frac{t^2}{h} \right. \right) - V^2 F \left(k_F \left| \frac{t^2}{h} \right. \right) \right].
 \end{aligned} \tag{3.67}$$

The integrand in Eq. (3.67) is

$$f(k) = -\frac{(tV \sin k)^2}{(V^2 + t^2 \cos^2 k)^{\frac{3}{2}}}. \tag{3.68}$$

This function reaches its maximum at $k = \pm \frac{\pi}{2}$,

$$f\left(\pm \frac{\pi}{2}\right) = -\frac{t^2}{|V|}. \tag{3.69}$$

In finite systems with $N = 4n$ lattice sites, the k -points $\pm \frac{\pi}{2}$ belong to the Brillouin zone. This leads to the divergence of the Drude weight to $-\infty$ for vanishing hybridization V . In the next section we look at the model on four lattice sites in more detail. In the thermodynamic limit, the Drude weight stays finite, because the area below the function $f(k)$ and not the value of the function $f(k)$ contributes to the Drude weight. If we add both terms contributing to the Drude weight, we obtain

$$D = \frac{t}{\pi} \left[1 + \frac{t \cos k_F}{\sqrt{t^2 \cos^2 k_F + V^2}} \right] \sin k_F. \tag{3.70}$$

On the other hand, the Drude weight in the thermodynamic limit can be calculated from half the ground state energy per site. For less than half filling, where

3.2 Example: The periodic Anderson model

only the lower band is populated (half filling means two electrons per site), it is

$$\begin{aligned}
 D &= \frac{\partial^2 E_0(\phi)}{\partial \phi^2} \frac{1}{2L} \\
 &= \frac{1}{2\pi} \frac{\partial^2}{\partial \phi^2} \int_{-k_F}^{k_F} E_k^-(\phi) dk \\
 &= \frac{t}{\pi} \left[1 + \frac{\epsilon^f + 2t \cos k_F}{\sqrt{(\epsilon^f + 2t \cos k_F)^2 + 4V^2}} \right] \sin k_F.
 \end{aligned} \tag{3.71}$$

For the symmetric case, the Drude weight is shown in Fig. 3.12. It is consistent with the result in Eq. (3.70). The lower band of the symmetric periodic Anderson

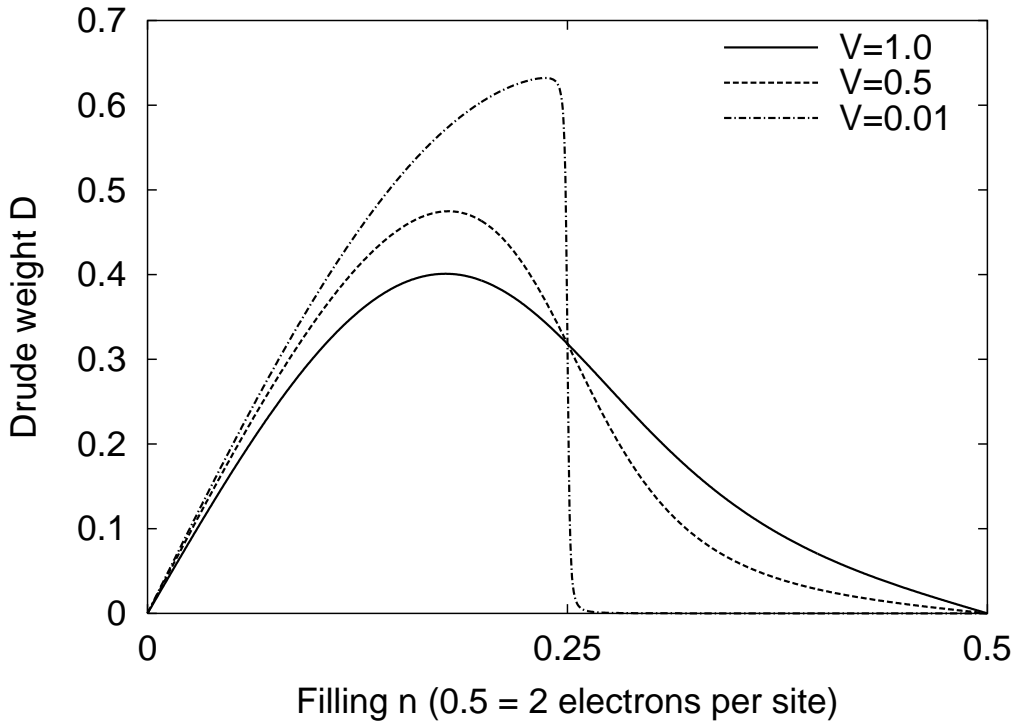


Figure 3.12: Drude weight for the symmetric periodic Anderson model with $t = 1$, $\epsilon^f = 0$, $U^f = 0$ and different values for the hybridization V .

model is flat in the region $|k| > \frac{\pi}{2}$ for small hybridizations. At quarter filling, the states in the flat area are populated, leading to a higher effective mass and a smaller conductivity of the charge carriers. For vanishing hybridization, the Drude weight between quarter and half filling is zero.

Finite systems

The simplest configuration to find negative Drude weight in the periodic Anderson model is the noninteracting model with 4 sites and 2 electrons of the same spin.

However, to proof that the negative Drude weight is not an open-shell effect, like in the Hubbard model (this will be explained in Sec. 3.3.2), we take 3 electrons of the same spin. The ground state is a combination of the one-particle states with momentum $-\frac{\pi}{2}$, 0 and $+\frac{\pi}{2}$. The dependence of the energy of the ground state on the magnetic flux is plotted in Fig. 3.13. As the hybridization becomes lower,

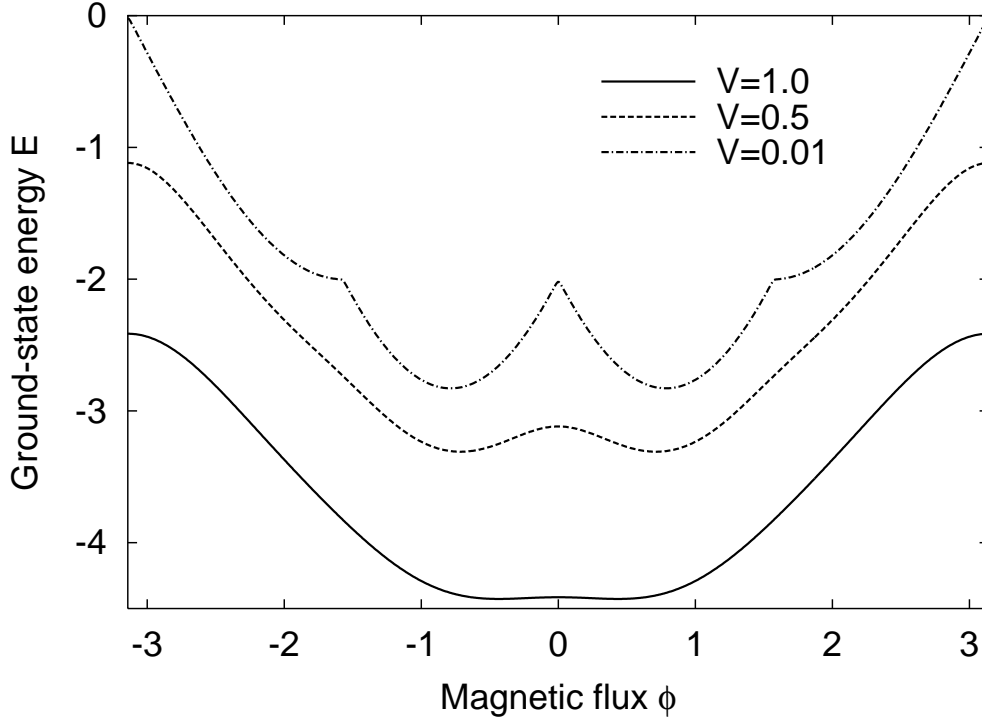


Figure 3.13: The ground-state energy for the noninteracting 4-site symmetric periodic Anderson model with 3 spin-up electrons for different hybridizations.

the spikes in the ground-state energy become sharper, leading to a higher absolute value of the Drude weight. The Drude weight is negative, because the curvature at $\phi = 0$ is negative. The Drude weight for this system is

$$D = \frac{t}{8} \left[1 - \frac{2t}{|V|} + \frac{t}{\sqrt{t^2 + V^2}} \right]. \quad (3.72)$$

The Drude weight diverges to minus infinity for vanishing hybridizations. The convergence to the thermodynamic limit is shown in Fig. 3.14.

3.3 Systems with negative Drude weight

For finite systems described by the Hubbard model, the periodic Anderson model or the Kronig-Penney model, a negative Drude weight is found in certain parameter ranges. We explain the reasons for this behavior in this section and give

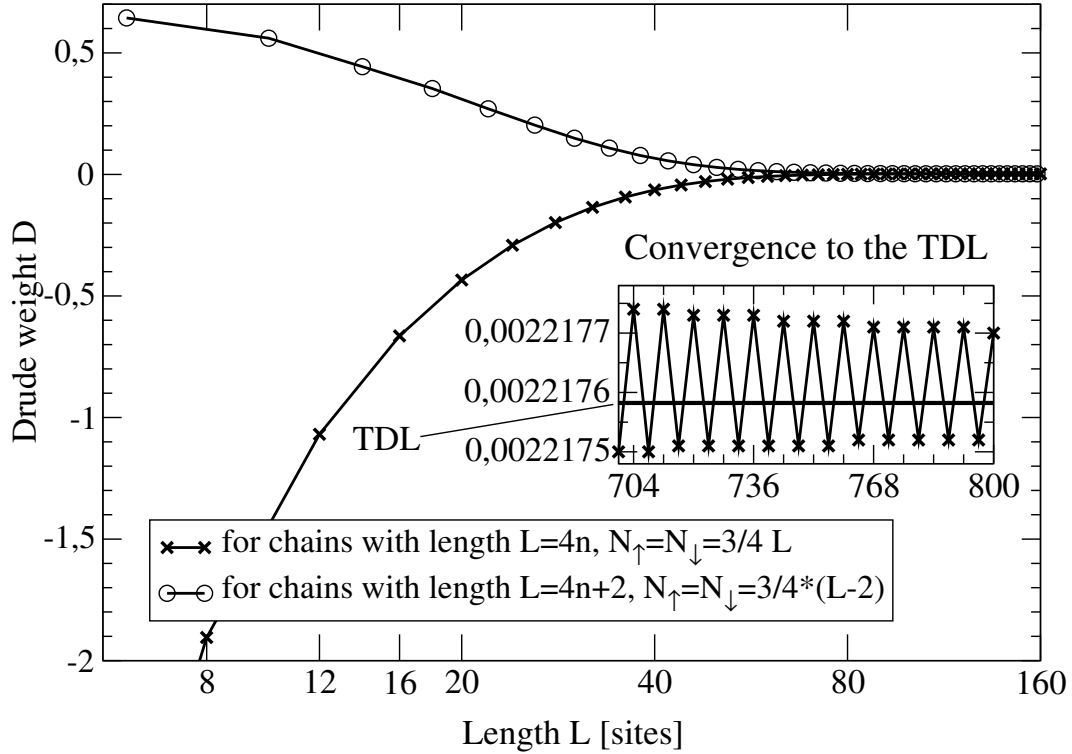


Figure 3.14: This figure shows the convergence of the Drude weight of the one-dimensional periodic Anderson model ($t = 1$, $V = 0.1$, $\epsilon^f = 0$, $U^f = 0$) to its value in the thermodynamic limit. The value of the Drude weight in the thermodynamic limit is $D = 0.00221758$. Each line is plotted at alternating open- and closed-shell configurations. The crossed dots are for systems that include the point $\pi/2$, where the band has a large negative second derivative in the Brillouin zone. Therefore the Drude weight is negative. The circled dots do not include this point in the Brillouin zone. The systems with open-shell configuration (e.g., $L = 600$) converge slightly worse to the thermodynamic limit than the closed-shell systems. The systems of size $L = 4n + 2$ converge much slower to the thermodynamic limit. Therefore these data are not shown in the inset.

criteria for the occurrence of a negative Drude weight in general. Whether or not it is possible to find a negative Drude weight depends on particle-hole symmetry and degeneracy of the ground state of the model under consideration. Negative Drude weight is a finite-size effect and corresponds to a paramagnetic response of the ring. The persistent current in the ring generates a magnetic field that enhances the magnetic field in the ring. However, the Drude weight is positive semidefinite in the thermodynamic limit, as has been exemplified for the periodic Anderson model in Fig. 3.14.

The occurrence of a negative Drude weight has been found first for a finite half-

filled Hubbard ring (SMS91; FMS⁺91; KEH99) if the number of sites is a multiple of four. The Hubbard model is an effective model for strongly interacting fermions. In contrast to the periodic Anderson model, it contains only one band of dispersive electrons. These electrons interact through an effective on-site Coulomb repulsion like the f -electrons in the periodic Anderson model. In a half-filled Hubbard ring on $4n$ lattice sites, the electrons are in an open-shell configuration. It will be shown in the next section, that open-shell configurations can potentially lead to a negative Drude weight.

A second characteristic of an electron system, which can lead to a negative Drude weight is an asymmetric band structure. In the next section, we start examining the asymmetric band structure of the lower band of the periodic Anderson model. Also in other finite systems, a negative Drude weight due to band asymmetry is present.

3.3.1 Asymmetric band structure

In the periodic Anderson model, the Drude weight is negative, because the curvature at $\phi = 0$ is negative, as has been shown in Fig. 3.13. The lowering of the ground-state energy can be understood from Fig. 3.15. If a magnetic flux

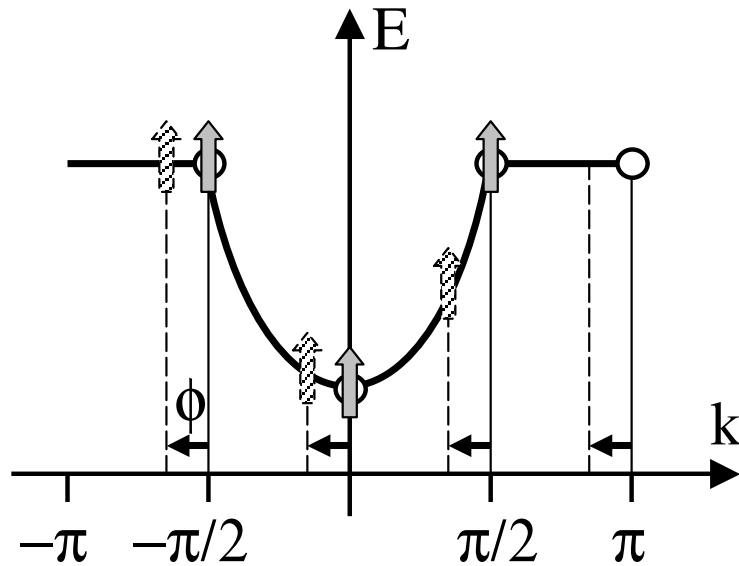


Figure 3.15: In the ground state of the 4-site symmetric periodic Anderson model on a ring with 3 spin-up electrons, the three lowest lying states are occupied. Only the lower band is plotted in the limit $V \rightarrow 0^+$ (see Fig. 3.11).

through the ring is switched on, the points in the Brillouin zone are shifted by an amount of ϕ . Due to the asymmetric structure of the lower band in the periodic Anderson model, the energy of the ground state can be lowered by the flux.

3.3 Systems with negative Drude weight

The symmetric case is not the only configuration where negative Drude weight appears in the periodic Anderson model even without interaction. Whenever the point k_1 where the f -level intersects the tight-binding band (see Fig. 3.11),

$$\epsilon^f = -2t \cos k_1, \quad (3.73)$$

is an element of the Brillouin zone, and the resulting hybridized band is filled at least up to that point, the Drude weight is negative for small hybridizations and diverges to minus infinity in the limit of vanishing hybridization. For example for $\epsilon^f = -1$, $k_1 = \pi/3$ is the point where the f -level intersects the tight-binding band. For rings with $N = 6n$ sites and at least 2 electrons of each spin direction, the Drude weight is negative.

The periodic Anderson model is not the only model where negative Drude weight is possible. Another example for an asymmetric band structure that leads to a negative Drude weight is the Kronig-Penney ring, mentioned in chapter 2.1. The point with the maximal negative curvature of the first band is $k_1 = \pi$ (see Fig. 3.16). So the band has to be completely filled for a negative Drude weight to appear. Of course, in the thermodynamic limit the Drude weight goes to zero.

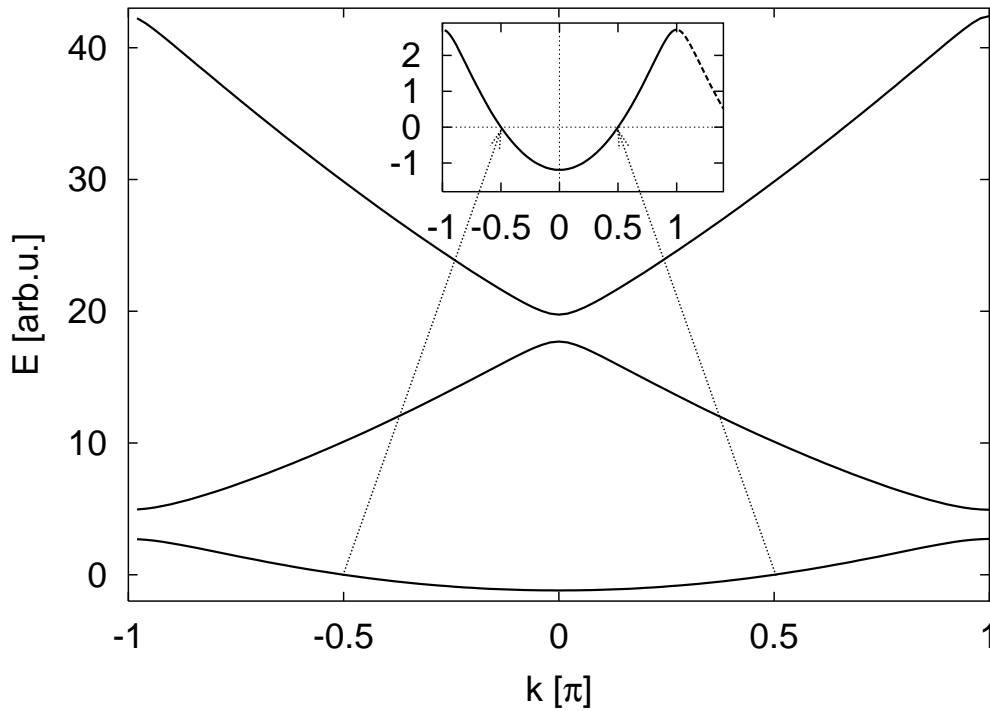


Figure 3.16: The first three bands of the Kronig-Penney model. The first band is extracted and shown in the inset. The absolute value of the curvature at the point $k_1 = \pi$ is much higher than the curvature at the point $k = 0$.

In conclusion, negative Drude weight in finite one-dimensional electronic rings due to particle-hole asymmetry exists, if there is a point k_1 in the Brillouin zone

B , where the curvature of the band is negative $E''(k_1) < 0$, and the absolute value of the curvature at this point is higher than the curvature at any other point in the Brillouin zone. This point in the Brillouin zone has to be filled with electrons.

3.3.2 Open shells

Besides of an asymmetric band structure, the electron-electron interaction can lead to a negative Drude weight. If there are several crossing levels for the ground state of the noninteracting model, the electron-electron interaction can lead to a level repulsion, which may end up in a negative curvature of the ground state with respect to the magnetic flux. We explain this in the following section for the special case of the Hubbard model.

The reason for the existence of a negative Drude weight in the Hubbard model,

$$H = -t \sum_{l,\sigma} \left(e^{-\frac{ie\phi}{N}} c_{l,\sigma}^\dagger c_{l+1,\sigma} + e^{\frac{ie\phi}{N}} c_{l+1,\sigma}^\dagger c_{l,\sigma} \right) + U \sum_l n_{l\uparrow} n_{l\downarrow}, \quad (3.74)$$

with periodic boundary conditions, which was found by Stafford *et al.* (SMS91; FMS⁺91; KEH99) lies in the open-shell configuration of such systems ($n_\uparrow = n_\downarrow$, n_\uparrow even). The ground state for the noninteracting system is fourfold degenerate. The degenerate states are $|\uparrow, \downarrow\rangle$, $|\downarrow, \uparrow\rangle$, $|\uparrow\downarrow, 0\rangle$ and $|0, \uparrow\downarrow\rangle$. Only the spins of the electrons at the Fermi points are given in this notation. All states below k_F are filled and all states above k_F are empty.

Finite Hubbard rings at half filling with $S_z = 0$ must have an even number of lattice sites. If the number of lattice sites is a multiple of four, $N = 4n$, the electrons are in an open-shell configuration. If the number of lattice sites is $N = 4n + 2$, the ground state is nondegenerate for the noninteracting system. In the second case, the Drude weight is positive semidefinite. For an open-shell configuration, the interaction matrix in first-order perturbation theory is

$$\begin{pmatrix} \frac{n_\uparrow n_\downarrow}{N} U & \frac{1}{N} U & 0 & 0 \\ \frac{1}{N} U & \frac{n_\uparrow n_\downarrow}{N} U & 0 & 0 \\ 0 & 0 & \frac{n_\uparrow n_\downarrow}{N} U & \left[\frac{1}{N} U \right] \\ 0 & 0 & \left[\frac{1}{N} U \right] & \frac{n_\uparrow n_\downarrow}{N} U \end{pmatrix}, \quad (3.75)$$

where the bracketed terms occur only at half filling when the number of lattice sites is a multiple of four ($k_F = \frac{\pi}{2a}$). This is due to an Umklapp process, that causes the $|\uparrow\downarrow, 0\rangle$ state with total momentum $-\pi/a$ to mix with the $|0, \uparrow\downarrow\rangle$ state with total momentum $+\pi/a$. The antisymmetric combination of $|\uparrow\downarrow, 0\rangle$ and $|0, \uparrow\downarrow\rangle$ is responsible for the finding of a negative Drude weight (see Fig. 3.17). In systems with open-shell configurations, but $k_F \neq \frac{\pi}{2a}$, the antisymmetric combination of $|\uparrow, \downarrow\rangle$ and $|\downarrow, \uparrow\rangle$ forms the ground state for small interactions (see Fig. 3.17).

3.3 Systems with negative Drude weight

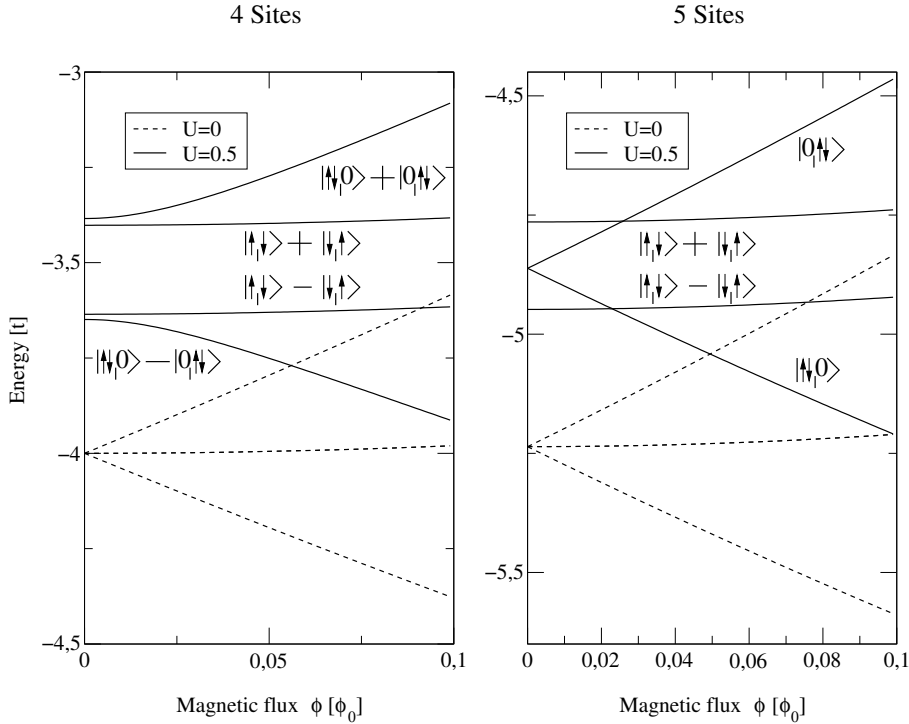


Figure 3.17: The energy levels of the first four states of the four- and five-site Hubbard ring with two up-spin and two down-spin electrons. The curvature of the ground state of the four-site ring is negative, whereas the curvature of the ground state of the five-site ring is positive for finite interactions. The lines are smoothly connected data from exact diagonalization. The states are labeled according to their closest equivalents in first order perturbation theory.

For the extended Hubbard model with nearest-neighbor interaction

$$V \sum_i n_i n_{i+1}, \quad (3.76)$$

the sign of the Drude weight stays the same for small interaction strengths V . As V approaches $U/2$ in $N = 4n$ half-filled systems, the gap between the antisymmetric and symmetric states becomes smaller. They cross over and for $V > U/2$ the Drude weight becomes positive. This is also true for negative U . In the U - V -plane, the Drude weight is negative in the region below the $V = U/2$ line and positive above (see Fig. 3.18). This was verified in a large number of points ranging from $-5t < U < 5t$, $-5t < V < 5t$ for the half-filled 4-site and 8-site Hubbard rings with exact diagonalization.

The finding of a negative Drude weight does not depend on the special band structure of the Hubbard model. All models with half-filled bands and $N = 4n$

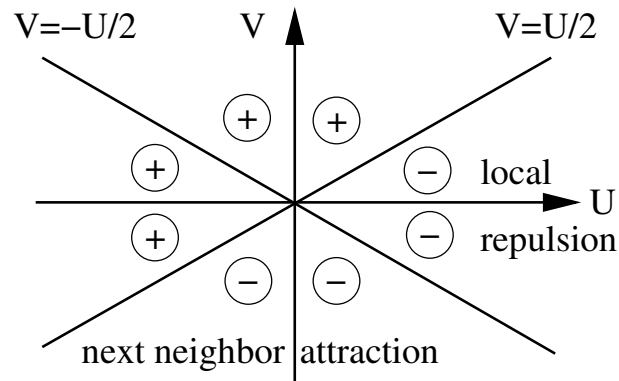


Figure 3.18: The sign of the Drude weight in the U - V -plane for the half-filled extended Hubbard model on a ring of $N = 4n$ sites. The Drude weight is positive for predominantly on-site repulsion and nearest-neighbor attraction.

sites with predominantly local repulsion or nearest-neighbor attraction should exhibit negative Drude weight at zero temperature as long as the dispersion of the noninteracting electrons is symmetric around the origin.

4 A second-quantized model for quantum rings

Starting from the expression for the free energy of a superconducting ring with a single junction, we construct a model for a strongly correlated one-dimensional quantum ring. The stationary persistent currents in static magnetic fields in superconducting rings, which stem from the gauge invariance of the superconducting wave function, create an internal magnetic flux in the ring. The proportionality constant between the internal flux and the persistent current is the inductivity. This constant also enters the relation between the energy stored in the internal field and the persistent current. The persistent current in *quantum rings* also generates an internal magnetic field. Therefore, the model that is constructed in the second part of this chapter includes an inductivity. Although up to now there is no method to estimate the inductivity of a quantum ring, the inclusion of inductivity terms can be considered a simple approximation for the mechanism of flux generation in a quantum ring. The persistent current determined from the Schrödinger equation is plugged into the classical Maxwell equations to calculate the flux that is generated. While there might be quantum electro-dynamical corrections to this approach, it should contain interesting novel effects that can be measured in custom-tailored experiments. These effects include spontaneous persistent currents in quantum rings for zero external field.

To evaluate the novel effects sparked by the model constructed, a robust solution scheme is needed. Such a solution scheme based on the exact diagonalization of the Hamiltonian after finding a fixed point for the current operator is presented. An examination of the fixed points of the current operator reveals the critical inductivity below which there is only a single solution for the current operator and above which there are multiple solutions. The different self-consistently determined solutions of the current operator can lead to multiple stable expectation values of the current. The interaction between the electrons plays a decisive role in mixing the energy levels with several minima with respect to the current, that would otherwise be too high energetically, into the ground state of the quantum ring. For weak interactions, the inductivity of the ring has to be even higher in order to drive the expectation value of the current at low temperatures into the realm of different stable solutions.

Although it is probably not physically meaningful to have non-diagonal current operators in momentum space, the existence of such non-diagonal current

operators cannot formally be ruled out. For the special case of a ring with two lattice sites and one electron, a proof for the non-existence of non-diagonal current operators is demonstrated.

4.1 Motivation through SQUIDS

4.1.1 Minimization of the free energy

According to Ref. (SR95), the free energy of a superconducting ring with a 0- or a π -junction is

$$F(j, \phi_{\text{ext}}) = \frac{1}{2}Lj^2 - \frac{\phi_0^{\text{sc}}j_c}{2\pi} \cos \left[\frac{2\pi}{\phi_0^{\text{sc}}}(\phi_{\text{ext}} + Lj) + \alpha \right], \quad (4.1)$$

with $\alpha = 0$ for unfrustrated SQUIDS and $\alpha = \pi$ for π -SQUIDS. The properties of the free energy are determined by the dimensionless parameter $\gamma = 2\pi Lj_c/\phi_0^{\text{sc}}$, where j_c is the critical current through the junction and ϕ_0^{sc} is the superconducting flux quantum $\phi_0^{\text{sc}} = \frac{h}{2|e|}$. In the following, we normalize the current to the critical current $j \rightarrow j/j_c$. For small inductivities L ($\gamma < 1$), the behavior of the free energy is dominated by Lj^2 . Clear enough, this term represents the energy that is stored in the magnetic field that the current in the SQUID generates. The boundaries of the superconducting wavefunction are twisted by the Aharonov-Bohm flux in the SQUID. This leads to the oscillatory term containing the total magnetic flux in the SQUID consisting of external flux ϕ_{ext} and the internal flux $\phi_{\text{int}} = Lj$. In special geometric arrangements of the junction, the d -wave pairing in the superconductor can be exploited to give antiperiodic boundary conditions. This is a π -junction (TK00).

For larger inductivities, the cosine term oscillates with higher frequency with respect to the current. This leads to a multivalued current for $\gamma > 1$ and $\phi_{\text{ext}} \approx (2m+1)\phi_0^{\text{sc}}/2$ ($\alpha = 0$, m integer) and $\phi_{\text{ext}} \approx m\phi_0^{\text{sc}}$ ($\alpha = \pi$). A persistent current for $\phi_{\text{ext}} = 0$ in π -SQUIDS is a consequence of the multivaluedness (see Fig. 4.1). We have plotted the stable current states of the SQUID with respect to the external flux in Fig. 4.2 and 4.3. These graphs were obtained by minimizing the free energy with respect to the current for a given external flux with a bisection search algorithm.

4.1.2 Iterative scheme

The dimensionless free energy is

$$F_{\phi_{\text{ext}}}(j) = \frac{\gamma}{2}j^2 - \cos(\phi_{\text{ext}} + \gamma j + \alpha). \quad (4.2)$$

The free energy has a minimum under the condition

$$F'_{\phi_{\text{ext}}}(j) = \gamma j + \gamma \sin(\phi_{\text{ext}} + \gamma j + \alpha) = 0. \quad (4.3)$$

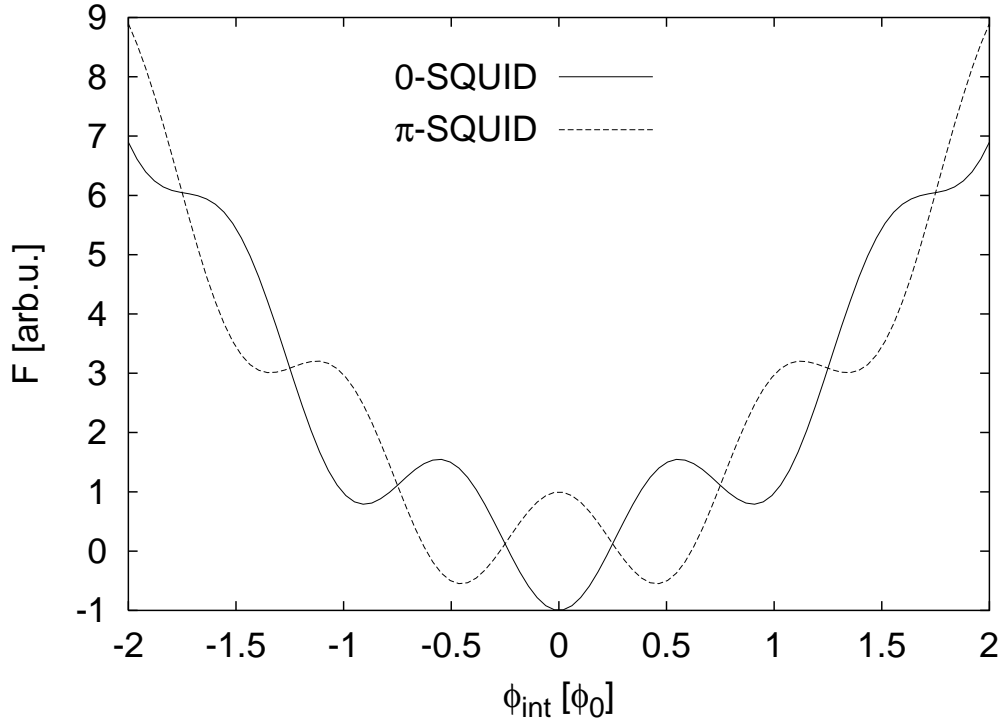


Figure 4.1: The free energy of a superconducting ring with a single junction for a large inductivity. The external flux is zero.

This condition can be easily rewritten to give a fixed-point equation for the current, which can be solved iteratively:

$$j_{(n)} = G(j_{(n-1)}) = -\sin(\phi_{\text{ext}} + \gamma j_{(n-1)} + \alpha). \quad (4.4)$$

G is a contraction ($|G(j_1) - G(j_2)| < g|j_1 - j_2|$, $0 \leq g < 1$) on \mathbb{R} for small inductivities. Since G is continuously differentiable, it is a contraction, if the absolute value of the first derivative is smaller than g , with g between 0 and 1. This can be shown using the mean-value theorem. The absolute value of the first derivative of G is always smaller than γ . For $\gamma < 1$ it is a contraction. Therefore, the equation $j = G(j)$ has a unique solution according to Banach's fixed point theorem for $\gamma < 1$ and the iterative scheme converges for every starting value $j_0 \in \mathbb{R}$ (Wal92).

Equation (4.4) is equivalent to the thermodynamic equation for the current:

$$j = -\frac{\partial F}{\partial \phi_{\text{ext}}} = -\sin(\phi_{\text{ext}} + \gamma j + \alpha). \quad (4.5)$$

The convergence is best if the starting value $j_{(0)}(\phi_{\text{ext}} + \epsilon)$ is chosen to be $j_{(n \rightarrow \infty)}(\phi_{\text{ext}})$, for small ϵ . Thus starting with zero flux and increasing the current in small steps results in the same graphs as the minimization process.

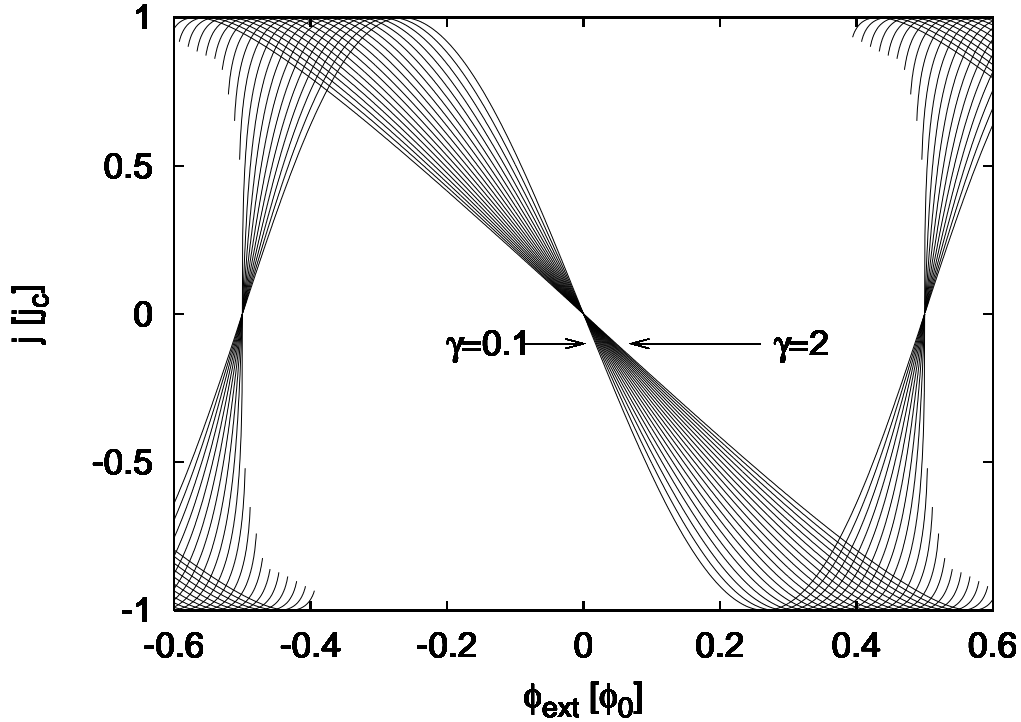


Figure 4.2: The unfrustrated SQUID is diamagnetic for small fields. For external fluxes near odd multiples of the flux quantum, the current is multivalued for high inductivities $\gamma > 1$.

Of course, for large inductivities $\gamma > 1$, the series of currents $j_{(n)}$ diverges, because G is no longer a contraction. It has to be stabilized with

$$j_{(n)} = [(1 - \lambda)j_{(n-1)} - \lambda \sin(\phi_{\text{ext}} + \gamma j_{(n-1)} + \alpha)], \quad (4.6)$$

with $\lambda = \frac{1}{\gamma+1}$ according to Hillam's theorem (Hil75). The images below were thus produced with the use of this algorithm (see Fig. 4.4). A quantum-mechanical equivalent of this iterative method is now motivated and applied to quantum rings.

4.2 The model and its analytic properties

In this section, we propose a model Hamiltonian for electrons on a quantum ring. The model is a close relative of the Hubbard model. In addition to the Hubbard model, the internal flux that the persistent current generates is taken into account. After explaining the Fourier transform that transforms the many-particle states from real space (the space where the Hamiltonian can be most comfortably written down) to momentum space (where the eigenstates are easier to be found), an iterative solution scheme for the model is introduced. This solution scheme

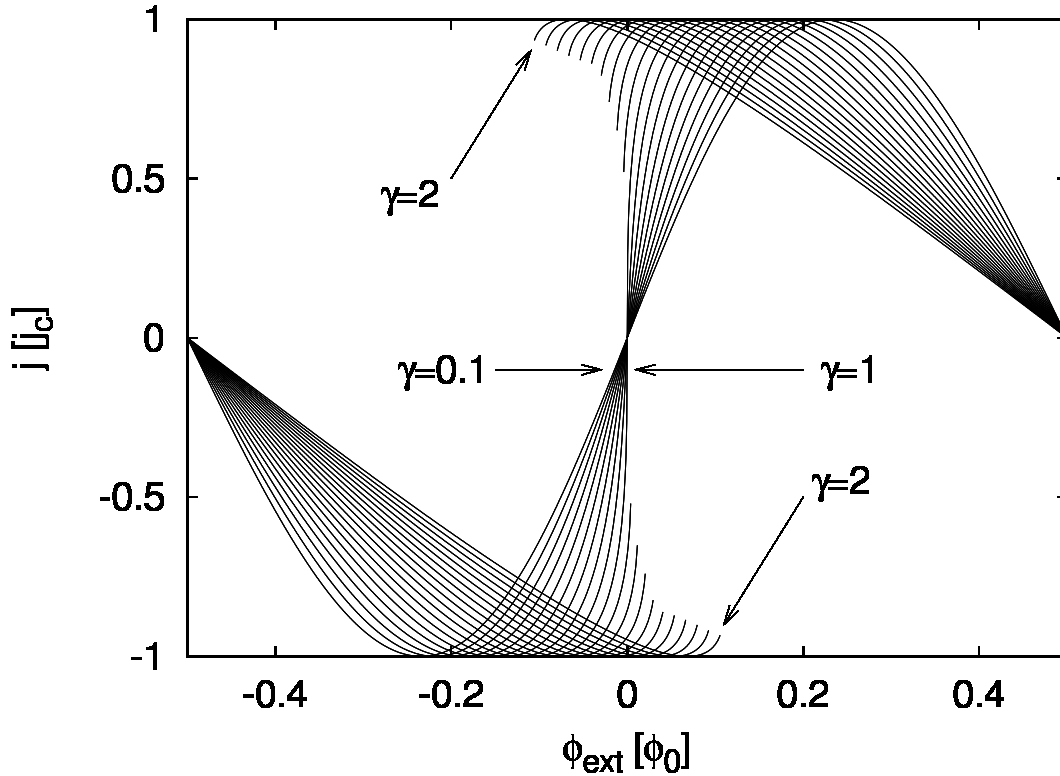


Figure 4.3: The π -SQUID is paramagnetic at small field strengths and small inductivities $\gamma < 1$. For high inductivities ($\gamma > 1$), the π -SQUID is ferromagnetic.

minimizes the diagonal matrix elements of the Hamiltonian matrix in momentum space with respect to the eigenvalues of the current operator. The current operator is diagonal in momentum space. A rather important subsection is devoted to proving that the Hamiltonian matrix with the minimal diagonal elements in momentum space leads to the minimal eigenvalues of the Hamiltonian. Thus, it is proven that the iterative solution scheme leads to the persistent current that minimizes the free energy of the quantum ring. Afterwards, the circumstances under which the proposed model allows for one or more solutions for the persistent current are investigated. For inductivities of the ring below a certain bound (the critical inductivity), there is only one fixed-point for the persistent current. However, above the critical inductivity, there may be more than one fixed-point for the persistent current. An asymptotic expansion for very high inductivities elucidates the behavior of the solutions in this limit. Whether the model also allows for the existence of non-diagonal—but probably physically meaningless—current operators is examined in the last subsection of this section.

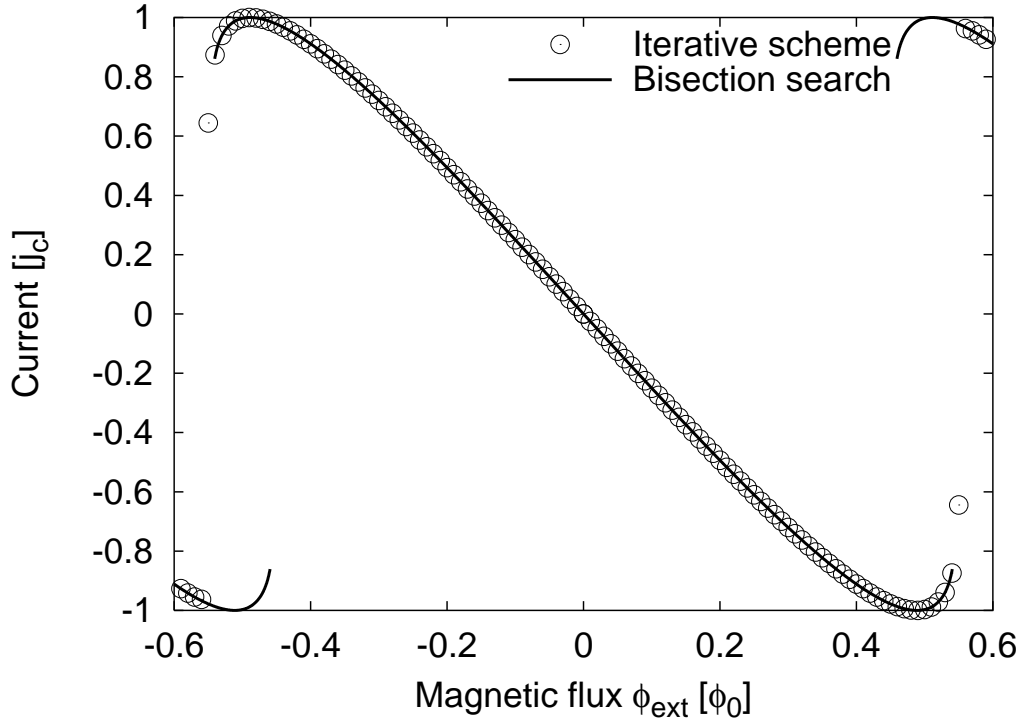


Figure 4.4: For a 0-SQUID with inductivity $\gamma = 1.5$, the iterative scheme is tested vs. the bisection search minimization. The iterative scheme is started at zero flux and continued stepwise to larger external fluxes, setting the initial value of the current to the converged current of the last step. This procedure keeps the current on one branch of fixed points as long as there is a solution on the branch. The graph was produced using a fixed number of 8 iterations.

4.2.1 The model Hamiltonian

We use semi-empirical one-band models with only nearest-neighbor hybridization t to describe the π -electrons of cyclic hydrocarbons, for example, the Hubbard model, the extended Hubbard model, or the Pariser-Parr-Pople (PPP) model. These models are described by the Hamiltonian

$$\begin{aligned}
 H = & -t \sum_{l\sigma} (c_{l+1,\sigma}^\dagger c_{l,\sigma} + c_{l,\sigma}^\dagger c_{l+1,\sigma}) \\
 & + U \sum_l n_{l\uparrow} n_{l\downarrow} + \frac{1}{2} \sum_{l \neq m} V_{lm} n_l n_m,
 \end{aligned} \tag{4.7}$$

where $c_{l\sigma}^\dagger$ creates an electron with spin σ on site l , $n_{l\sigma} = c_{l\sigma}^\dagger c_{l\sigma}$, and $n_l = n_{l\uparrow} + n_{l\downarrow}$. The sums are taken over all N sites, and periodic boundary conditions are used. The Coulomb interaction between the electrons is modeled by an on-site repulsion U and by a long-range repulsion V_{lm} (which is zero for the Hubbard model). The

4.2 The model and its analytic properties

extended Hubbard model also includes a nearest-neighbor repulsion ($V_{lm} \neq 0$ for $|l - m| = 1$). In the PPP model, the Coulomb repulsion can be parameterized by the Ohno (Ohn64) potential with a dielectric constant $\epsilon_r > 1$ (CB02):

$$V_{lm} = \frac{U}{\epsilon_r \sqrt{1 + \zeta r_{lm}^2}}, \quad (4.8)$$

where we must choose

$$\zeta = \left(\frac{U}{1.4397 \text{ nm eV}} \right)^2, \quad (4.9)$$

in order to ensure that $V_{lm} \rightarrow e^2/4\pi\epsilon_0\epsilon_r r_{lm}$ as $r_{lm} \rightarrow \infty$ (BCB98). The dielectric constant originates from the screening of the π -electrons by the σ -electrons and from screening effects from the environment.

In these models, the twist of the phase in the wave function in the presence of an Aharonov-Bohm flux can be partitioned into phase shifts for every hopping process. Therefore, the kinetic energy part of the Hamiltonian is modified with the usual Peierls phase factor $\exp(\frac{2\pi i}{N\phi_0}\phi_{\text{ext}})$, where $\phi_0 = h/|e|$ is the flux quantum. In natural units ($e = c = \hbar = k_B = 1$, [Energy] = 1 eV), the flux quantum equals 2π . The Hamiltonian shown in Eq. (4.14) is the Hamiltonian needed to calculate the Drude weight D , which is the dc conductivity of an electronic system in the thermodynamic limit. The thermodynamic limit for one-dimensional systems is the limit in which the number of sites N approaches infinity. However, for small rings, the quantum nature of the system could lead to equilibrium persistent currents, leading the concept of conductivity ad absurdum. This corresponds to systems with two minima in the ground-state energy E_0 , with respect to the external flux. The curvature of the ground-state energy between those minima is negative, leading to a negative Drude weight (SMS91; FMS⁺91).

If the system is given the opportunity to generate an internal flux itself, by letting a persistent current

$$\mathbf{j} = -\frac{\partial H}{\partial \phi_{\text{ext}}} \quad (4.10)$$

flow, the system falls into the minimum of the ground-state energy with respect to the internally generated flux

$$\phi_{\text{int}} = L\mathbf{j}. \quad (4.11)$$

We assume the inductivity L —which depends only upon the geometry of the system—to be a valid concept down to the scale of organic molecules. This approximation corresponds to a time-averaged linearization of the coupling between the moving charges and the magnetic field. The inductivity is a fit parameter in our calculations; it can only be roughly estimated for molecules. The internal flux leads to an additional phase shift represented by the unitary phase-shift operator

$$P \equiv e^{-\frac{i}{N}L\mathbf{j}}. \quad (4.12)$$

The current operator appears in the exponential because the eigenstates carry different quantities of current, leading to a different phase shift for different eigenstates.

The energy that is stored in the internal magnetic field of an electronic quantum ring, e.g., a cyclic hydrocarbon,

$$\frac{L}{2} j^2, \quad (4.13)$$

must be added to the model under consideration. This term boosts the eigenenergies of the current carrying eigenstates.

The complete Hamiltonian is:

$$\begin{aligned} H = & -t \sum_{l\sigma} \left[e^{\frac{i}{N}(\phi_{\text{ext}} + Lj)} c_{l+1,\sigma}^\dagger c_{l,\sigma} \right. \\ & \left. + c_{l,\sigma}^\dagger c_{l+1,\sigma} e^{-\frac{i}{N}(\phi_{\text{ext}} + Lj)} \right] \\ & + U \sum_l n_{l\uparrow} n_{l\downarrow} + \frac{1}{2} \sum_{l \neq m} V_{lm} n_l n_m \\ & + \frac{1}{2} L j^2. \end{aligned} \quad (4.14)$$

This Hamiltonian is motivated by the free energy of superconducting rings with a conventional or a π -junction given in Ref. (SR95).

Let us simplify the notation by introducing operators for the sum of leftward hopping and the sum of rightward hopping terms as well as for the interaction:

$$\begin{aligned} C & \equiv -t e^{-\frac{i}{N}\phi_{\text{ext}}} \sum_{l\sigma} c_{l,\sigma}^\dagger c_{l+1,\sigma} \\ & = -t e^{-\frac{i}{N}\phi_{\text{ext}}} \sum_{k\sigma} e^{ik} n_{k\sigma}, \\ C^\dagger & = -t e^{\frac{i}{N}\phi_{\text{ext}}} \sum_{l\sigma} c_{l+1,\sigma}^\dagger c_{l,\sigma}, \\ W & \equiv U \sum_l n_{l\uparrow} n_{l\downarrow} + \frac{1}{2} \sum_{l \neq m} V_{lm} n_l n_m. \end{aligned} \quad (4.15)$$

The kinetic energy can then be expressed as

$$K = C P + P^\dagger C^\dagger. \quad (4.16)$$

The current operator is

$$j = -\frac{\partial H}{\partial \phi_{\text{ext}}} = \frac{i}{N} (C P - P^\dagger C^\dagger). \quad (4.17)$$

The kinetic energy and the current are obviously Hermitian operators. Although it is difficult to prove rigorously, it is physically obvious that the kinetic energy and the current are diagonal in momentum space (see 4.2.8). Consequently, any two operators from the set $\{C, C^\dagger, P, P^\dagger, j, K\}$ commute with each other.

4.2.2 Fourier transform of the many-particle states

We derive a transformation matrix from real space to momentum space. The current and the kinetic energy of our model are diagonal in momentum space. With the transformation, we can reduce the problem of finding a fixed point for the current operator to a set of one-dimensional problems of finding fixed points for every eigenvalue of the current operator. Therefore, the following transformation is essential in finding the eigenstates of the model Hamiltonian (4.14).

For a system with n spinless fermions on N lattice sites, the basis states in real space are

$$|x^l\rangle = c_{l_1}^\dagger \cdots c_{l_n}^\dagger |0\rangle, \quad l \longmapsto (l_1, \dots, l_n). \quad (4.18)$$

The number $l \in \{1, \dots, \dim \mathcal{H}\}$ counts the basis states. It can be mapped to a set of integers (l_1, \dots, l_n) denoting the occupied lattice sites. Analogously, the basis states in momentum space are $|p^\kappa\rangle$. The transformation matrix transforms the expansion coefficients of a state $|\psi\rangle$ from one basis to the other:

$$\langle p^\kappa | \psi \rangle = \sum_{l=1}^{\dim \mathcal{H}} \underbrace{\langle p^\kappa | x^l \rangle}_{U_{\kappa l}} \langle x^l | \psi \rangle. \quad (4.19)$$

The following transformation for every single creation operator in the many-particle state is needed to perform the transformation:

$$c_{l_i}^\dagger = \frac{1}{\sqrt{N}} \sum_{\kappa_j=0}^{N-1} e^{-\frac{2\pi i \kappa_j l_i}{N}} c_{\kappa_j}^\dagger. \quad (4.20)$$

The transformation matrix is thus

$$\begin{aligned} U_{\kappa l} &= \langle 0 | c_{\kappa_n} \cdots c_{\kappa_1} c_{l_1}^\dagger \cdots c_{l_n}^\dagger | 0 \rangle \\ &= \left(\frac{1}{\sqrt{N}} \right)^n \sum_{\kappa'_1, \dots, \kappa'_n=0}^{N-1} e^{-\frac{2\pi i}{N}(\kappa'_1 l_1 + \cdots + \kappa'_n l_n)} \langle 0 | c_{\kappa_n} \cdots c_{\kappa_1} c_{\kappa'_1}^\dagger \cdots c_{\kappa'_n}^\dagger | 0 \rangle. \end{aligned} \quad (4.21)$$

The sum in (4.21) does not have to be taken over all combinations of $(\kappa'_1, \dots, \kappa'_n)$. The permutations of $(\kappa_1, \dots, \kappa_n)$ are sufficient, since the other addenda do not contribute to the sum. Depending on the sign of the permutation, the scalar product is ± 1 :

$$U_{\kappa l} = \left(\frac{1}{\sqrt{N}} \right)^n \sum_{(\kappa'_1, \dots, \kappa'_n) = P(\kappa_1, \dots, \kappa_n)} \text{sgn}(P) e^{-\frac{2\pi i}{N}(\kappa'_1 l_1 + \cdots + \kappa'_n l_n)}. \quad (4.22)$$

This matrix is easily generalized to electrons with spin:

$$U_{\kappa l} = \prod_{\sigma \in \{\downarrow, \uparrow\}} \left(\frac{1}{\sqrt{N}} \right)^{n_\sigma} \sum_{(\kappa'_{1\sigma}, \dots, \kappa'_{n\sigma}) = P(\kappa_{1\sigma}, \dots, \kappa_{n\sigma})} \text{sgn}(P) e^{-\frac{2\pi i}{N}(\kappa'_{1\sigma} l_{1\sigma} + \cdots + \kappa'_{n\sigma} l_{n\sigma})}. \quad (4.23)$$

With this matrix it is possible to comfortably switch between the representations of the operators and states in momentum and real space.

4.2.3 Iterative scheme

The current operator is defined implicitly to be the current operator that minimizes the free energy resulting from the model Hamiltonian (4.14). The metastable current states are found as the local minima of the free energy. We will derive a solution scheme of the model in this section. The current operator will be determined iteratively. We first state the iterative scheme and afterwards prove that it minimizes the free energy with respect to the current operator.

Before starting the iteration ($n = 1$), we choose the current to be

$$\mathbf{j}_{(0)} = 0. \quad (4.24)$$

The iterative scheme is the search for a fixed point of the current operator:

$$\begin{aligned} P_{(n)} &= e^{-\frac{i}{N} L \mathbf{j}_{(n-1)}} \\ \mathbf{j}_{(n)} &= -\frac{\partial H}{\partial \phi_{\text{ext}}} = \frac{i}{N} \left(C P_{(n)} - P_{(n)}^\dagger C^\dagger \right). \end{aligned} \quad (4.25)$$

The corresponding fixed-point equation is

$$\mathbf{j} = G(\mathbf{j}) \equiv \frac{i}{N} \left[C P(\mathbf{j}) - P^\dagger(\mathbf{j}) C^\dagger \right]. \quad (4.26)$$

Thus, the current operator is determined without linearizing the Hamiltonian with respect to the external field. In momentum space, we may think of the above equations as $\dim(\mathcal{H})$ uncoupled equations for the eigenvalues of the operators instead of the operators themselves, because of diagonality.

In the following, we show that the free energy is minimized with respect to the current operator by the iterative scheme. In fact, every single energy eigenvalue is minimized. In momentum space, the alternation of the eigenvalues due to a change in the current operator is determined by the diagonal elements of the matrix representing the Hamiltonian. The off-diagonal matrix elements correspond to the interaction of the electrons and are independent of the current operator.

4.2.4 Minimization of the free energy

The iterative solution scheme of the last subsection is useless, if it just minimizes the diagonal elements of the Hamiltonian matrix in momentum space. Here, we will prove that the current operator that minimizes the diagonal elements of the Hamiltonian in momentum space also minimizes the eigenvalues of the Hamiltonian and therefore the free energy.

Assuming the minimal diagonal elements of the Hamiltonian matrix in momentum space were found, every other possible Hamiltonian matrix could be described by the sum of the minimal Hamiltonian matrix and a positive semidefinite matrix. Any alternation with a positive semidefinite matrix leads to an increase of

4.2 The model and its analytic properties

some eigenvalues. In section 4.2.5 we will develop a criterion under which the iterative scheme converges and minimizes the diagonal elements of the Hamiltonian in momentum space.

In the notation defined above, the Hamiltonian can be written as:

$$H = C P + P^\dagger C^\dagger + \frac{1}{2} L j^2 + W. \quad (4.27)$$

The first three terms are diagonal in momentum space with diagonal entries composed of the eigenvalues of the hopping, phase-shift, and current operator (C^κ , P^κ , j^κ). Let the eigenstates of the noninteracting many-particle system in momentum space be $|p^\kappa\rangle$ with $\kappa \in \{1, \dots, \dim \mathcal{H}\}$. The Jacobian

$$\frac{\partial H_{\kappa\xi}}{\partial j^\zeta} = \delta_{\kappa\xi} \delta_{\xi\zeta} L \left\{ \frac{i}{N} [(P^\kappa)^* (C^\kappa)^* - C^\kappa P^\kappa] + j^\kappa \right\} \quad (4.28)$$

of the Hamiltonian with respect to the current eigenvalues must be

$$\frac{\partial H_{\kappa\xi}}{\partial j^\zeta} = 0, \quad \forall \kappa, \xi, \zeta \in \{1, \dots, \dim \mathcal{H}\}. \quad (4.29)$$

This condition is necessary for the elements of the Hamiltonian matrix in this representation to have minima and is automatically fulfilled if the iterative scheme converges. It is sufficient for the existence of minima that the diagonal elements of the tensor containing the second derivatives are positive:

$$\begin{aligned} \frac{\partial^2 H_{\kappa\xi}}{\partial (j^\zeta)^2} &= \delta_{\kappa\xi} \delta_{\xi\zeta} L \left\{ 1 - \frac{L}{N^2} [C^\kappa P^\kappa + (P^\kappa)^* (C^\kappa)^*] \right\} \\ &> 0, \quad \forall \kappa = \xi = \zeta \in \{1, \dots, \dim \mathcal{H}\}. \end{aligned} \quad (4.30)$$

Since the off-diagonal elements of the Hamiltonian are constant, the tensor is diagonal.

We assume that the current $j_{(\infty)}$ minimizes the diagonal elements of the Hamiltonian. Any deflection of the current from this position corresponds to a small perturbation of the Hamiltonian with a positive semidefinite matrix M . The Hamiltonians from previous iterations exhibit larger diagonal elements than the converged Hamiltonian $H_{(\infty)}$ in momentum space:

$$H_{(n)} = C P_{(n)} + P_{(n)}^\dagger C^\dagger + \frac{L}{2} j_{(n)}^2 + W \quad (4.31)$$

$$H_{(n)} - H_{(\infty)} = M = \text{diag}(d^1, \dots, d^{\dim \mathcal{H}}), \quad \forall 1 \leq l \leq \dim \mathcal{H} : d^l \geq 0. \quad (4.32)$$

Adding a diagonal matrix to a normal matrix changes the eigenvalues within well defined boundaries. So for every eigenvalue $E_{(\infty)}^\kappa$ of $H_{(\infty)}$ there is an eigenvalue $E_{(n)}^\kappa$ of $H_{(n)}$ with

$$|E_{(\infty)}^\kappa - E_{(n)}^\kappa| \leq \|M\| = \max_l |d^l|. \quad (4.33)$$

Therefore, the eigenvalues of the Hamiltonian lie within disks around the eigenvalues of the n th approximation to the Hamiltonian, if the iterative scheme converges. For the special case of the Hermitian Hamiltonian and the *real* diagonal perturbation M , these disks are simple intervals. Furthermore, if the Hamiltonian is nondegenerate (i.e., the eigenvectors and eigenvalues are differentiable functions with respect to a small perturbation), it can be proven that the energy eigenvalues are minimal at the current $j_{(\infty)}$, because a perturbation with a *positive* semidefinite matrix M to a Hermitian matrix $H_{(\infty)}$ makes the eigenvalues larger (Har01). The first derivative of the eigenvalues with respect to the perturbation is positive or zero. The eigenvalue equation is

$$(H_{(\infty)} + \xi M) |p^\kappa\rangle(\xi) = E^\kappa(\xi) |p^\kappa\rangle(\xi) \quad (4.34)$$

for small values of the positive parameter ξ . Differentiation with respect to ξ leads us to:

$$\begin{aligned} & H_{(\infty)} \left[\frac{\partial}{\partial \xi} |p^\kappa\rangle \right](\xi) + M |p^\kappa\rangle(\xi) + \xi M \left[\frac{\partial}{\partial \xi} |p^\kappa\rangle \right](\xi) \\ &= |p^\kappa\rangle(\xi) \left[\frac{\partial}{\partial \xi} E^\kappa \right](\xi) + E^\kappa(\xi) \left[\frac{\partial}{\partial \xi} |p^\kappa\rangle \right](\xi). \end{aligned} \quad (4.35)$$

At $\xi = 0$ [$|p^\kappa\rangle \equiv |p^\kappa\rangle(0)$] we get

$$H_{(\infty)} \frac{\partial}{\partial \xi} |p^\kappa\rangle - E^\kappa(0) \frac{\partial}{\partial \xi} |p^\kappa\rangle = \left[\frac{\partial}{\partial \xi} E^\kappa \right](0) |p^\kappa\rangle - M |p^\kappa\rangle. \quad (4.36)$$

Multiplication with the left eigenvector of $H_{(\infty)}$ results in

$$0 = \left[\frac{\partial}{\partial \xi} E^\kappa \right](0) \langle p^\kappa | p^\kappa \rangle - \langle p^\kappa | M | p^\kappa \rangle. \quad (4.37)$$

Thus the first derivative of the eigenvalues is a positive semidefinite Hermitian form:

$$\left[\frac{\partial}{\partial \xi} E^\kappa \right](0) = \frac{\langle p^\kappa | M | p^\kappa \rangle}{\langle p^\kappa | p^\kappa \rangle} \geq 0. \quad (4.38)$$

This result holds for any perturbation ($\xi \geq 0$) of the current from its minimizing position. Consequently we obtain that

$$E_{(\infty)}^\kappa \equiv E^\kappa(j_{(\infty)}) \leq E^\kappa(j), \quad (4.39)$$

for all κ and for all possible current operators in some finite neighborhood of $j_{(\infty)}$. We can now partition the current space into small finite neighborhoods and extend the above calculation to a larger neighborhood of $j_{(\infty)}$. If the minimum of the diagonal matrix elements is global, the minimum of the eigenvalues is also global. The above relation (4.39) is only strictly valid if the Hamiltonian is nondegenerate near $j_{(\infty)}$. However, if we look at the maximally degenerate case of zero

interaction, the eigenvalues of the Hamiltonian are identical to the diagonal matrix elements. Equation (4.39) also holds trivially in that case. Therefore, there is strong evidence that the following statement is always true: The minima of the eigenenergies of the system with respect to the current are the eigenvalues of the Hamiltonian whose diagonal matrix elements are minimized in momentum space. The minimal diagonal matrix elements are found if the two criteria (4.29) and (4.30) are matched.

4.2.5 The critical inductivity

The convergence of the iterative scheme is investigated here. Below a certain bound of the inductivity, the critical inductivity, the iterative solution scheme converges to one fixed-point of the current operator. Above the critical inductivity, more than one fixed-point for the current operator can be found. The critical inductivity is therefore a very important point at which the physical characteristics of quantum rings change dramatically.

The condition (4.29) is automatically fulfilled if the iterative scheme (4.25) converges. A criterion for the convergence of the sequence of currents is the Banach fixed point theorem. We apply it to determine the parameter range for which there is only one stable current state for each external flux.

The space of linear operators on the Hilbert space \mathcal{H} is a complete vector space with the operator norm

$$\|O\| = \sup_{\substack{|\psi\rangle \neq 0 \\ |\psi\rangle \in \mathcal{H}}} \frac{|O|\psi\rangle|}{||\psi\rangle|}, \quad (4.40)$$

and therefore a Banach space. A contraction O on a Banach space is defined to be a mapping from a closed subset D of the Banach space onto D , fulfilling a Lipschitz condition

$$\|O(x_2) - O(x_1)\| \leq g\|x_2 - x_1\| \quad (4.41)$$

for all $x_1, x_2 \in D$, where $0 \leq g < 1$. The Banach fixed point theorem states the convergence of the iterative scheme $x_{(n+1)} = O(x_{(n)})$ to one and only one fixed point of O for any starting value $x_{(0)} \in X$.

The operator G in the fixed point equation (4.26) fulfills a Lipschitz condition:

$$\|G(j_2) - G(j_1)\| \leq g\|j_2 - j_1\|. \quad (4.42)$$

It is a contraction if $0 \leq g < 1$. The operator G is diagonal and Hermitian in momentum space. Therefore it is considered as a simple continuously differentiable function $G : \mathbb{R}^{\dim \mathcal{H}} \rightarrow \mathbb{R}^{\dim \mathcal{H}}$. We derive an estimation for the smallest possible Lipschitz constant of G in the following. Let $\frac{\partial G}{\partial j}$ be the Jacobian matrix of the

operator G :

$$\begin{aligned} \left(\frac{\partial G}{\partial j} \right)_{\kappa\xi} &\equiv \frac{\partial G^\kappa}{\partial j^\xi} \\ &= \delta_{\kappa\xi} \frac{L}{N^2} [C^\kappa P^\kappa + (P^\kappa)^* (C^\kappa)^*], \end{aligned} \quad (4.43)$$

with

$$\begin{aligned} \|G(j+\Delta j) - G(j)\| &= \left\| \int_0^1 \frac{\partial G}{\partial j}(j+t\Delta j) \cdot \Delta j dt \right\| \\ &\leq \int_0^1 \left\| \frac{\partial G}{\partial j}(j+t\Delta j) \right\| \|\Delta j\| dt \\ &\leq \left(\sup_{0 \leq t \leq 1} \left\| \frac{\partial G}{\partial j}(j+t\Delta j) \right\| \right) \|\Delta j\|. \end{aligned} \quad (4.44)$$

The smallest possible global Lipschitz constant can be estimated as:

$$\begin{aligned} g &= \sup \left\| \frac{\partial G}{\partial j} \right\| \\ &= \frac{L}{N^2} \sup \|C P(j) + P^\dagger(j) C^\dagger\| \\ &\leq \frac{L}{N^2} (\|C\| + \|C^\dagger\|) \\ &= \frac{2L}{N^2} |\lambda_{\max}(C)|. \end{aligned} \quad (4.45)$$

The Hermiticity of j , unitarity of P , normality of C , and the triangle inequality have been used. Here $\lambda_{\max}(C)$ denotes the complex eigenvalue of the operator C with the largest absolute value. It follows that G is a contraction ($g < 1$) if the condition

$$L < L_c = \frac{N^2}{2|\lambda_{\max}(C)|} \quad (4.46)$$

is satisfied. The hopping operator is diagonal in momentum space. Thus we obtain

$$L_c = \frac{N^2}{2t \max_{\kappa} \left| \sum_{k\sigma} e^{ik} \langle p^\kappa | \mathbf{n}_{k\sigma} | p^\kappa \rangle \right|}, \quad (4.47)$$

where the maximum is taken over all normalized configurations of the electrons in momentum space $|p^\kappa\rangle$.

The sufficient criterion (4.30) is also fulfilled. The supremum g of the norm of the Jacobian matrix of G is smaller than one, therefore the entries in the Jacobian

matrix are also smaller than one. In terms of the Jacobian matrix the criterion (4.30) reads

$$\begin{aligned} \frac{\partial^2 H_{\kappa\xi}}{\partial(j^\zeta)^2} &= \delta_{\kappa\xi} \delta_{\xi\zeta} \left\{ 1 - \left(\frac{\partial G}{\partial j} \right)_{\kappa\kappa} \right\} \\ &> 0, \quad \forall \kappa = \xi = \zeta \in \{1, \dots, \dim \mathcal{H}\}. \end{aligned} \quad (4.48)$$

The physical essence of this result is that for inductivities smaller than the critical inductivity L_c , the current is a unique, single valued function of the external flux.

Furthermore, the expectation value of the current is an antisymmetric function of the external flux. The current operator is antisymmetric in ϕ_{ext} . This can be verified by looking at the eigenvalues of the current operator. The eigenvalues are proportional to the imaginary part of $e^{i\phi_{\text{ext}}/N}$, which is clearly antisymmetric. The density matrix of the problem is symmetric, because the external flux enters the Hamiltonian only through the kinetic energy operator and the square of the current operator. Both are symmetric in ϕ_{ext} . Therefore, there is no persistent current for zero external flux ($\langle j(\phi_{\text{ext}}) \rangle = 0$, for $\phi_{\text{ext}} = 0$) and for inductivities $L \leq L_c$. States with a spontaneous orbital magnetic moment without external magnetic field are only possible for inductivities $L > L_c$.

The convergence of the scheme can be tested numerically by the operator norm of the difference of current operators of two successive iteration steps:

$$\|\Delta j_{(n)}\| \equiv \|j_{(n)} - j_{(n-1)}\| \xrightarrow{n \rightarrow \infty} 0. \quad (4.49)$$

The iterative procedure may be considered to have reached convergence once the spectral norm $\|\Delta j_{(n)}\|$ drops below a certain bound. The convergence for very small rings becomes exponential in n after sufficiently many steps (see Fig. 4.5). The expectation value of the free energy is seen to be lowered in each iteration step while the expectation value of the current reaches its equilibrium value.

4.2.6 Modification for large inductivities

Above the critical inductivity the iterative scheme does not converge in general. This can occur for certain values of the external flux. In this case, there is more than one stable current state. Since the current operator and the phase-shift operator in Eq. (4.25) are diagonal, it is possible to reduce the scheme to $\dim \mathcal{H}$ one-dimensional searches for fixed points. For fixed points of one-dimensional functions, Hillam's theorem (Hil75) provides an iterative scheme to find a fixed point for every single eigenvalue of the current operator. Let g^κ be the Lipschitz constant for the κ -th eigenvalue of the current operator [analog to Eq. (4.45)]:

$$g^\kappa = \frac{2L|C^\kappa|}{N^2}. \quad (4.50)$$

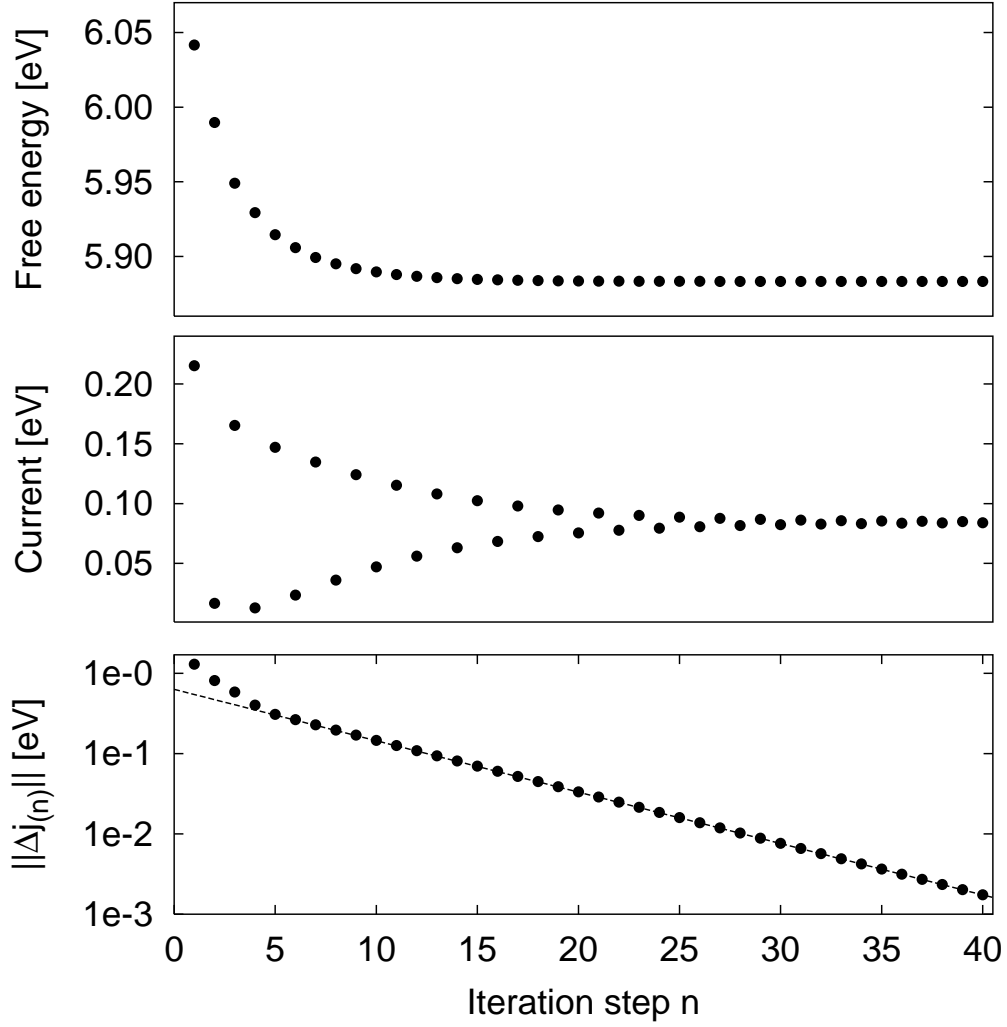


Figure 4.5: Free energy, current and the difference of the norm of successive current operators on a logarithmic scale were obtained for the extended Hubbard model on 4 sites with 2 up and 2 down electrons with $t = 1$ eV, $U = 4$ eV, $V = 3$ eV, $L = 2.5/\text{eV}$, $\phi_{\text{ext}} = 1.5$ at $T = 0.01$ eV. The critical inductivity for this model is $L_c = 2\sqrt{2}/\text{eV} \approx 2.8284/\text{eV}$.

Hillam's theorem states that the iterative scheme

$$\begin{aligned}
 P_{(n)}^\kappa &= e^{-\frac{i}{N}Lj_{(n-1)}^\kappa} \\
 j_{(n)}^\kappa &= -\frac{2}{N} \text{Im}(C^\kappa P_{(n)}^\kappa) \\
 j_{(n)}^\kappa &= \lambda^\kappa j_{(n)}^\kappa + (1 - \lambda^\kappa) j_{(n-1)}^\kappa \\
 \Delta j_{(n)}^\kappa &= \frac{1}{\lambda^\kappa} (j_{(n)}^\kappa - j_{(n-1)}^\kappa)
 \end{aligned} \tag{4.51}$$

4.2 The model and its analytic properties

will converge when $\lambda^\kappa = \frac{1}{g^\kappa + 1}$. The iteration starts with $n = 1$. The current eigenvalues $\{j_{(0)}^\kappa\}$ can be set in order to find different branches of the solution. A criterion for the convergence of the scheme is $\max_\kappa (\Delta j_{(n)}^\kappa) < \epsilon$. After the convergence criterion is satisfied, it still has to be verified that the current minimizes the energy eigenvalues. Consequently, the criterion

$$\min_\kappa \left| 1 - \frac{2L}{N^2} \operatorname{Re}(C^\kappa P_{(\infty)}^\kappa) \right| > 0 \quad (4.52)$$

needs to be checked up, in analogy to Eq. (4.30).

4.2.7 Asymptotic expansion for large inductivities

We can expand the solution for every eigenvalue of the current operator in momentum space asymptotically for high inductivities. The implicit equations that determine the eigenvalues of the current operator are

$$j^\kappa = \frac{2t\tilde{n}}{N} \sin \left[K - \frac{1}{N} (Lj^\kappa + \phi_{\text{ext}}) \right]. \quad (4.53)$$

Here \tilde{n} and K are defined by the equation

$$e^{iK\tilde{n}} = \sum_{k\sigma} e^{ik} \langle p^\kappa | n_{k\sigma} | p^\kappa \rangle, \quad (4.54)$$

where \tilde{n} is a positive real number. $|p^\kappa\rangle$ denotes the eigenstates of the noninteracting Hamiltonian in momentum space. We define $J^\kappa = Lj^\kappa$, so that

$$\frac{J^\kappa}{L} = \frac{2t\tilde{n}}{N} \sin \left[K - \frac{1}{N} (J^\kappa + \phi_{\text{ext}}) \right]. \quad (4.55)$$

We recognize that there are infinitely many solutions for the lowest order coefficient of the expansion $J^\kappa = \sum_{n=0}^{\infty} \frac{1}{L^n} J_n^\kappa$, namely

$$J_0^{\kappa,m} = N (K + 2m\pi) - \phi_{\text{ext}}, \quad m \in \frac{1}{2}\mathbb{Z}. \quad (4.56)$$

From the equation of the energy eigenvalues

$$E^\kappa = -2t\tilde{n} \cos \left[K - \frac{1}{N} (J^{\kappa,m} + \phi_{\text{ext}}) \right] + \frac{1}{2} \frac{(J^{\kappa,m})^2}{L}, \quad (4.57)$$

it is evident that the $J_0^{\kappa,m}$ for $m \in \mathbb{Z}$ are in fact the minima of the eigenenergies (for $L \rightarrow \infty$). The expansion to second order in $\frac{1}{L}$ is $J^{\kappa,m} = \sum_{n=0}^2 \left(-\frac{N^2}{2tL\tilde{n}} \right)^n J_0^{\kappa,m}$. This is the beginning of an alternating series of terms that are linear in $J_0^{\kappa,m}$. These terms are therefore also linear in ϕ_{ext} . The gradient of the sequence of the

partial sums of this series with respect to ϕ_{ext} alternates around the gradient of the tangent to the real solution at the point $\phi_{\text{ext}} = N(K + 2m\pi)$. The sum of all terms of the expansion that are linear in ϕ_{ext} is

$$\begin{aligned} J^{\kappa,m} &= \sum_{n=0}^{\infty} \left(-\frac{N^2}{2tL\tilde{n}} \right)^n J_0^{\kappa,m} + O\left(\frac{1}{L^3}\right) \\ &= \frac{2tL\tilde{n}}{N^2 + 2tL\tilde{n}} J_0^{\kappa,m} - \frac{N^3 (J_0^{\kappa,m})^3}{48t^3 L^3 \tilde{n}^3} + (J_0^{\kappa,m})^3 O\left(\frac{1}{L^4}\right), \\ j^{\kappa,m} &= \frac{2t\tilde{n}}{N^2 + 2tL\tilde{n}} [N(K + 2\pi m) - \phi_{\text{ext}}] + O\left(\frac{1}{L^4}\right). \end{aligned} \quad (4.58)$$

We take the sum of the terms linear in ϕ_{ext} for the following reason: the $j^{\kappa,m}(\phi_{\text{ext}})$ are good approximations for large inductivities (to third order in $1/L$), they are also tangents of the real solutions at the points $\phi_{\text{ext}} = N(K + 2\pi m)$, $m \in \mathbb{Z}$ for small inductivities. Therefore, the approximation is also a second-order approximation if $J_0^{\kappa,m} = N(K + 2\pi m) - \phi_{\text{ext}}$ is considered as a small parameter. The next-order contribution is a third order term in $J_0^{\kappa,m}$ which is fourth order in $1/L$. This shows that the real solutions of j are bounded from above by the lines $j^{\kappa,m}$ for $\phi_{\text{ext}} < N(K + 2\pi m)$ and are bounded from below for $\phi_{\text{ext}} > N(K + 2\pi m)$ for sufficiently high inductivities. This is important for the following estimation of the possible number of simultaneous solutions of the current at a given ϕ_{ext} . We can compare the value of the critical inductivity with the value of the inductivity for which we first detect two solutions.

The maximum of the current that can be a solution of Eq. (4.53) is $|j^\kappa| \leq \frac{2t}{N}$. We obtain the following interpretation of Fig. 4.6: The closer the solutions lie to the line $j = 0$, the lower is their energy, because of the $\frac{1}{2}L(j^\kappa)^2$ contribution. The real solutions jump from one m -level $j^{\kappa,m}$ to the next $j^{\kappa,m\pm 1}$ or interpolate between them continuously at low inductivities.

The number of solutions N_s for $j^\kappa(\phi_{\text{ext}})$ at a given value of ϕ_{ext} can be approximated as the number of lines $j^{\kappa,m}$ intersecting the line $\phi_{\text{ext}} = 0$ in the interval $j \in [-2t/N, 2t/N]$ (circles in Fig. 4.6), which can be evaluated to be roughly

$$\begin{aligned} N_s &= \frac{1}{2\pi} \left(2 - K + \frac{4tL\tilde{n}}{N^2} \right) + 1 \\ &\stackrel{L \rightarrow \infty}{\approx} \frac{2tL\tilde{n}}{\pi N^2}. \end{aligned} \quad (4.59)$$

We can draw the following conclusion from the above calculations: The ring current is a finite size effect that decreases with the reciprocal system size for all $L > 0$. The possibility to find several stable current states decreases even more strongly with $1/N^2$. However, it grows linearly with the inductivity. The value of one solution $j^{\kappa,m}$ goes to zero like $1/L$ for high inductivities.

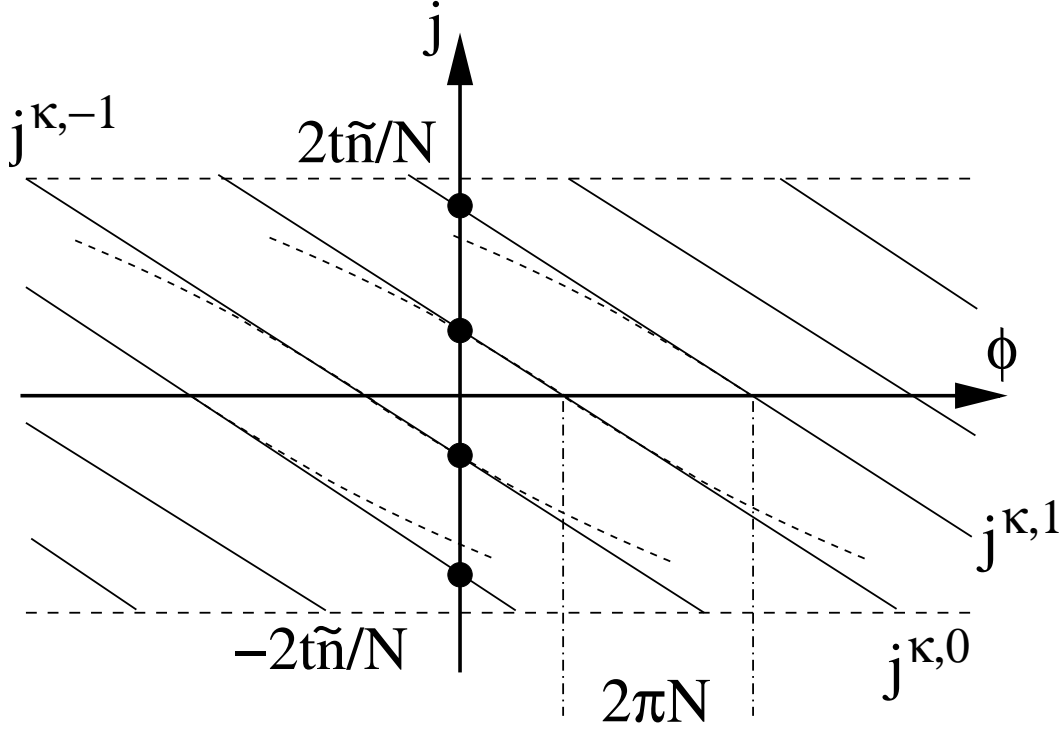


Figure 4.6: Sketch of the asymptotic expansion (solid lines) and the real solution (dashed lines).

4.2.8 Examination of the diagonality of the current operator

The kinetic energy and the current have been assumed to be diagonal in momentum space for physical reasons. This can be verified for low inductivities. For low inductivities the phase shift operator is close to the identity and the hopping operator is diagonal [see Eq. (4.15)], leading to a diagonal current and kinetic energy. However, it is not clear whether the above equations allow for non-diagonal solutions and whether there is a physical meaning of these solutions if they exist at all. For a two-site model we prove below that there are only diagonal solutions of the equation (4.17). It is therefore plausible to expect that the physical solutions of the current operator are always diagonal in momentum space.

We start with the operators constituting the Hamiltonian of the system:

$$\begin{aligned}
 P &\equiv e^{-\frac{i}{N}Lj}, \\
 C &\equiv -te^{-\frac{i}{N}\phi_{\text{ext}}}\sum_{k\sigma}e^{ik}n_{k\sigma}, \\
 j &= \frac{i}{N}(CP - P^\dagger C^\dagger).
 \end{aligned} \tag{4.60}$$

For a system with two lattice sites and one electron, the matrix representing the

hopping operator in momentum space is

$$C = -te^{-\frac{i}{2}\phi_{\text{ext}}}\sigma_3. \quad (4.61)$$

The current operator is a Hermitian matrix. Every Hermitian 2×2 matrix can be expressed as a linear combination of the Pauli matrices and the identity. Therefore, the current is

$$\mathbf{j} = a_0\mathbb{1} + \mathbf{a} \cdot \boldsymbol{\sigma}, \quad (4.62)$$

where $\boldsymbol{\sigma}$ denotes the vector of the three Pauli matrices:

$$\boldsymbol{\sigma} = \begin{pmatrix} \begin{pmatrix} 0 & 1 \\ 1 & 0 \end{pmatrix} \\ \begin{pmatrix} 0 & -i \\ i & 0 \end{pmatrix} \\ \begin{pmatrix} 1 & 0 \\ 0 & -1 \end{pmatrix} \end{pmatrix}. \quad (4.63)$$

The expansion coefficients a_i are real. The direction of the current operator is determined by $\hat{\mathbf{a}}$:

$$\begin{aligned} \mathbf{a} &= a\hat{\mathbf{a}} \\ \hat{\mathbf{a}} &= \begin{pmatrix} \cos \varphi \sin \vartheta \\ \sin \varphi \sin \vartheta \\ \cos \vartheta. \end{pmatrix} \end{aligned} \quad (4.64)$$

The current operator is diagonal in momentum space if the angle ϑ is zero. Then the current operator can be purely expanded in terms of the identity and the σ_3 matrix.

With the use of these definitions, we obtain the current operator

$$\mathbf{j} = \frac{it}{2} \left(e^{\frac{i}{2}Lj} e^{\frac{i}{2}\phi_{\text{ext}}}\sigma_3 - e^{-\frac{i}{2}\phi_{\text{ext}}}\sigma_3 e^{-\frac{i}{2}Lj} \right), \quad (4.65)$$

or, inserting the Pauli matrix expansion,

$$a_0\mathbb{1} + \mathbf{a} \cdot \boldsymbol{\sigma} = \frac{it}{2} \left(e^{\frac{i}{2}(\phi_{\text{ext}}+La_0)} e^{\frac{i}{2}L\mathbf{a}\cdot\boldsymbol{\sigma}}\sigma_3 - e^{-\frac{i}{2}(\phi_{\text{ext}}+La_0)}\sigma_3 e^{-\frac{i}{2}L\mathbf{a}\cdot\boldsymbol{\sigma}} \right). \quad (4.66)$$

4.2 The model and its analytic properties

The matrix exponential can be evaluated to be

$$\begin{aligned}
 e^{-\frac{iL}{2}\mathbf{a}\cdot\boldsymbol{\sigma}} &= \sum_{n=0}^{\infty} \frac{\left(\frac{iL}{2}\mathbf{a}\cdot\boldsymbol{\sigma}\right)^{2n}}{(2n)!} - \sum_{n=0}^{\infty} \frac{\left(\frac{iL}{2}\mathbf{a}\cdot\boldsymbol{\sigma}\right)^{2n+1}}{(2n+1)!} \\
 &= \sum_{n=0}^{\infty} \frac{(-1)^n}{(2n)!} \left(\frac{L}{2}\mathbf{a}\right)^{2n} \mathbb{1} - i \frac{\mathbf{a}\cdot\boldsymbol{\sigma}}{\mathbf{a}} \sum_{n=0}^{\infty} \frac{(-1)^n}{(2n+1)!} \left(\frac{L}{2}\mathbf{a}\right)^{2n+1} \\
 &= \mathbb{1} \cos \frac{L\mathbf{a}}{2} - i \frac{\mathbf{a}\cdot\boldsymbol{\sigma}}{\mathbf{a}} \sin \frac{L\mathbf{a}}{2} \\
 &= \begin{pmatrix} \cos \frac{L\mathbf{a}}{2} - i \cos \vartheta \sin \frac{L\mathbf{a}}{2} & -i \sin \vartheta e^{-i\varphi} \sin \frac{L\mathbf{a}}{2} \\ -i \sin \vartheta e^{i\varphi} \sin \frac{L\mathbf{a}}{2} & \cos \frac{L\mathbf{a}}{2} + i \cos \vartheta \sin \frac{L\mathbf{a}}{2} \end{pmatrix} \\
 &\equiv \begin{pmatrix} a & b \\ -b^* & a^* \end{pmatrix},
 \end{aligned} \tag{4.67}$$

where we used

$$\begin{aligned}
 (\mathbf{a}\cdot\boldsymbol{\sigma})^2 &= \begin{pmatrix} \mathbf{a}_3 & \mathbf{a}_1 - i\mathbf{a}_2 \\ \mathbf{a}_1 + i\mathbf{a}_2 & -\mathbf{a}_3 \end{pmatrix} \begin{pmatrix} \mathbf{a}_3 & \mathbf{a}_1 - i\mathbf{a}_2 \\ \mathbf{a}_1 + i\mathbf{a}_2 & -\mathbf{a}_3 \end{pmatrix} \\
 &= \begin{pmatrix} \mathbf{a}^2 & 0 \\ 0 & \mathbf{a}^2 \end{pmatrix} = \mathbf{a}^2 \mathbb{1}.
 \end{aligned} \tag{4.68}$$

The exponential is a unitary operator because of the Hermiticity of the exponent. Therefore we get

$$e^{+\frac{iL}{2}\mathbf{a}\cdot\boldsymbol{\sigma}} = \begin{pmatrix} \cos \frac{L\mathbf{a}}{2} + i \cos \vartheta \sin \frac{L\mathbf{a}}{2} & i \sin \vartheta e^{-i\varphi} \sin \frac{L\mathbf{a}}{2} \\ i \sin \vartheta e^{i\varphi} \sin \frac{L\mathbf{a}}{2} & \cos \frac{L\mathbf{a}}{2} - i \cos \vartheta \sin \frac{L\mathbf{a}}{2} \end{pmatrix} = \begin{pmatrix} a^* & -b \\ b^* & a \end{pmatrix}. \tag{4.69}$$

For the further calculations, the effect of multiplying an arbitrary matrix by one of the Pauli matrices is needed to be known:

$$\begin{aligned}
 \begin{pmatrix} a & b \\ c & d \end{pmatrix} \sigma_1 &= \begin{pmatrix} b & a \\ d & c \end{pmatrix} \\
 \begin{pmatrix} a & b \\ c & d \end{pmatrix} \sigma_2 &= \begin{pmatrix} ib & -ia \\ id & -ic \end{pmatrix} \\
 \begin{pmatrix} a & b \\ c & d \end{pmatrix} \sigma_3 &= \begin{pmatrix} a & -b \\ c & -d \end{pmatrix} \\
 \sigma_3 \begin{pmatrix} a & b \\ c & d \end{pmatrix} &= \begin{pmatrix} a & b \\ -c & -d \end{pmatrix}.
 \end{aligned} \tag{4.70}$$

Applying the trace to Eq. (4.66) results in a first self-consistency equation:

$$\begin{aligned}
 \mathbf{a}_0 &= \frac{1}{2} \text{Tr} (\mathbf{a}_0 \mathbf{1} + \mathbf{a} \cdot \boldsymbol{\sigma}) \\
 &= \frac{it}{4} \text{Tr} \left[e^{\frac{i}{2}(\phi_{\text{ext}} + L\mathbf{a}_0)} \begin{pmatrix} a^* & b \\ b^* & -a \end{pmatrix} - e^{-\frac{i}{2}(\phi_{\text{ext}} + L\mathbf{a}_0)} \begin{pmatrix} a & b \\ b^* & -a^* \end{pmatrix} \right] \\
 &= \frac{it}{4} (a^* - a) \left[e^{\frac{i}{2}(\phi_{\text{ext}} + L\mathbf{a}_0)} + e^{-\frac{i}{2}(\phi_{\text{ext}} + L\mathbf{a}_0)} \right] \\
 &= -\frac{t}{2} \cos \vartheta \sin \frac{L\mathbf{a}}{2} \left[e^{\frac{i}{2}(\phi_{\text{ext}} + L\mathbf{a}_0)} + e^{-\frac{i}{2}(\phi_{\text{ext}} + L\mathbf{a}_0)} \right] \\
 &= -t \cos \vartheta \sin \frac{L\mathbf{a}}{2} \cos \frac{\phi_{\text{ext}} + L\mathbf{a}_0}{2} \\
 &= -t \frac{\mathbf{a}_3}{\mathbf{a}} \sin \frac{L\mathbf{a}}{2} \cos \frac{\phi_{\text{ext}} + L\mathbf{a}_0}{2}.
 \end{aligned} \tag{4.71}$$

The second equation is obtained by multiplying the initial equation (4.66) with the first Pauli matrix and taking the trace afterwards:

$$\begin{aligned}
 \mathbf{a}_1 &= \frac{1}{2} \text{Tr} [(\mathbf{a}_0 \mathbf{1} + \mathbf{a} \cdot \boldsymbol{\sigma}) \sigma_1] \\
 &= \frac{it}{4} \text{Tr} \left[e^{\frac{i}{2}(\phi_{\text{ext}} + L\mathbf{a}_0)} \begin{pmatrix} a^* & b \\ b^* & -a \end{pmatrix} \sigma_1 - e^{-\frac{i}{2}(\phi_{\text{ext}} + L\mathbf{a}_0)} \begin{pmatrix} a & b \\ b^* & -a^* \end{pmatrix} \sigma_1 \right] \\
 &= \frac{it}{4} \text{Tr} \left[e^{\frac{i}{2}(\phi_{\text{ext}} + L\mathbf{a}_0)} \begin{pmatrix} b & a^* \\ -a & b^* \end{pmatrix} - e^{-\frac{i}{2}(\phi_{\text{ext}} + L\mathbf{a}_0)} \begin{pmatrix} b & a \\ -a^* & b^* \end{pmatrix} \right] \\
 &= \frac{it}{4} (b + b^*) \left[e^{\frac{i}{2}(\phi_{\text{ext}} + L\mathbf{a}_0)} - e^{-\frac{i}{2}(\phi_{\text{ext}} + L\mathbf{a}_0)} \right] \\
 &= -\frac{it}{2} \sin \vartheta \sin \frac{L\mathbf{a}}{2} \sin \varphi \left(e^{\frac{i}{2}(\phi_{\text{ext}} + L\mathbf{a}_0)} - e^{-\frac{i}{2}(\phi_{\text{ext}} + L\mathbf{a}_0)} \right) \\
 &= t \sin \vartheta \sin \frac{L\mathbf{a}}{2} \sin \varphi \sin \frac{\phi_{\text{ext}} + L\mathbf{a}_0}{2} \\
 &= t \frac{\mathbf{a}_2}{\mathbf{a}} \sin \frac{L\mathbf{a}}{2} \sin \frac{\phi_{\text{ext}} + L\mathbf{a}_0}{2}.
 \end{aligned} \tag{4.72}$$

Analogously, a third and a fourth self-consistency equation are obtained:

$$\begin{aligned}
 \mathbf{a}_2 &= \frac{1}{2} \text{Tr} [(\mathbf{a}_0 \mathbf{1} + \mathbf{a} \cdot \boldsymbol{\sigma}) \sigma_2] \\
 &= \frac{it}{4} \text{Tr} \left[e^{\frac{i}{2}(\phi_{\text{ext}} + L\mathbf{a}_0)} \begin{pmatrix} a^* & b \\ b^* & -a \end{pmatrix} \sigma_2 - e^{-\frac{i}{2}(\phi_{\text{ext}} + L\mathbf{a}_0)} \begin{pmatrix} a & b \\ b^* & -a^* \end{pmatrix} \sigma_2 \right] \\
 &= \frac{it}{4} \text{Tr} \left[e^{\frac{i}{2}(\phi_{\text{ext}} + L\mathbf{a}_0)} \begin{pmatrix} ib & -ia^* \\ -ia & -ib^* \end{pmatrix} - e^{-\frac{i}{2}(\phi_{\text{ext}} + L\mathbf{a}_0)} \begin{pmatrix} ib & -ia \\ -ia^* & -ib^* \end{pmatrix} \right] \\
 &= -\frac{t}{4} (b - b^*) \left[e^{\frac{i}{2}(\phi_{\text{ext}} + L\mathbf{a}_0)} - e^{-\frac{i}{2}(\phi_{\text{ext}} + L\mathbf{a}_0)} \right] \\
 &= \frac{it}{2} \sin \vartheta \sin \frac{L\mathbf{a}}{2} \cos \varphi \left[e^{\frac{i}{2}(\phi_{\text{ext}} + L\mathbf{a}_0)} - e^{-\frac{i}{2}(\phi_{\text{ext}} + L\mathbf{a}_0)} \right] \\
 &= -t \sin \vartheta \sin \frac{L\mathbf{a}}{2} \cos \varphi \sin \frac{\phi_{\text{ext}} + L\mathbf{a}_0}{2} \\
 &= -t \frac{\mathbf{a}_1}{\mathbf{a}} \sin \frac{L\mathbf{a}}{2} \sin \frac{\phi_{\text{ext}} + L\mathbf{a}_0}{2},
 \end{aligned} \tag{4.73}$$

$$\begin{aligned}
 \mathbf{a}_3 &= \frac{1}{2} \text{Tr} [(\mathbf{a}_0 \mathbf{1} + \mathbf{a} \cdot \boldsymbol{\sigma}) \sigma_3] \\
 &= \frac{it}{4} \text{Tr} \left[e^{\frac{i}{2}(\phi_{\text{ext}} + L\mathbf{a}_0)} \begin{pmatrix} a^* & -b \\ b^* & a \end{pmatrix} - e^{-\frac{i}{2}(\phi_{\text{ext}} + L\mathbf{a}_0)} \begin{pmatrix} a & -b \\ b^* & a^* \end{pmatrix} \right] \\
 &= \frac{it}{4} (a + a^*) \left[e^{\frac{i}{2}(\phi_{\text{ext}} + L\mathbf{a}_0)} - e^{-\frac{i}{2}(\phi_{\text{ext}} + L\mathbf{a}_0)} \right] \\
 &= -\frac{t}{2} (a + a^*) \sin \frac{\phi_{\text{ext}} + L\mathbf{a}_0}{2} \\
 &= -t \cos \frac{L\mathbf{a}}{2} \sin \frac{\phi_{\text{ext}} + L\mathbf{a}_0}{2}.
 \end{aligned} \tag{4.74}$$

The equations for \mathbf{a}_1 and \mathbf{a}_2 are of the form $\mathbf{a}_1 = \xi \mathbf{a}_2$ and $\mathbf{a}_2 = -\xi \mathbf{a}_1$. Since the only solution of these equations is $\mathbf{a}_1 = \mathbf{a}_2 = 0$, the current operator can be expanded in terms of the identity and the σ_3 Pauli matrix, which are diagonal. The current operator for the special case of a two-site model with one electron has thus been proven to possess only diagonal solutions in momentum space.

4.3 Numerical examination and physical consequences

In this section, we apply the proposed method to physical systems. Realistic parameters for cyclic hydrocarbon, especially the π -electrons in benzene are given and applied. The magnetic properties of benzene due to ring-current effects are evaluated.

In the last part of this section, we exhibit a system with a hysteresis loop in the magnetization with respect to the external field. The hysteresis loop is centered around the external field value of half a flux quantum in the ring. The system is a half filled four-site Hubbard ring. The phenomenon of the hysteresis loop is not restricted to this system; it should be found in any system with a negative Drude weight. Apart from half filled Hubbard rings, rings of noninteracting electrons with a band structure that cannot be approximated by a straight line around the Fermi points can possess a negative Drude weight. In a system with a negative Drude weight and six lattice sites, the hysteresis loop would be centered around zero external flux. Thus there would exist a spontaneous orbital magnetic moment without external magnetic field.

4.3.1 Realistic parameters

The work of Castleton, Bursill and Barford (CB02; BCB98) makes it seem reasonable to choose the parameters of the PPP model for benzene as follows:

$$\begin{aligned}t &= 2.64 \text{ eV}, \\U &= 8.9 \text{ eV}, \\ \epsilon_r &= 1.28.\end{aligned}\tag{4.75}$$

We estimate the inductivity of a molecule. If we take a look at the inductivity of a non-ferromagnetic classical conducting ring in vacuum of the size of a benzene molecule, we find that the inductivity

$$L = \mu_0 R \left\{ \frac{1}{4} + \left[\ln \left(\frac{8R}{r} \right) - 2 \right] \right\}\tag{4.76}$$

will be very small. The radius of the ring R in the above equation is about 140 pm. If the radius r of the conductor itself were about $R/5$, the inductivity would be about $L \approx 0.02/\text{eV}$ in natural units. However, the inductivity is a phenomenological parameter that has to be fitted to experiments. We try a large range of inductivities to show what kind of effects might arise because of the inductivity of a molecule or a ring of coupled quantum dots.

4.3.2 Benzene

The magnetic susceptibility of aromatic compounds is anisotropic. In benzene, the diamagnetic susceptibility perpendicular to the molecular plane ($\chi_{\perp}^{\text{mol}} = -119 \times$

4.3 Numerical examination and physical consequences

$10^{-11} \text{ m}^3 \text{ mol}^{-1}$) is about three times larger than the diamagnetic susceptibility parallel to the molecular plane ($\chi_{\parallel}^{\text{mol}} = -43.8 \times 10^{-11} \text{ m}^3 \text{ mol}^{-1}$) (Lue99). With the proposed model, the total magnetic susceptibility cannot be described because the influence of the core electrons is neglected. Moreover, the π -electrons are not able to move perpendicular to the plane of the molecule. Therefore, the orbital magnetic susceptibility in the plane of the benzene molecules is zero within our model. However, the part of the magnetic susceptibility that stems from the delocalization of the π -electrons—and this is the part that is important to determine the degree of aromaticity—is extracted.

If only the ring-current effect in benzene were anisotropic, the magnetic susceptibility anisotropy,

$$\begin{aligned} \Delta\chi^{\text{mol}} &\equiv \chi_{\perp}^{\text{mol}} - \chi_{\parallel}^{\text{mol}} \\ &= 75.2 \times 10^{-11} \text{ m}^3 \text{ mol}^{-1}, \end{aligned} \quad (4.77)$$

would be a good number to test the model. But according to Pople, the ring current effect makes up only 30% of the anisotropy (Pop64; FP64). The rest is caused by van Vleck paramagnetism. Other calculations have produced different results (Dai64). The van Vleck paramagnetism is a local contribution that can be captured by incremental schemes that ascribe a certain amount of the total magnetic susceptibility to every atom or bond in the molecule.

This observation has led to the definition of the magnetic susceptibility exaltation as the difference between the measured susceptibility (averaged over all orientations of the molecule) and the susceptibility calculated from incremental schemes:

$$\Lambda \equiv \bar{\chi}^{\text{mol}} - \left(\sum \chi_{\text{atom},i}^{\text{mol}} + n\chi_{\text{C}=\text{C}}^{\text{mol}} \right). \quad (4.78)$$

Another method to determine the magnetic susceptibility exaltation is to take the difference between the measured magnetic susceptibility of the aromatic molecule and the susceptibility of molecules built from the same atoms but without cyclic delocalization. The magnetic susceptibility exaltation should therefore be a good measure for the delocalization of electrons in a molecule. In current magnetochemistry textbooks, the value

$$\Lambda = -17.2 \times 10^{-11} \text{ m}^3 \text{ mol}^{-1} = -13.7 \text{ ppm cgs} \quad (4.79)$$

is found for the ring-current contribution to the total susceptibility in benzene (Lue99). This value stems from the articles of Dauben (DWL68; DWL69). It was calculated using the incremental schemes that were developed by Haberditzl, Pacault, and Hoarau. We compare it in the following with the susceptibility of our model.

The response current of benzene to an externally applied Aharonov-Bohm flux would look like that displayed in Fig. 4.7. The data was obtained with the parameters in Eq. (4.75) and including the electron-electron interaction according to the Ohno potential in Eq. (4.8). The diamagnetic response of benzene and the

shape of the free energy in Fig. 4.8 is reminiscent of SC rings with a conventional junction. The existence of a large almost linear regime around zero flux clarifies why linear approximations were so successful in explaining the magnetic response. The critical inductivity is ($t = 2.64 \text{ eV}$)

$$L_c = \frac{9}{2t} \approx 1.70455/\text{eV}. \quad (4.80)$$

Since this inductivity is very high, we expect the effect of the inductivity to be negligible in benzene rings. The slope of the curves at zero magnetic flux was determined as $j_{L=0}(\phi_{\text{ext}}) = -\frac{1.73 \text{ eV}}{\pi} \phi_{\text{ext}}$, $j_{L=0.05/\text{eV}}(\phi_{\text{ext}}) = -\frac{1.68 \text{ eV}}{\pi} \phi_{\text{ext}}$, $j_{L=0.1/\text{eV}}(\phi_{\text{ext}}) = -\frac{1.63 \text{ eV}}{\pi} \phi_{\text{ext}}$. It should be noted that the plots are not intended to be representative of the real ring current in benzene over the whole range of flux shown in the figures. This would only be true if it were possible to create a thin flux tube threading the molecule. In a homogeneous magnetic field the Zeeman interaction of the electron spins with the magnetic field would make the oversimplified model chosen invalid. However, in small fields the spins are not polarized in the benzene molecule and the diagrams can be used to extract the ring-current effect in small homogeneous magnetic fields.

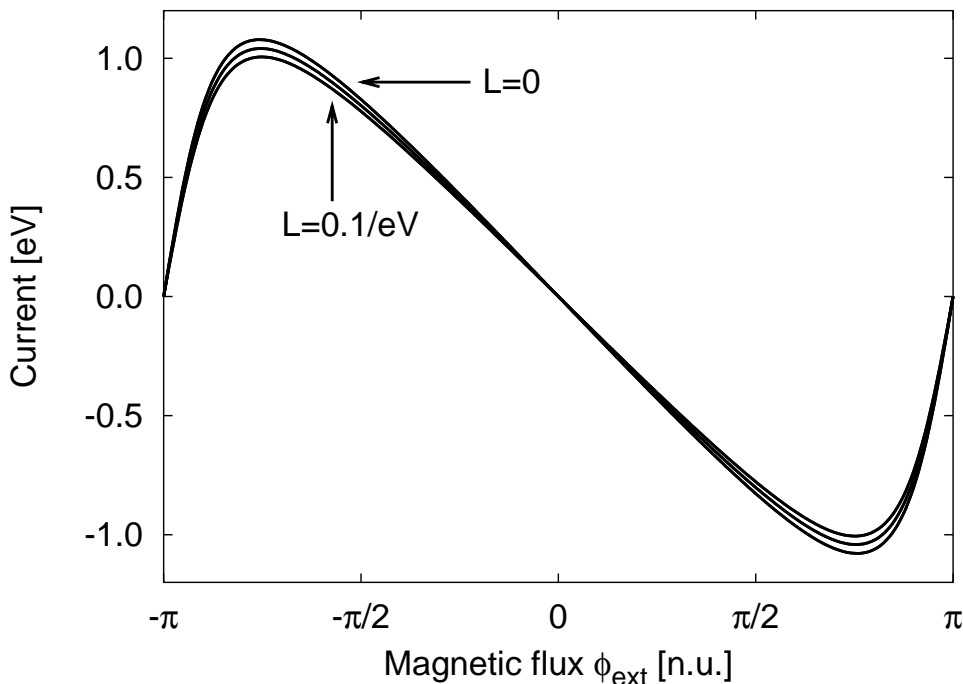


Figure 4.7: The PPP model on 6 sites with 3 up and 3 down electrons, $t = 2.64 \text{ eV}$, $U = 8.9 \text{ eV}$, $\epsilon_r = 1.28$, $T = 0.025 \text{ eV}$, $L = 0.0, 0.05/\text{eV}, 0.1/\text{eV}$ was used to model benzene.

The molar magnetic susceptibility

$$\chi^{\text{mol}} \equiv \frac{\chi}{\rho} M_r, \quad (4.81)$$

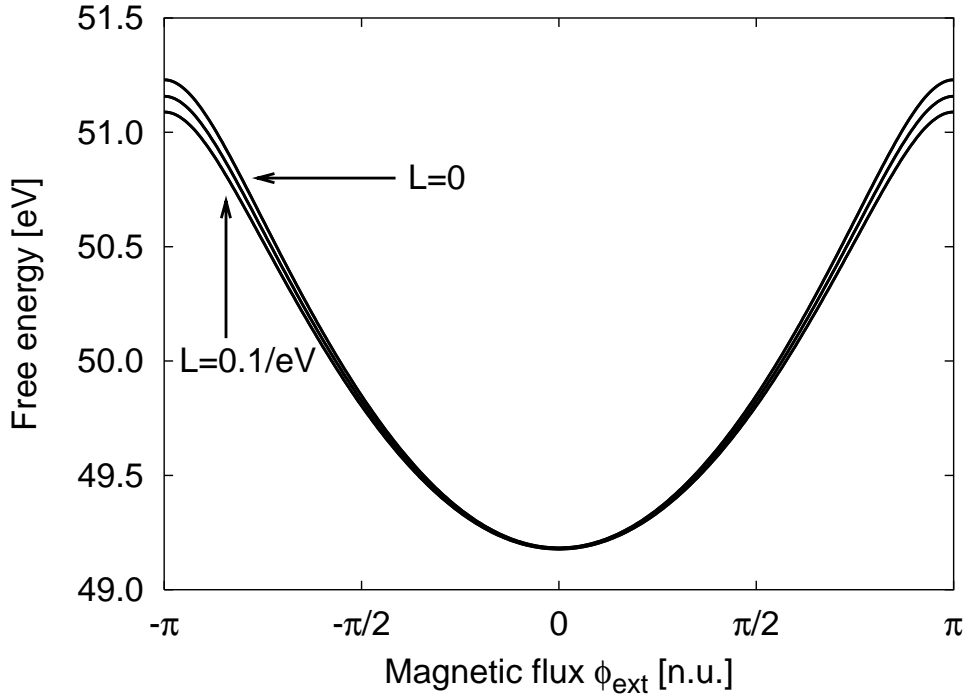


Figure 4.8: The free energy as a function of the magnetic flux for the system shown in Fig. 4.7.

is the magnetic susceptibility divided by the density of the material and multiplied by the molecular weight. In the framework of the model proposed above, the magnetic susceptibility is equal to the magnetic susceptibility exaltation

$$\Lambda = \bar{\chi}^{\text{mol}} = \frac{\mu_0 j A^2}{3 \phi_{\text{ext}}}. \quad (4.82)$$

With the values of $\frac{j}{\phi_{\text{ext}}} \approx -\frac{1.73 \text{ eV}}{\pi}$ and $A = \frac{3\sqrt{3}}{2}(140 \text{ pm})^2$ we obtain

$$\Lambda = -13.3 \times 10^{-11} \text{ m}^3 \text{ mol}^{-1}, \quad (4.83)$$

which agrees reasonably well with the value that was cited above [see Eq. (4.79)].

4.3.3 Systems with negative Drude weight

Systems with a negative Drude weight were first found by Stafford (SMS91) and Fye (FMS⁺91). These systems are finite, half filled Hubbard rings with a multiple of 4 lattice sites. As the ring reaches the thermodynamic limit, the Drude weight becomes positive semidefinite. These rings are paramagnetic and correspond to $[4n]$ annulenes. The negative Drude weight is related to the paramagnetism of these substances. However, we cannot expect to capture every property of the

[4n]annulenes with the simple Hubbard model. Bond length alternation and the long range Coulomb interaction counteract such an oversimplified description.

In this section we simply examine the new physical features that emerge from the proposed model. There can be states with a permanent orbital magnetic moment for these systems if the inductivity is tuned to values above the critical inductivity. We have calculated a hysteresis loop centered around half a flux quantum of the external field. There are two current states reached by entering the hysteresis loop from above or below. This is shown in Fig. 4.9. For small fields and small inductivities, the response is paramagnetic, and the overall characteristics are reminiscent of a π -SQUID, although for large inductivities, the response current of the 4-site system differs from that of a π -SQUID. The magnitude of the current becomes smaller for larger inductivities. The critical inductivity is ($t = 2.64$ eV)

$$L_c = \frac{2\sqrt{2}}{t} \approx 1.07137/\text{eV}. \quad (4.84)$$

States with a permanent orbital magnetic moment occur above the critical inductivity. They evolve around half a flux quantum. The free energy at $T = 0.01$ eV is plotted in Fig. 4.10. The current in a ring that is exposed to a magnetic field is the negative first derivative of the free energy with respect to the external flux.

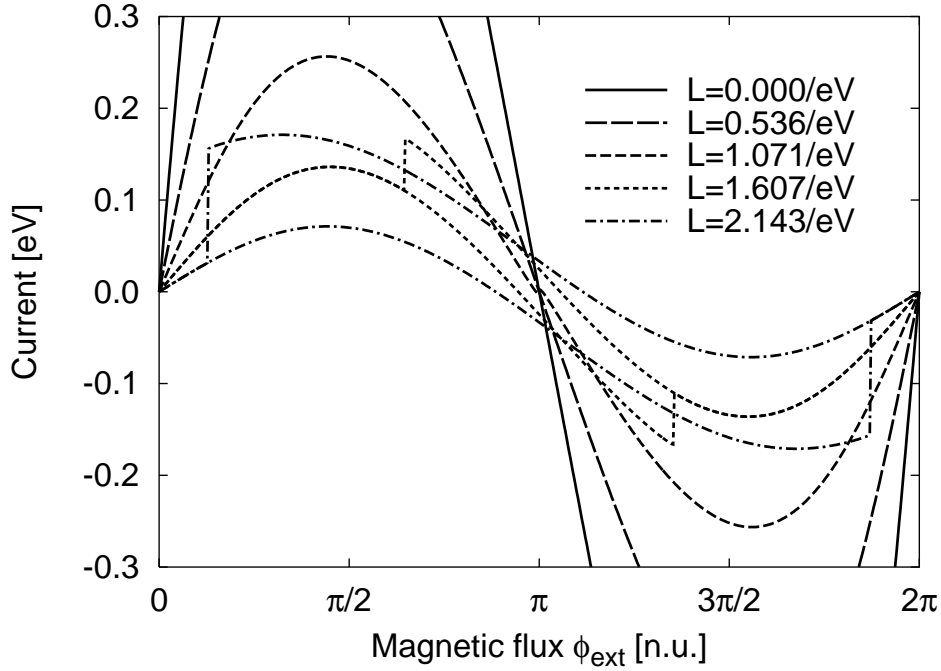


Figure 4.9: Current for the Hubbard model on 4 sites with 2 up and 2 down electrons, $t = 2.64$ eV, $U = 8.9$ eV, $V_{lm} = 0$, $T = 0.01$ eV, at inductivities $L = 0, \frac{1}{2}, 1, \frac{3}{2}, 2L_c$.

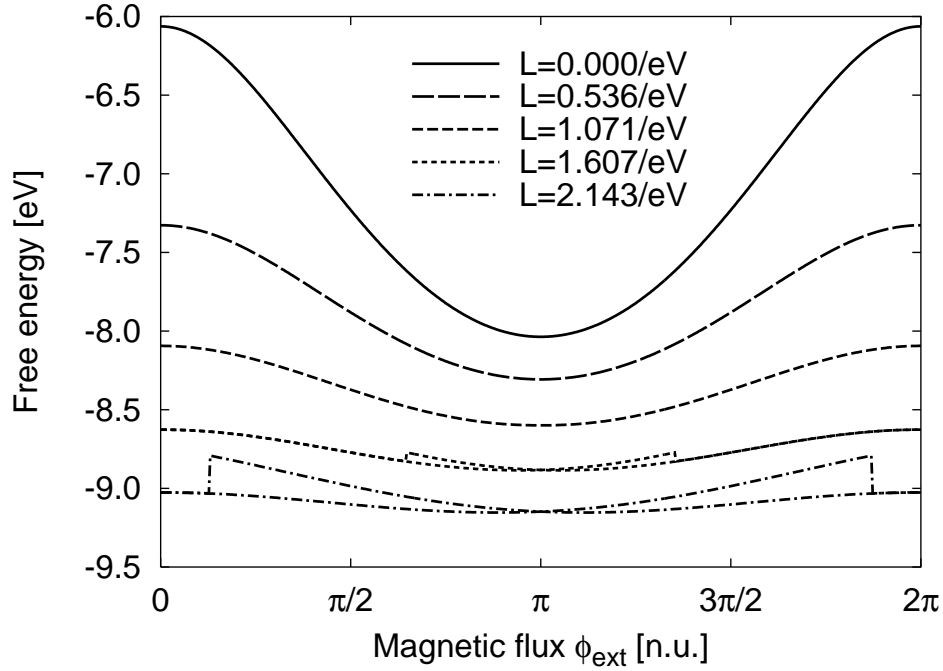


Figure 4.10: Here the free energy for the current curves shown in Fig. 4.9 is illustrated.

Although the electron interaction plays a subordinate role in the iterative scheme for the fixed point of the current operator, it is important for the occurrence of a permanent orbital magnetic moment in the 4-site system. We can ask which energy eigenstate of the noninteracting system is the first to cross from a single minimum with respect to the corresponding eigenvalue of the current operator to two minima. For the noninteracting system, the eigenenergies are

$$H^\kappa = 2 \operatorname{Re} \left[e^{-\frac{i}{N} L j^\kappa} C^\kappa \right] + \frac{1}{2} L (j^\kappa)^2. \quad (4.85)$$

For a single-particle system the eigenvalues of the hopping operator C^k lie on a circle in the complex plane. The radius of the circle is the hopping amplitude t . The eigenvalues on the circle correspond to the points in momentum space. As the external flux increases, they are rotated by an angle ϕ_{ext}/N in negative direction. All this is clear from Eq. (4.15). We are able to construct every possible eigenvalue of the hopping operator of the many-particle system by successively filling up the states in momentum space with electrons. Most of all, we are interested in the properties of the state that crosses first from one minimum to two minima as the inductivity is increased (see Fig. 4.11). The crossover takes place at L_c . This state has to be the state that produces the highest amplitude of the exponential term in Eq. (4.85). Occupying the single particle states $-\frac{\pi}{2}$ and π in momentum space with two electrons each yields the highest real part of the hopping operator in Eq. (4.85) [see Fig. 4.12]. Let us call this state $|\psi\rangle$. The state $|\psi\rangle$ is the

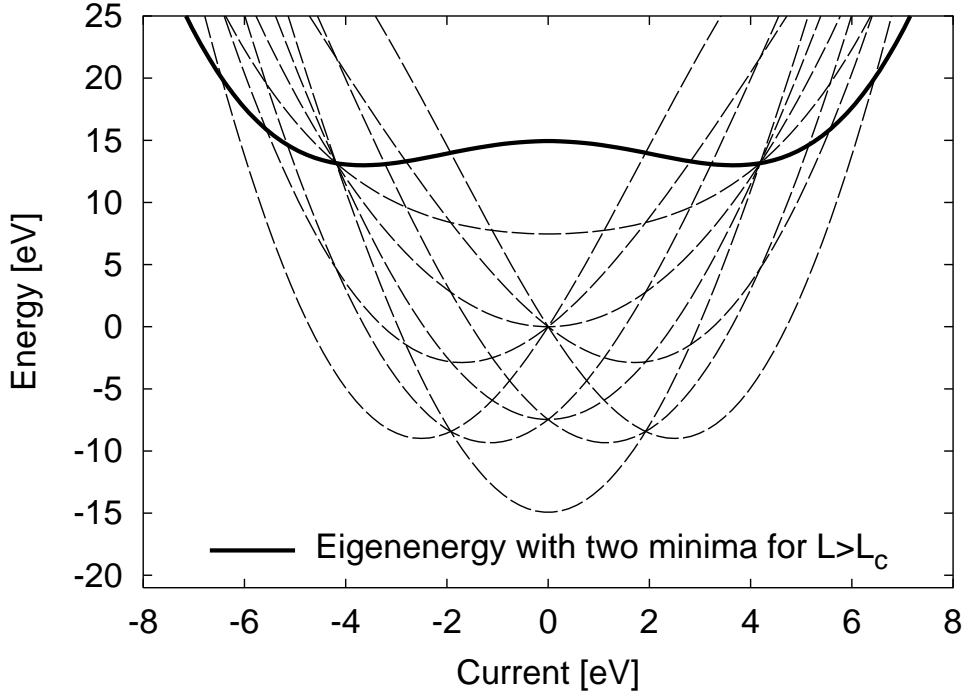


Figure 4.11: The eigenenergies for the noninteracting model on four lattice sites with two up and two down electrons with respect to the corresponding eigenvalues of the current operator. The state with the highest energy is nondegenerate and crosses first from one to two minima. The inductivity chosen for the graph is $L = 1.5/\text{eV}$ ($U = 0$, all other parameters taken from Fig. 4.9). The eigenvalues of the current operator will be adjusted by the fixed point method so as to minimize the eigenenergies.

state with the highest energy for the noninteracting system. Hence we expect the expectation value of the current at low temperatures not to exhibit a spontaneous orbital magnetic moment. The interaction of the electrons plays a vital role in mixing the state $|\psi\rangle$ with the ground state and thus adding a spontaneous orbital magnetic moment to the ground state (see Fig. 4.13). The hysteresis loop of the spontaneous orbital magnetic moment is seen to evolve for high interaction strengths. There is no hysteresis for the noninteracting system.

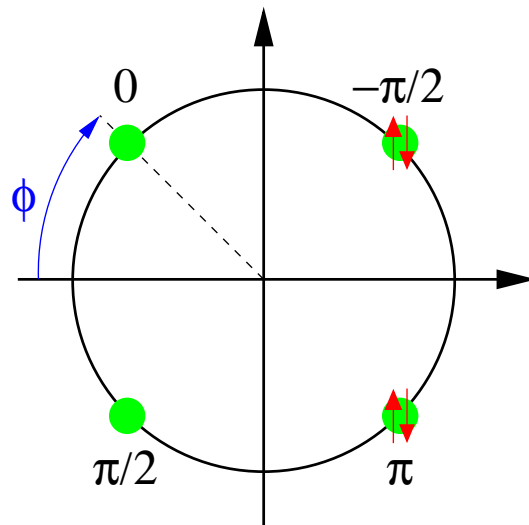


Figure 4.12: The eigenvalues of the hopping operator lie on a circle in the complex plane. For four lattice sites, there are also four sites in momentum space. The position of the points is influenced by the external flux ϕ applied to the system. The largest positive eigenvalue is reached if the points $-\frac{\pi}{2}$ and π are occupied with two electrons. Every possible eigenvalue can be constructed from this sketch.

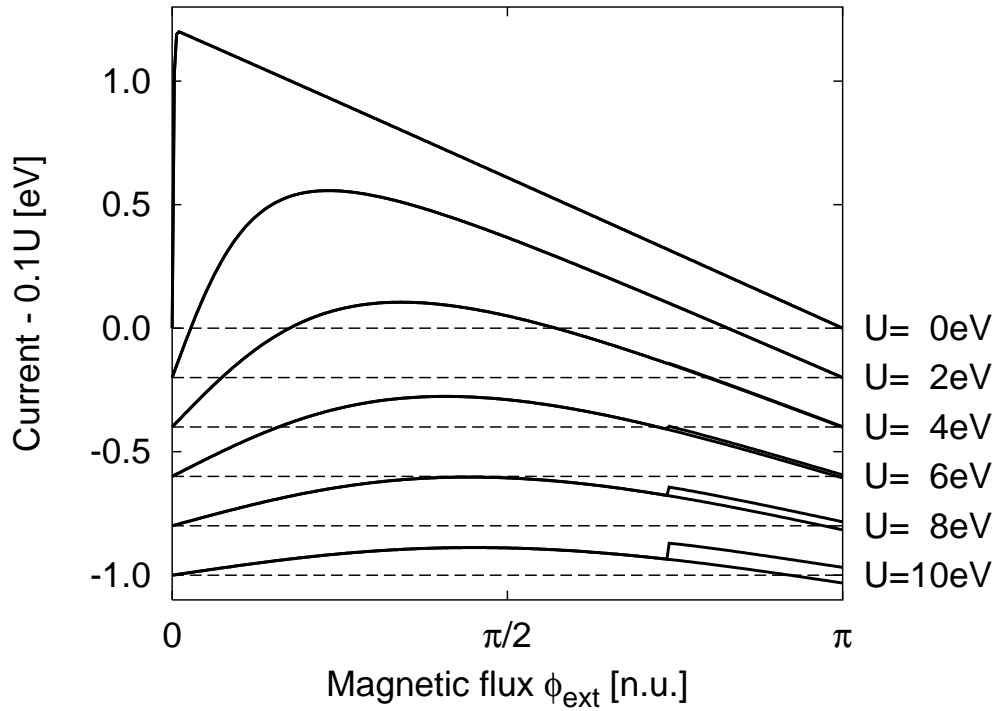


Figure 4.13: The expectation value of the current at $T = 0.01$ eV for the Hubbard model on four lattice sites with two up and two down electrons. The inductivity is held constant at $L = 1.5/\text{eV}$. The on-site interaction varies from $U = 0$ eV to $U = 10$ eV in steps of 2 eV.

5 Conclusion

5.1 What has been achieved?

The work described in this thesis has demonstrated the existence of three different types of quantum rings. There are quantum rings with *diamagnetic*, *paramagnetic*, or *spontaneous* persistent currents. In all of these rings, the strength of the persistent current is periodic in the number of flux quanta threading the ring. This is a consequence of the Aharonov-Bohm effect. However, it should be noted once again, that this result is strictly valid only for a flux tube threading the ring. In a homogeneous field, the magnetic field penetrating the ring area leads to a non-periodic contribution due to the Zeeman interaction of the electron spin with the magnetic field, if there is a total spin component in the direction of the field. Also the relativistic corrections, of which the spin-orbit coupling is most important, potentially change the periodic behavior of the physical quantities in quantum rings. A very important factor that influences the Aharonov-Bohm oscillations in quantum rings in homogeneous magnetic fields is the width of the ring. The leading-order corrections in terms of the ring width have been systematically derived with the use of perturbation theory. In two- and three-dimensional rings, the simple Peierls substitution, which multiplies the wave function by a phase factor depending on the magnetic flux in the ring, breaks down. The Peierls substitution describes, however, the leading order effect of a homogeneous magnetic field on narrow rings.

Diamagnetic and paramagnetic ring currents have been known for many years, if the connection between quantum rings and aromatic and antiaromatic molecules, that was emphasized in this thesis, is accepted. A theoretical criterion to distinguish between these types of ring currents has been given. The *Drude weight*, which was introduced as the singular part of the conductivity of systems in the thermodynamic limit, can be positive or negative for finite systems. It is calculated as the second derivative of the ground-state energy with respect to the flux in the ring. The current in a ring is the negative first derivative of the ground-state energy with respect to the magnetic flux at zero temperature. Therefore, the Drude weight is related to the first derivative of the current in the ring with respect to the flux. A positive Drude weight indicates diamagnetic ring currents whereas a negative Drude weight indicates paramagnetic ring currents. The existence of paramagnetic ring currents is astonishing at first sight. However, paramagnetic persistent currents, which enhance the magnetic field in the quantum rings, do

not contradict Lenz's law. Lenz's law makes a prediction for *ac* currents induced in alternating magnetic fields. In these fields, the ring currents have to counteract their cause, which is the alternating magnetic field. In contrast, the persistent currents in quantum rings are stemming from the Aharonov-Bohm effect that a static magnetic vector potential has on the wave function of the electrons in the ring.

Two different conditions under which the Drude weight can be negative have been described in this thesis. The first one concerns the band structure of the system under consideration. A system with a band structure where at a certain point the curvature is negative and larger in its absolute value than the absolute value of the curvature of the band at the other points in the Brillouin zone can lead to a negative Drude weight, if that point is occupied by one or more electrons. The second condition is concerned with the degeneracy of the ground state of the system, which in connection with Umklapp scattering and level repulsion due to the electron-electron interaction can lead to a negative Drude weight. Negative Drude weight and therefore paramagnetic currents have thus been found in three different models in this thesis, namely the periodic Anderson model and the Kronig-Penney model which fulfill the first condition, and the Hubbard model, which fulfills the second condition. Of course, parameters could be adjusted to find negative Drude weight due to fulfilling of the second condition in the periodic Anderson model.

It was also pointed out in this thesis, that another criterion to distinguish between diamagnetic and paramagnetic quantum rings is the sign of the Meissner fraction. This quantity would probably be better suited at finite temperature. It was also suggested to make use of the Meissner fraction in forthcoming investigations on the phase-coherence length. The Meissner fraction is different from zero for systems whose energy depends on the magnetic flux threading them. Such a dependency can only occur in systems with a phase-coherent electron motion. Therefore, the Meissner fraction is correlated to the phase-coherence length, and a definition of the phase-coherence length not resorting to the one-particle picture of the electrons seems possible with the use of the Meissner fraction.

The Meissner fraction, which is also called the superfluid density, hints at an analogy between quantum and superconducting rings. This analogy was explored to find a novel effect in quantum rings: spontaneous persistent currents. These have been measured in so-called π -SQUIDs. These are superconducting rings with a junction which turns the phase of the superconducting wave function by π . Due to this phase change, the free energy of the ring has two minima with respect to the flux. At zero external flux, the system has a maximum of the free energy, but there is no possibility to fall into one of the minima, because the system cannot generate magnetic flux. The model that was developed to describe spontaneous persistent currents in π -SQUIDs includes an inductivity. This inductivity enables the persistent current flowing through the ring to generate the internal magnetic flux needed to come closer to one of the minima in the free energy.

In complete analogy to this model, we have proposed a model including a feed-

5.1 What has been achieved?

back term through which the persistent current in a quantum ring can generate magnetic flux. Current and generated magnetic flux are coupled linearly by an inductivity. The energy of the generated magnetic field is quadratic in the current. However, the current is an operator. Within the framework of this model, the magnetic field is approximated classically in the following sense: The eigenvalues of the current operator are inserted into the Maxwell equations in order to obtain the magnetic field generated by the eigenstates of the current operator. Afterwards, the additional phase generated by the additional flux is inserted into the Schrödinger equation. Due to the linearity of the Maxwell equations, this process should lead to the correct expectation values if the state of the system under consideration is a superposition of different eigenstates of the current operator.

An iterative solution scheme for the model was developed, corresponding to iteratively inserting the current operator from the Schrödinger equation into the Maxwell equations and thus obtaining a change in the phase until a fixed point is found. It was proved that the eigenvalues of the Hamiltonian are minimized with respect to the eigenvalues of the current operator with this scheme. This method is conducted in momentum space, where the Hamiltonian of the noninteracting system and the current operator are diagonal. Therefore, the method can be applied to each eigenvalue separately. It has been shown, that the minimization of the energy eigenvalues of the noninteracting Hamiltonian corresponds to a minimization of the eigenvalues of the complete Hamiltonian.

For high inductivities, a state with a spontaneous orbital magnetic moment has been found. This is a state where at zero external field there is a persistent current flowing through the ring, generating a magnetic moment. It is not clear whether the critical inductivities we estimated can be reached in molecules. However, it should be possible to tune the inductivity of a ring of coupled quantum dots to the required values.

The ring-current effect contributes to the anisotropy of the magnetic susceptibility in benzene. It has been found that the inductivity of a benzene ring should be almost negligible. This is due to the extremely small diameter (240pm) of the molecule. However, for an exact determination of the inductivity of the π -system of benzene, the part of the anisotropy of the magnetic susceptibility that is induced by ring currents would have to be clearly separated from the part of the anisotropy that stems from Van Vleck paramagnetism.

The proposed model has been applied to extract the ring current contribution to the magnetic susceptibility in benzene. It should be possible to apply this method to other substances and thus establish a theoretical criterion for aromaticity. The advantage over the theoretical predictions of aromaticity from density-functional-theory calculations is the full consideration of the Coulomb interaction. Of course, here we have only considered relatively simple models with four parameters.

5.2 What remains to be investigated?

- Further investigation should be undertaken to determine the inductivity of quantum rings. A theory for calculating the value of the inductivity and the parameters on which it depends has to be constructed. With the use of such a theory, hints could be given to experimentalists, how quantum dots should be coupled to build up quantum rings resulting in the largest possible inductivity, and thus making it possible to measure spontaneous persistent currents in quantum rings.
- The effect of the Zeeman interaction should be included in all calculations. The Zeeman effect is a linear contribution to the energy of the quantum ring. The exact-diagonalization calculations would have to be separately conducted in the subspaces with different values of the total spin. We were concerned mostly with systems with zero total spin. These calculations are therefore also valid if the Landé factor of the electrons is switched on in the low field limit of a homogeneous magnetic field. However, for strong fields, the Zeeman interaction is also very important for systems, that show no resulting spin component in weak fields.
- It should be tried to incorporate the solution of the model into the density-matrix-renormalization formalism to reach larger system sizes. This should be possible in momentum space for weak electron-electron interactions. It is inevitable to work in momentum space, for the eigenstates of the current operator are needed.
- Relativistic corrections should be examined more rigorously to estimate the effect they have on quantum rings.
- We have neglected the quantization of the electro-magnetic field. The length scale down to which the model is valid should be determined.

A Units

The natural units (Tom99) in this thesis are defined by: $\hbar = c = e = k_B = 1$ (and $4\pi\epsilon_0 = 1$, whence $\mu_0 = 4\pi$). The remaining unit is chosen to be the energy 1eV.

Quantity	Symbol	natural units	SI	Explanation
Length	l	1/eV	$1.9732705 \times 10^{-7}\text{m}$	$= ct$
Mass	m	1 eV	$1.7826627 \times 10^{-36}\text{kg}$	$= E/c^2$
Time	t	1/eV	$6.5821220 \times 10^{-16}\text{s}$	$= \hbar/E$
Frequency	f	eV	$1.5192669 \times 10^{15}\text{Hz}$	$= 1/t$
Speed	v	1	$2.99792458 \times 10^8\text{m/s}$	$c \stackrel{!}{=} 1$
Momentum	p	1 eV	$5.3442883 \times 10^{-28}\text{kg m/s}$	$= cm$
Force	F	1 eV ²	$8.1194003 \times 10^{-13}\text{N}$	$= p/t$
Power	P	1 eV ²	0.24341350mW	$= E/t$
Energy	E	1 eV	$1.6021773 \times 10^{-19}\text{J}$	$\stackrel{!}{=} 1\text{ eV}$
Charge	q	1	$1.6021773 \times 10^{-19}\text{C}$	$e \stackrel{!}{=} 1$
Charge density	ρ	1 eV ³	20.852143C/m^2	$= e/l^3$
Current	J	1 eV	$2.4341349 \times 10^{-4}\text{A}$	$= e/t$
Current density	j	1 eV ³	$6.2513152 \times 10^9\text{A/m}^2$	$= J/l^2$
Potential	U	1 eV	1V	$= E/e$
Electrical field	E	1 eV ²	$5.0677289 \times 10^6\text{V/m}$	$= U/l$
Polarization	P	1 eV ²	$4.114692 \times 10^{-6}\text{C/m}^2$	$= e/l^2$
Resistance	R	1	$4.1082357 \times 10^3\Omega$	$= U/J$
Conductivity	σ	1 eV	$1.2335536 \times 10^3\text{S/m}$	$= \frac{J}{U/l}$
Capacitance	C	1/eV	$1.60217733 \times 10^{-19}\text{F}$	$= e/U$
Magnetic flux	ϕ	1	$6.5821217 \times 10^{-16}\text{Wb}$	$= \frac{\hbar}{e} = \frac{\phi_0^{\text{S.C.}}}{\pi}$
Magnetic induction	B	1 eV ²	$1.6904124 \times 10^{-2}\text{T}$	$= \phi/l^2$
Magnetization	M	1 eV ²	$1.2335536 \times 10^3\text{A/m}$	$= J/l$
Inductance	L	1/eV	$2.07040908 \times 10^{-12}\text{H}$	$= \phi/J$
Temperature	T	1 eV	$1.1604447 \times 10^4\text{K}$	$= E/k_B$

B Continuum model for quantum rings

This appendix provides additional information needed for the calculations in Sec. 2. The Schrödinger equation of a quantum ring with an infinite potential wall, threaded by a flux tube has been examined in Sec. 2.2. The expansion of the radial ground-state wave function in orders of the ring width was verified with the use of the MATHEMATICA notebook in Sec. 2.2.

The influence of a homogeneous magnetic field on a quantum ring has been expanded in orders of the ring width. The usual formulas of perturbation theory have been applied to the problem. In the course of the calculations, an integral over the product of the azimuthal wave function and the first derivative of the azimuthal wave function appeared. The value of this integral is calculated in Sec. B.2.

B.1 Asymptotic expansion of a two-dimensional ring

In the following, the MATHEMATICA notebook for the evaluation of the asymptotic expansion of the radial ground-state wave function and the lowest energy levels of a ring threaded by a magnetic flux tube is shown.

Separation of the radius r_n , the radial wave function ψ , the differential operator d and the energy eng into different orders of the ring width ϵ .

```
In[1]:= rn = r0 + eps r;
psi[r_] =
  1/Sqrt[eps] psi0[r] + Sqrt[eps] psi1[r] + eps^(3/2) psi2[r] +
  eps^(5/2) psi3[r] + eps^(7/2) psi4[r] + eps^(9/2) psi5[r];
d = (r0^2/eps^2 psi''[r] + 2r0 r/eps psi''[r] + r0/eps psi'[r] +
  r^2 psi''[r] + r psi'[r]); dlinks =
Normal[Series[Collect[d, eps], {eps, 0, 3}]];
eng = em2/eps^2 + em1/eps + e0 + e1 eps + e2 eps^2 + e3 eps^3;
drechts = Normal[Series[-(eng rn^2 - ksi^2) psi[r], {eps, 0, 3}]];
```

The first equation that has to be solved is of the order $-5/2$ in ϵ .

```
In[6]:= g11 =
Simplify[
  Coefficient[dlinks, eps^(-5/2)] -
  Coefficient[drechts, eps^(-5/2)] == 0]
```

```
Out[6]= r0 (em2 psi0[r] + psi0''[r]) == 0
```

```
In[7]:= DSolve[%,psi0[r],r]
```

B Continuum model for quantum rings

```
Out[7]= {{psi0[r]->C[1] Cos[Sqrt[em2] r] + C[2] Sin[Sqrt[em2] r]}}
```

Applying the boundary condition for the radial wave function leads to the first order of the energy em_2 and the first order of the wave function psi_0 .

```
In[8]:= em2 = Pi^2;
psi0[r_] = Cos[Pi r]/Sqrt[Pi r0];
```

The scalar product is separated into its orders of ϵ as well. The normalization of the proposed wave function psi_0 is tested in lowest order (with the symmetric scalar product).

```
In[10]:= symska[f_, g_] := 2 Pi Integrate[r0 f[r] g[r], {r, -1/2, +1/2}];
asymska[f_, g_] := 2Pi Integrate[r f[r] g[r], {r, -1/2, 1/2}];
symska[psi0[#] &, psi0[#] &]
```

```
Out[12]= 1
```

The second order equation leads to the second order energy and the second order wave function.

```
In[13]:= dgl2 = FullSimplify[
  Coefficient[dlinks, eps^(-3/2)] ==
  Coefficient[drechts, eps^(-3/2)], {Element[r, Reals]
  , eps > 0, r0 > 0}]
DSolve[dgl2, psi1[r], r];
psi11[r_] = psi1[r] /. Flatten[%];
gl211 = psi11[-1/2] == 0;
gl212 = psi11[+1/2] == 0;
rule211 = Solve[{gl211, gl212}, {em1, C[2], C[1]}];
psi12[r_] = psi11[r] /. Flatten[{rule211}];
em1 = em1 /. Flatten[{rule211}]
gl213 = eps asymska[psi0[#] &, psi0[#] &]
+ 2 symska[psi0[#] &, psi12[#] &] == 0;
rule213 = Solve[gl213, {C[1], C[2]}];
psi1[r_] =
  FullSimplify[
  psi12[r] /. Flatten[{rule213}],
  {Element[r, Reals], eps > 0, r0 > 0}]
```

```
Out[13]= em1 r0^(3/2) Cos[Pi r] + Sqrt[Pi] r0^2
(Pi^2 psi1[r] + psi1''[r]),
== Pi Sqrt[r0] Sin[Pi r]
```

```
Out[20]= 0
```

```
Out[23]= -r Cos[Pi r]/(2 Sqrt[Pi] r0^(3/2))
```

The third order follows:

```
In[24]:= dgl3 = FullSimplify[
  Coefficient[dlinks, eps^(-1/2)] ==
  Coefficient[drechts, eps^(-1/2)],
  {Element[r, Reals], eps > 0, r0 > 0}]
DSolve[dgl3, psi2[r], r];
psi21[r_] = psi2[r] /. Flatten[%];
```

B.1 Asymptotic expansion of a two-dimensional ring

```

gl311 = psi21[-1/2] == 0;
gl312 = psi21[+1/2] == 0;
rule311 = Solve[{gl311, gl312}, {e0, C[2], C[1]}];
psi22[r_] = psi21[r] /. Flatten[{rule311}];
e0 = e0 /. Flatten[{rule311}];
gl313 = 2 asymska[psi0[#] &, psi1[#] &]
+ symska[psi1[#] &, psi1[#] &]
+ 2 symska[psi0[#] &, psi22[#] &] == 0;
rule313 = Solve[gl313, {C[1], C[2]}];
psi2[r_] =
FullSimplify[
psi22[r] /. Flatten[{rule313}],
{Element[r, Reals], eps > 0, r0 > 0}]

```

```

Out[24]= 1/Sqrt[r0](( - 1 - 2 ksi^2 + 2 e0 r0^2) Cos[Pi r]
+3 Pi r Sin[Pi r]
+ 2 Sqrt[Pi] r0^(5/2) (Pi^2 psi2[r]+psi2''[r])) == 0

```

```

Out[31]= -(1 - 4 ksi^2)/(4 r0^2)

```

```

Out[34]= 3 r^2 Cos[Pi r]/(8 Sqrt[Pi] r0^(5/2))

```

The fourth order is:

```

In[35]:= dgl4 = FullSimplify[
Coefficient[dlinks, eps^(1/2)] ==
Coefficient[drechts, eps^(1/2)], {Element[r, Reals], eps > 0, r0 > 0}]
DSolve[dgl4, psi3[r], r];
psi31[r_] = psi3[r] /. Flatten[%];
gl411 = psi31[-1/2] == 0;
gl412 = psi31[+1/2] == 0;
rule411 = Solve[{gl411, gl412}, {e1, C[2], C[1]}];
psi32[r_] =
FullSimplify[
psi31[r] /. Flatten[{rule411}],
{Element[r, Reals], eps > 0, r0 > 0}];
e1 = e1 /. Flatten[{rule411}];
gl413 = 2 asymska[psi0[#] &, psi2[#] &] + asymska[psi1[#] &, psi1[#] &] +
2 symska[psi0[#] &, psi32[#] &] + 2symska[psi1[#] &, psi2[#] &] == 0;
rule413 = Solve[gl413, {C[1], C[2]}];
psi3[r_] =
FullSimplify[
psi32[r] /. Flatten[{rule413}], {Element[r, Reals], eps > 0, r0 > 0}]

```

```

Out[35]= ((11+16 ksi^2) r Cos[Pi r]-15 Pi r^2 Sin[Pi r]+
8 Sqrt[Pi] r^(7/2) ((-2 r (-2+8 ksi^2 +5 Pi^2 r^2)
Cos[Pi r]-(-1+4 ksi^2) Pi (-1+4 r^2) Sin[Pi r]))/(32 Sqrt[Pi] r0^(7/2))+
(-60 Pi^2 r Cos[Pi r]+
2 Pi^2 r (-2+8 ksi^2 + 5 Pi^2 r^2) Cos[Pi r]+
4 Pi (-2+8 ksi^2+15 Pi^2 r^2) Sin[Pi r]-
(-1+4ksi^2) Pi
(16 Pi r Cos[Pi r]+ 8 Sin[Pi r]-
Pi^2 (-1+4 r^2) Sin[Pi r]))/(32 Pi^(5/2) r^(7/2)))/Sqrt[r0]==0

```

```

Out[42]= 0

```

```

Out[45]= (-2 r (-2+8 ksi^2+5 Pi^2 r^2) Cos[Pi r]-
(-1+4 ksi^2) Pi (-1+4 r^2) Sin[Pi r])/((32 Pi^(5/2) r0^(7/2))

```

The fourth order correction to a $\text{Cos}[\text{Pi } r]/\text{Sqrt}[\text{Pi } \text{eps } (r_0+\text{eps } r)]$ function is:

```

In[46]:= FullSimplify[psi0[r] eps^(-1/2)+psi1[r] eps^(1/2)+psi2[r] eps^(3/2)+

```

```

psi3[r] eps^(5/2)-
Normal[Series[Cos[Pi r]/Sqrt[Pi eps(r0 + eps r)], {eps, 0, 3}]]
Out[46]= -(eps^(5/2) (-1+4 ksi^2) (4 r Cos[Pi r]+Pi (-1+4r^2) Sin[Pi r]))/
(32 Pi^(5/2) r0^(7/2))

```

B.2 Perturbation theory

The problem of a quantum ring in a homogeneous magnetic field was expanded in terms of a quantum ring threaded by a flux tube in Sec. 2.3. The perturbation expansion is the standard perturbation expansion. The integral on p. 115 over the complex conjugated wave function and the first derivative of the wave function plays an important role in this expansion. The result has been used in Eq. 2.65. The first derivative of the azimuthal wave function is discontinuous at the locations of the δ -functions in the potential. In fact, there are δ -functions appearing in the first derivative of the wave function. Integrating over a product of a discontinuous function and a δ -function leads to the result

$$\int_{-\infty}^{\infty} \delta(x) f(x) dx = \lim_{\epsilon \rightarrow 0} \frac{1}{2} [f(-\epsilon) + f(\epsilon)]. \quad (\text{B.1})$$

We use the definition $\xi = \xi_\nu$ on the next page.

The last four terms in the penultimate equation on the next page can be analytically shown to vanish with the use of the continuity of the absolute value of the wave function at $\varphi = 0$.

$$\begin{aligned}
 & \int_0^{2\pi} \chi_{\nu}^* \chi_{\nu}' d\varphi \\
 &= \int_0^{2\pi} \left(A_0^* e^{-i\xi[\varphi-s(\varphi)]} + B_0^* e^{i\xi[\varphi-s(\varphi)]} \right) \\
 & \quad \left\{ \left[-i\beta + ik's'(\varphi) \right] \left(A_0 e^{i\xi[\varphi-s(\varphi)]} + B_0 e^{-i\xi[\varphi-s(\varphi)]} \right) + i\xi \left[1 - s'(\varphi) \right] \left(A_0 e^{i\xi[\varphi-s(\varphi)]} - B_0 e^{-i\xi[\varphi-s(\varphi)]} \right) \right\} d\varphi \\
 &= \lim_{\epsilon \rightarrow 0} N \int_{-\epsilon}^{\frac{2\pi}{N}-\epsilon} \left(A_0^* e^{-i\xi[\varphi-s(\varphi)]} + B_0^* e^{i\xi[\varphi-s(\varphi)]} \right) \\
 & \quad \left\{ \left[-i\beta + ik a \delta(\varphi) \right] \left(A_0 e^{i\xi[\varphi-s(\varphi)]} + B_0 e^{-i\xi[\varphi-s(\varphi)]} \right) + i\xi \left[1 - a \delta(\varphi) \right] \left(A_0 e^{i\xi[\varphi-s(\varphi)]} - B_0 e^{-i\xi[\varphi-s(\varphi)]} \right) \right\} d\varphi \\
 &= -2\pi i \beta + 2\pi i k \left[|A_0|^2 + |B_0|^2 + 2 \operatorname{Re}(A_0^* B_0) \right] + i\xi N \int_0^{\frac{2\pi}{N}} \left(|A_0|^2 e^{-2i \operatorname{Im} \xi \varphi} - |B_0|^2 e^{2i \operatorname{Im} \xi \varphi} - A_0^* B_0 e^{-2i \operatorname{Re} \xi \varphi} + B_0^* A_0 e^{2i \operatorname{Re} \xi \varphi} \right) d\varphi \\
 & \quad - 2\pi i \xi \frac{1}{2} \left[(A_0^* + B_0^*) (A_0 - B_0) \left(A_0^* e^{\frac{2\pi}{N} i \xi^*} + B_0^* e^{-\frac{2\pi}{N} i \xi^*} \right) \left(A_0 e^{-\frac{2\pi}{N} i \xi} - B_0 e^{\frac{2\pi}{N} i \xi} \right) \right] \\
 &= -2\pi i \beta + 2\pi i k \left[|A_0|^2 + |B_0|^2 + 2 \operatorname{Re}(A_0^* B_0) \right] \\
 & \quad - \frac{i\xi N}{2 \operatorname{Im} \xi} \left(|A_0|^2 e^{-\frac{4\pi}{N} \operatorname{Im} \xi} + |B_0|^2 e^{\frac{4\pi}{N} \operatorname{Im} \xi} - |A_0|^2 - |B_0|^2 \right) + \frac{i\xi N}{2 \operatorname{Re} \xi} \left(A_0^* B_0 e^{-\frac{4\pi}{N} i \operatorname{Re} \xi} + B_0^* A_0 e^{\frac{4\pi}{N} i \operatorname{Re} \xi} - A_0^* B_0 - B_0^* A_0 \right) \\
 & \quad - i\pi \xi \left(|A_0|^2 e^{-\frac{4\pi}{N} \operatorname{Im} \xi} - |B_0|^2 e^{\frac{4\pi}{N} \operatorname{Im} \xi} + |A_0|^2 - |B_0|^2 \right) - i\pi \xi \left(-A_0^* B_0 e^{\frac{4\pi}{N} i \operatorname{Re} \xi} + B_0^* A_0 e^{-\frac{4\pi}{N} i \operatorname{Re} \xi} - A_0^* B_0 + B_0^* A_0 \right) \\
 &= -2\pi i \beta + 2\pi i k \left[|A_0|^2 + |B_0|^2 + 2 \operatorname{Re}(A_0^* B_0) \right] \\
 &= -2\pi i \beta + 2\pi i k |A_0^* + B_0|^2
 \end{aligned} \tag{B.2}$$

C The periodic Anderson model

In this appendix, additional information on the periodic Anderson model is supplied. The first section shows a table of the operators that are important for calculating the Drude weight. These are the Hamiltonian, the paramagnetic current operator and the operator of the kinetic energy. These operators are most useful in the space of the quasi-particles. To get these operators, they are shown in real space (\mathfrak{R}), transformed to momentum space (\mathfrak{K}) and then, after a Bogoliubov transformation, obtained in the space of the quasi-particles (\mathfrak{B}). Only the results are given in the table.

A chapter about particle-hole symmetry shows how calculations for the symmetric periodic Anderson model for less than half filling could be mapped on the model for more than half filling. Although we have frequently described the lower band of the periodic Anderson model as being asymmetric (and thus leading to a negative Drude weight), the two bands together are in fact particle-hole symmetric.

In chapter 3, we have studied the noninteracting periodic Anderson model. To gain insight how the electron-electron coupling in the f -orbitals influences the behavior of the electrons in the model, we added a short section about the Hartree-Fock approximation in the antiferromagnetic phase. There is strong evidence that the ground state of the symmetric periodic Anderson model at half filling in one-dimension with local hybridization is antiferromagnetic.

C.1 Overview: Operators of the noninteracting PAM

	LH	NNH
\mathfrak{N}	$-t \sum_{l\delta\sigma} d_{l+\delta,\sigma}^\dagger d_{l\sigma} - V \sum_{l\sigma} (d_{l\sigma}^\dagger f_{l\sigma} + f_{l\sigma}^\dagger d_{l\sigma}) + \epsilon^f \sum_{l\sigma} n_{l\sigma}^f$	$-t \sum_{l\delta\sigma} d_{l+\delta,\sigma}^\dagger d_{l\sigma} - V \sum_{l\delta\sigma} (d_{l+\delta,\sigma}^\dagger f_{l\sigma} + f_{l+\delta,\sigma}^\dagger d_{l\sigma}) + \epsilon^f \sum_{l\sigma} n_{l\sigma}^f$
τ	$-t \sum_{l\delta\sigma} d_{l+\delta,\sigma}^\dagger d_{l\sigma}$	$-t \sum_{l\delta\sigma} d_{l+\delta,\sigma}^\dagger d_{l\sigma} - V \sum_{l\delta\sigma} (d_{l+\delta,\sigma}^\dagger f_{l\sigma} + f_{l+\delta,\sigma}^\dagger d_{l\sigma})$
j_p	$it \sum_{l\delta\sigma} \delta d_{l+\delta,\sigma}^\dagger d_{l\sigma}$	$it \sum_{l\delta\sigma} \delta d_{l+\delta,\sigma}^\dagger d_{l\sigma} + iV \sum_{l\delta\sigma} \delta (d_{l+\delta,\sigma}^\dagger f_{l\sigma} + f_{l+\delta,\sigma}^\dagger d_{l\sigma})$
\mathfrak{R}	$\sum_{\mathbf{k}\sigma} \left[\epsilon_{\mathbf{k}} d_{\mathbf{k}\sigma}^\dagger d_{\mathbf{k}\sigma} - V (d_{\mathbf{k}\sigma}^\dagger f_{\mathbf{k}\sigma} + f_{\mathbf{k}\sigma}^\dagger d_{\mathbf{k}\sigma}) + \epsilon^f n_{\mathbf{k}\sigma}^f \right]$	$\sum_{\mathbf{k}\sigma} \left\{ \epsilon_{\mathbf{k}} [d_{\mathbf{k}\sigma}^\dagger d_{\mathbf{k}\sigma} + \frac{V}{t} (d_{\mathbf{k}\sigma}^\dagger f_{\mathbf{k}\sigma} + f_{\mathbf{k}\sigma}^\dagger d_{\mathbf{k}\sigma})] + \epsilon^f n_{\mathbf{k}\sigma}^f \right\}$
τ	$\sum_{\mathbf{k}\sigma} \epsilon_{\mathbf{k}} d_{\mathbf{k}\sigma}^\dagger d_{\mathbf{k}\sigma}$	$\sum_{\mathbf{k}\sigma} \epsilon_{\mathbf{k}} [d_{\mathbf{k}\sigma}^\dagger d_{\mathbf{k}\sigma} + \frac{V}{t} (d_{\mathbf{k}\sigma}^\dagger f_{\mathbf{k}\sigma} + f_{\mathbf{k}\sigma}^\dagger d_{\mathbf{k}\sigma})]$
j_p	$\sum_{\mathbf{k}\sigma} \eta_{\mathbf{k}} d_{\mathbf{k}\sigma}^\dagger d_{\mathbf{k}\sigma}$	$\sum_{\mathbf{k}\sigma} \eta_{\mathbf{k}} [d_{\mathbf{k}\sigma}^\dagger d_{\mathbf{k}\sigma} + \frac{V}{t} (d_{\mathbf{k}\sigma}^\dagger f_{\mathbf{k}\sigma} + f_{\mathbf{k}\sigma}^\dagger d_{\mathbf{k}\sigma})]$
\mathfrak{B}	$\sum_{\mathbf{k}\sigma} [E_{\mathbf{k}}^+ b_{\mathbf{k}\sigma}^\dagger b_{\mathbf{k}\sigma} + E_{\mathbf{k}}^- a_{\mathbf{k}\sigma}^\dagger a_{\mathbf{k}\sigma}]$	$\sum_{\mathbf{k}\sigma} [E_{\mathbf{k}}^+ b_{\mathbf{k}\sigma}^\dagger b_{\mathbf{k}\sigma} + E_{\mathbf{k}}^- a_{\mathbf{k}\sigma}^\dagger a_{\mathbf{k}\sigma}]$
$E_{\mathbf{k}}^\pm$	$\frac{1}{2} [\epsilon_{\mathbf{k}} + \epsilon^f \pm \sqrt{(\epsilon_{\mathbf{k}} - \epsilon^f)^2 + 4V^2}]$	$\frac{1}{2} [\epsilon_{\mathbf{k}} + \epsilon^f \pm \sqrt{(\epsilon_{\mathbf{k}} - \epsilon^f)^2 + 4\frac{V^2 \epsilon_{\mathbf{k}}^2}{t^2}}]$
τ	$\sum_{\mathbf{k}\sigma} \epsilon_{\mathbf{k}} [\Xi_{\mathbf{k}}^+ b_{\mathbf{k}\sigma}^\dagger b_{\mathbf{k}\sigma} + \Xi_{\mathbf{k}}^- a_{\mathbf{k}\sigma}^\dagger a_{\mathbf{k}\sigma} + \Upsilon_{\mathbf{k}} (b_{\mathbf{k}\sigma}^\dagger a_{\mathbf{k}\sigma} + a_{\mathbf{k}\sigma}^\dagger b_{\mathbf{k}\sigma})]$	$\sum_{\mathbf{k}\sigma} \epsilon_{\mathbf{k}} [\Xi_{\mathbf{k}}^+ b_{\mathbf{k}\sigma}^\dagger b_{\mathbf{k}\sigma} + \Xi_{\mathbf{k}}^- a_{\mathbf{k}\sigma}^\dagger a_{\mathbf{k}\sigma} + \Upsilon_{\mathbf{k}} (b_{\mathbf{k}\sigma}^\dagger a_{\mathbf{k}\sigma} + a_{\mathbf{k}\sigma}^\dagger b_{\mathbf{k}\sigma})]$
$\Xi_{\mathbf{k}}^\pm$	$\frac{1}{2} \pm \frac{\epsilon_{\mathbf{k}} - \epsilon^f}{2\sqrt{(\epsilon_{\mathbf{k}} - \epsilon^f)^2 + 4V^2}}$	$\frac{1}{2} \pm \frac{(\epsilon_{\mathbf{k}} - \epsilon^f) + 4\frac{V^2 \epsilon_{\mathbf{k}}}{t^2}}{2\sqrt{(\epsilon_{\mathbf{k}} - \epsilon^f)^2 + 4\frac{V^2 \epsilon_{\mathbf{k}}^2}{t^2}}}$
$\Upsilon_{\mathbf{k}}$	$-\frac{V}{\sqrt{(\epsilon_{\mathbf{k}} - \epsilon^f)^2 + 4V^2}}$	$-\frac{\epsilon^f V}{t\sqrt{(\epsilon_{\mathbf{k}} - \epsilon^f)^2 + 4\frac{V^2 \epsilon_{\mathbf{k}}^2}{t^2}}}$
j_p	$\sum_{\mathbf{k}\sigma} \eta_{\mathbf{k}} [\Xi_{\mathbf{k}}^+ b_{\mathbf{k}\sigma}^\dagger b_{\mathbf{k}\sigma} + \Xi_{\mathbf{k}}^- a_{\mathbf{k}\sigma}^\dagger a_{\mathbf{k}\sigma} + \Upsilon_{\mathbf{k}} (b_{\mathbf{k}\sigma}^\dagger a_{\mathbf{k}\sigma} + a_{\mathbf{k}\sigma}^\dagger b_{\mathbf{k}\sigma})]$	$\sum_{\mathbf{k}\sigma} \eta_{\mathbf{k}} [\Xi_{\mathbf{k}}^+ b_{\mathbf{k}\sigma}^\dagger b_{\mathbf{k}\sigma} + \Xi_{\mathbf{k}}^- a_{\mathbf{k}\sigma}^\dagger a_{\mathbf{k}\sigma} + \Upsilon_{\mathbf{k}} (b_{\mathbf{k}\sigma}^\dagger a_{\mathbf{k}\sigma} + a_{\mathbf{k}\sigma}^\dagger b_{\mathbf{k}\sigma})]$
$\epsilon^f = 0$	$\frac{1}{2} \epsilon_{\mathbf{k}} \pm \frac{1}{2} \sqrt{\epsilon_{\mathbf{k}}^2 + 4V^2}$	$\frac{1}{2} \epsilon_{\mathbf{k}} \pm \frac{1}{2} \sqrt{\epsilon_{\mathbf{k}}^2 + 4\frac{V^2 \epsilon_{\mathbf{k}}^2}{t^2}}$
$E_{\mathbf{k}}^\pm$	$\frac{1}{2} \pm \frac{\epsilon_{\mathbf{k}}}{2\sqrt{\epsilon_{\mathbf{k}}^2 + 4V^2}}$	$\frac{1}{2} \pm \frac{\epsilon_{\mathbf{k}}}{2\sqrt{\epsilon_{\mathbf{k}}^2 + 4\frac{V^2 \epsilon_{\mathbf{k}}^2}{t^2}}}$
$\Xi_{\mathbf{k}}^\pm$	$-\frac{V}{\sqrt{\epsilon_{\mathbf{k}}^2 + 4V^2}}$	$-\frac{V}{\sqrt{\epsilon_{\mathbf{k}}^2 + 4\frac{V^2 \epsilon_{\mathbf{k}}^2}{t^2}}}$
$\Upsilon_{\mathbf{k}}$	0	0

C.2 Particle-hole symmetry in the PAM

To gain deeper insight into the physics and also to simplify calculations, conserved quantities of the periodic Anderson model have to be found. There are several known symmetries of the one-dimensional Hubbard model (similar to the PAM), e.g., its spin rotational invariance, making the total spin S and its z -component S_z good quantum numbers. In particular, particle-hole transformations turned out to be very helpful in finding useful relations between the filling and the chemical potential of all types of lattices. Special transformations are constructed to deal with bipartite lattices.

To apply those transformations to the periodic Anderson model, it is natural to use the grand canonical Hamiltonian:

$$\begin{aligned}
 K_{\text{PAM}} = & -t \sum_{(lm),\sigma} d_{l\sigma}^\dagger d_{m\sigma} + H_V \\
 & + U^f \sum_l n_{l\uparrow}^f n_{l\downarrow}^f \\
 & - \mu_d \sum_{l,\sigma} n_{l\sigma}^d - \mu_f \sum_{l,\sigma} n_{l\sigma}^f,
 \end{aligned} \tag{C.1}$$

where H_V is the local hybridization

$$-V \sum_{l,\sigma} \left(d_{l\sigma}^\dagger f_{l\sigma} + f_{l\sigma}^\dagger d_{l\sigma} \right), \tag{C.2}$$

or the nearest-neighbor hybridization

$$-V \sum_{(lm),\sigma} \left(d_{l\sigma}^\dagger f_{m\sigma} + f_{m\sigma}^\dagger d_{l\sigma} \right). \tag{C.3}$$

Independent chemical potentials μ_d and μ_f of the d and f sites are assumed in order to incorporate both, general fillings and general on-site energies.

For a lattice with a bipartite structure, the electrons can be transformed to holes and vice versa. With nearest-neighbor hybridization we use the transformation

$$\begin{aligned}
 d_{l\sigma}^\dagger & \rightarrow (-1)^{|l|} d_{l\sigma} & f_{l\sigma}^\dagger & \rightarrow (-1)^{|l|} f_{l\sigma} \\
 d_{l\sigma} & \rightarrow (-1)^{|l|} d_{l\sigma}^\dagger & f_{l\sigma} & \rightarrow (-1)^{|l|} f_{l\sigma}^\dagger,
 \end{aligned} \tag{C.4}$$

where $|l| = \sum_{\ell=1}^d |l_\ell|$. This ensures different signs on the different sub-lattices. This transformation is canonical, for it leaves the canonical anticommutator relations (3.37)

C The periodic Anderson model

unchanged. Inserting this transformation into the periodic Anderson model yields:

$$\begin{aligned}
\tilde{K}_{\text{PAM}} &= -t \sum_{(lm),\sigma} d_{l\sigma}^\dagger d_{m\sigma} - V \sum_{(lm),\sigma} \left(f_{m\sigma}^\dagger d_{l\sigma} + d_{l\sigma}^\dagger f_{m\sigma} \right) \\
&\quad + U^f \sum_l \left(1 - n_{l\uparrow}^f \right) \left(1 - n_{l\downarrow}^f \right) \\
&\quad - \mu_d \sum_{l,\sigma} \left(1 - n_{l\sigma}^d \right) - \mu_f \sum_{l,\sigma} \left(1 - n_{l\sigma}^f \right) \\
&= -t \sum_{(lm),\sigma} d_{l\sigma}^\dagger d_{m\sigma} - V \sum_{(lm),\sigma} \left(d_{l\sigma}^\dagger f_{m\sigma} + f_{m\sigma}^\dagger d_{l\sigma} \right) \\
&\quad + U^f \sum_l n_{l\uparrow}^f n_{l\downarrow}^f - (U^f - \mu_f) \sum_{l,\sigma} n_{l\sigma}^f - (-\mu_d) \sum_{l,\sigma} n_{l\sigma}^d \\
&\quad + L \left(U^f - 2(\mu_f + \mu_d) \right) \\
&= H_t + H_V + H_{U^f} + H_{\tilde{\mu}_f=U^f-\mu_f} + H_{\tilde{\mu}_d=-\mu_f} + L \left(U^f - 2(\mu_f + \mu_d) \right).
\end{aligned} \tag{C.5}$$

At half filling, the original and the transformed grand canonical Hamiltonians must be identical: $K_{\text{PAM}} \stackrel{!}{=} \tilde{K}_{\text{PAM}}$. By comparing them, we find:

$$\begin{aligned}
\mu_f &= \frac{U^f}{2}, \\
\mu_d &= 0.
\end{aligned} \tag{C.6}$$

By shifting the chemical potential of the f -sites by $U^f/2$, thus writing the interaction in a particle-hole symmetric manner, both chemical potentials are zero.

For local hybridization, the transformation has to be chosen according to

$$\begin{aligned}
d_{l\sigma}^\dagger &\rightarrow (-1)^{|l|} d_{l\sigma} & f_{l\sigma}^\dagger &\rightarrow -(-1)^{|l|} f_{l\sigma} \\
d_{l\sigma} &\rightarrow (-1)^{|l|} d_{l\sigma}^\dagger & f_{l\sigma} &\rightarrow -(-1)^{|l|} f_{l\sigma}^\dagger.
\end{aligned} \tag{C.7}$$

This transformation is also canonical and fulfills (3.37). The terms in (C.5) that contain a creator and an annihilator of f -electrons through $n_{l\sigma}^f$ are unchanged by the two supplementary signs. The terms that describe the hybridization contain a minus sign for next neighbor hybridization, because the operators for d - and f -electrons act on different sub-lattices. This effect is compensated by the two additional signs in the transformation.

The particle density n is transformed into the hole density \tilde{n} , thus, for the total density on a lattice site we get:

$$\begin{aligned}
\tilde{n} &= \frac{1}{N} \sum_{l,\sigma} \left(\langle \tilde{d}_{l\sigma}^\dagger \tilde{d}_{l\sigma} \rangle + \langle \tilde{f}_{l\sigma}^\dagger \tilde{f}_{l\sigma} \rangle \right) \\
&= \frac{1}{N} \sum_{l,\sigma} \left(2 - \langle d_{l\sigma}^\dagger d_{l\sigma} \rangle - \langle f_{l\sigma}^\dagger f_{l\sigma} \rangle \right) \\
&= \frac{1}{N} (4N - \langle n \rangle) \\
&= 4 - n.
\end{aligned} \tag{C.8}$$

This symmetry allows us to restrict ourselves to half filling or less.

C.3 Hartree-Fock study of the PAM

The periodic Anderson model is used to describe heavy-fermion materials. These materials exhibit different ground states: antiferromagnetic, superconducting, paramagnetic, or semiconducting. Therefore, it is useful to investigate the ground state of the Anderson lattice. Studies of this model have shown contradictory results regarding the magnetism of the ground state. Paramagnetic (Ris92), ferromagnetic (REH92) and antiferromagnetic (MW93) ground states have been found in the model with local hybridization depending on the approximation method being applied. The antiferromagnetic ground state for the symmetric case ($\epsilon^f = 0$) at half filling was confirmed by density-matrix renormalization group studies of Guerrero and Noack (GN96). There are two rigorous results for the half-filled symmetric periodic Anderson model: The ground state of the symmetric periodic Anderson model in any dimension at half filling for any coupling strength is unique and forms a total spin singlet [$S = 0$] (UTS92), and there is a short-range antiferromagnetic order in the ground state (Tia94).

Therefore, we study the periodic Anderson model within the Hartree-Fock approximation in the antiferromagnetic phase. Weak Coulomb interaction of the f -electrons is thus included. In order to implement this approximation, the Hamiltonian of the interaction,

$$H_U = U^f \sum_l n_{l\uparrow}^f n_{l\downarrow}^f, \quad (\text{C.9})$$

is replaced by a one-particle operator,

$$H_U = U^f \sum_l \left(\langle n_{l\uparrow}^f \rangle n_{l\downarrow}^f + \langle n_{l\downarrow}^f \rangle n_{l\uparrow}^f - \langle n_{l\uparrow}^f \rangle \langle n_{l\downarrow}^f \rangle \right). \quad (\text{C.10})$$

In the paramagnetic phase, this leads to an effective f -level:

$$\tilde{\epsilon}_{l\sigma}^f = \epsilon^f + U \langle n_{l,-\sigma}^f \rangle. \quad (\text{C.11})$$

In an antiferromagnet on a bipartite lattice, the magnetization on the two different sublattices points in opposite directions. Accordingly, we set [see, e.g., (vD93)]

$$\langle n_{l\uparrow}^f - n_{l\downarrow}^f \rangle = m_l = (-1)^{|l|} m \neq 0, \quad (\text{C.12})$$

which—at the filling $n = \langle n^f \rangle$ —results in

$$\left. \begin{aligned} \langle n_{l\uparrow}^f \rangle &= \frac{n}{2} [1 + (-1)^{|l|} m] \\ \langle n_{l\downarrow}^f \rangle &= \frac{n}{2} [1 - (-1)^{|l|} m] \end{aligned} \right\} \langle n_{l\sigma}^f \rangle = \frac{n}{2} [1 + \sigma(-1)^{|l|} m]. \quad (\text{C.13})$$

The terms that contribute to the Hamiltonian within the Hartree-Fock approximation

C The periodic Anderson model

are:

$$\begin{aligned}
-U^f \sum_l \langle n_{l\uparrow}^f \rangle \langle n_{l\downarrow}^f \rangle &= -U^f n^2 \sum_l \frac{1}{4} [1 + (-1)^{|l|} m] [1 - (-1)^{|l|} m] \\
&= -U^f n^2 \sum_l \frac{1}{4} [1 - (-1)^{2|l|} m^2] \\
&= -\frac{U^f n^2}{4} \sum_l (1 - m^2) \\
&= -\frac{U^f N_f n^2}{4} (1 - m^2)
\end{aligned} \tag{C.14}$$

and

$$\begin{aligned}
U^f \sum_l \left(\langle n_{l\downarrow}^f \rangle n_{l\uparrow}^f + \langle n_{l\uparrow}^f \rangle n_{l\downarrow}^f \right) \\
&= U^f n \sum_l \left(\frac{1}{2} [1 - (-1)^{|l|} m] n_{l\uparrow}^f + \frac{1}{2} [1 + (-1)^{|l|} m] n_{l\downarrow}^f \right) \\
&= U^f n \sum_l \left[\frac{1}{2} (n_{l\uparrow}^f + n_{l\downarrow}^f) - \frac{1}{2} (-1)^{|l|} m n_{l\uparrow}^f + \frac{1}{2} (-1)^{|l|} m n_{l\downarrow}^f \right] \\
&= \frac{U^f N_f n}{2} + \frac{U^f n m}{2} \sum_{l,\sigma} (-\sigma) (-1)^{|l|} n_{l\sigma}^f \\
&= \frac{U^f N_f n}{2} - \frac{U^f n m}{2} \sum_{l,\sigma} \sigma (-1)^{|l|} n_{l\sigma}^f.
\end{aligned} \tag{C.15}$$

For the symmetric periodic Anderson model ($\epsilon^f = 0$) at the filling $\langle n^f \rangle = n$, the Hamiltonian is

$$\begin{aligned}
H_{\text{PAM}}^{\text{HF}} &= -t \sum_{(lm),\sigma} d_{l\sigma}^\dagger d_{m\sigma} - V \sum_{(lm),\sigma} \left(d_{l\sigma}^\dagger f_{m\sigma} + f_{m\sigma}^\dagger d_{l\sigma} \right) \\
&\quad - \frac{U^f n m}{2} \sum_{l,\sigma} \sigma (-1)^{|l|} n_{l\sigma}^f + \frac{U^f N_f n}{2} \\
&\quad - \frac{U^f N_f n^2}{4} (1 - m^2) - \mu \sum_{l,\sigma} \left(n_{l\sigma}^d + n_{l\sigma}^f \right).
\end{aligned} \tag{C.16}$$

The third term has to be Fourier transformed. To this end, we insert the Fourier-transformed creators and annihilators into the interaction term in the Hamiltonian and obtain, replacing $(-1)^{|l|}$ by $e^{ix_l \mathbf{Q}}$, with $\mathbf{Q} = (\pi, \pi, \dots)$:

$$\begin{aligned}
& - \sum_{\sigma} \frac{U^f n m \sigma}{2N^d} \sum_{\mathbf{k}, \mathbf{k}'} \sum_l e^{ix_l \mathbf{Q}} e^{-i(\mathbf{k}-\mathbf{k}') \cdot \mathbf{x}_l} f_{\mathbf{k}\sigma}^\dagger f_{\mathbf{k}'\sigma} \\
&= - \sum_{\sigma} \frac{U^f n m \sigma}{2} \sum_{\mathbf{k}, \mathbf{k}'} \delta_{\mathbf{k}', \mathbf{k}-\mathbf{Q}} f_{\mathbf{k}\sigma}^\dagger f_{\mathbf{k}'\sigma} \\
&= - \frac{U^f n m}{2} \sum_{\mathbf{k}, \sigma} \sigma f_{\mathbf{k}\sigma}^\dagger f_{\mathbf{k}-\mathbf{Q}\sigma}.
\end{aligned} \tag{C.17}$$

C.3 Hartree-Fock study of the PAM

The sum over the momenta can be split up into a sum over the momenta with $\epsilon_{\mathbf{k}} > 0$ and $\epsilon_{\mathbf{k}} < 0$. After this splitting procedure, the Hamiltonian is

$$\begin{aligned}
H_{\text{PAM}}^{\text{HF}} = \sum_{\substack{\mathbf{k}, \sigma \\ \epsilon_{\mathbf{k}} > 0}} & \left[\epsilon_{\mathbf{k}} \left(n_{\mathbf{k}\sigma}^d - n_{\mathbf{k}-\mathbf{Q}\sigma}^d \right) \right. \\
& + V_{\mathbf{k}} \left(d_{\mathbf{k}\sigma}^\dagger f_{\mathbf{k}\sigma} + f_{\mathbf{k}\sigma}^\dagger d_{\mathbf{k}\sigma} - d_{\mathbf{k}-\mathbf{Q}\sigma}^\dagger f_{\mathbf{k}-\mathbf{Q}\sigma} - f_{\mathbf{k}-\mathbf{Q}\sigma}^\dagger d_{\mathbf{k}-\mathbf{Q}\sigma} \right) \\
& - U^f n m \sigma \left(f_{\mathbf{k}\sigma}^\dagger f_{\mathbf{k}-\mathbf{Q}\sigma} + f_{\mathbf{k}-\mathbf{Q}\sigma}^\dagger f_{\mathbf{k}\sigma} \right) \\
& \left. - \mu \left(n_{\mathbf{k}\sigma}^d + n_{\mathbf{k}-\mathbf{Q}\sigma}^d + n_{\mathbf{k}\sigma}^f + n_{\mathbf{k}-\mathbf{Q}\sigma}^f \right) \right] \\
& + \frac{U^f N_f n}{2} - \frac{U^f N_f n^2}{4} (1 - m^2) - \mu (N_d + N_f).
\end{aligned} \tag{C.18}$$

This Hamiltonian can be written in a more compact form with the use of the matrix

$$M_{\mathbf{k}\sigma} = \begin{pmatrix} \epsilon_{\mathbf{k}} & V_{\mathbf{k}} & 0 & 0 \\ V_{\mathbf{k}} & 0 & 0 & -U^f n m \sigma \\ 0 & 0 & -\epsilon_{\mathbf{k}} & -V_{\mathbf{k}} \\ 0 & -U^f n m \sigma & -V_{\mathbf{k}} & 0 \end{pmatrix} \tag{C.19}$$

and the vector

$$\psi_{\mathbf{k}\sigma} = \begin{pmatrix} d_{\mathbf{k}\sigma} \\ f_{\mathbf{k}\sigma} \\ d_{\mathbf{k}-\mathbf{Q}\sigma} \\ f_{\mathbf{k}-\mathbf{Q}\sigma} \end{pmatrix}. \tag{C.20}$$

The result is

$$H_{\text{PAM}}^{\text{HF}} = \sum_{\substack{\mathbf{k}, \sigma \\ \epsilon_{\mathbf{k}} > 0}} \psi_{\mathbf{k}\sigma}^\dagger M_{\mathbf{k}\sigma} \psi_{\mathbf{k}\sigma} + \frac{U^f N_f n}{2} - \frac{U^f N_f n^2}{4} (1 - m^2) - \mu (N_d + N_f). \tag{C.21}$$

The real symmetric matrix $M_{\mathbf{k}\sigma}$ is diagonalizable. For the thermodynamic behavior, the eigenvalues are most important. With the definitions

$$\begin{aligned}
a &= \epsilon_{\mathbf{k}}^2 + (nmU^f)^2 + 2V_{\mathbf{k}}^2, \\
b &= \sqrt{[\epsilon_{\mathbf{k}}^2 - (mnU^f)^2]^2 + 4[\epsilon_{\mathbf{k}}^2 + (mnU^f)^2] V_{\mathbf{k}}^2},
\end{aligned} \tag{C.22}$$

the eigenvalues are

$$\begin{aligned}
(+\lambda_+) &= \sqrt{\frac{1}{2}(a+b)}, \\
(-\lambda_+) &= -\sqrt{\frac{1}{2}(a+b)}, \\
(+\lambda_-) &= \sqrt{\frac{1}{2}(a-b)}, \\
(-\lambda_-) &= -\sqrt{\frac{1}{2}(a-b)}.
\end{aligned} \tag{C.23}$$

With the band index $\tau = \pm$, the four eigenvalues can be combined to two energy bands $[(\lambda_{\pm}) \text{ and } (-\lambda_{\pm}) \rightarrow E_{\mathbf{k}}^{\pm}]$:

$$E_{\mathbf{k}}^{\tau} = \tau \operatorname{sgn}(\epsilon_{\mathbf{k}}) \sqrt{\frac{1}{2}(a + \tau b)}. \quad (\text{C.24})$$

The obtained band structure is shown in Fig. C.1 for local hybridization and in Fig. C.2 for nearest-neighbor hybridization.

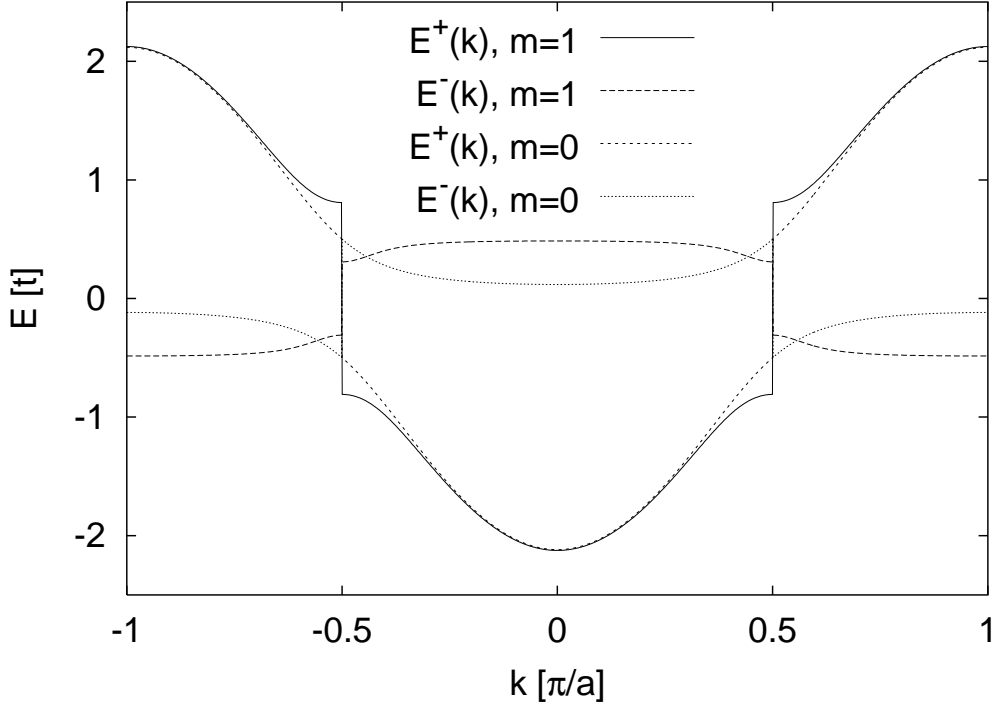


Figure C.1: Band structure of the one-dimensional symmetric periodic Anderson model with local hybridization in the antiferromagnetic phase, $U^f = 0.5$ and $V = 0.5$. The lowering of the ground state energy for the half-filled model due to the magnetization m is visualized by plotting the band structure for $m = 1$ and $m = 0$.

With the information provided above, the symmetry of the ground state can be studied. The ground-state energy needs to be expressed in terms of the magnetization m . Minimizing the ground-state energy with respect to the magnetization will show that for nearest-neighbor hybridization the ground state of the periodic Anderson model is antiferromagnetic within the Hartree-Fock approximation for weak Coulomb repulsion U^f . A critical interaction strength $U_c^f(V)$ is found below which the ground state is antiferromagnetic and above which the ground state becomes paramagnetic. In contrast, the model with local hybridization exhibits paramagnetism for weak interaction and antiferromagnetism for strong interaction (GKKR96; GN96).

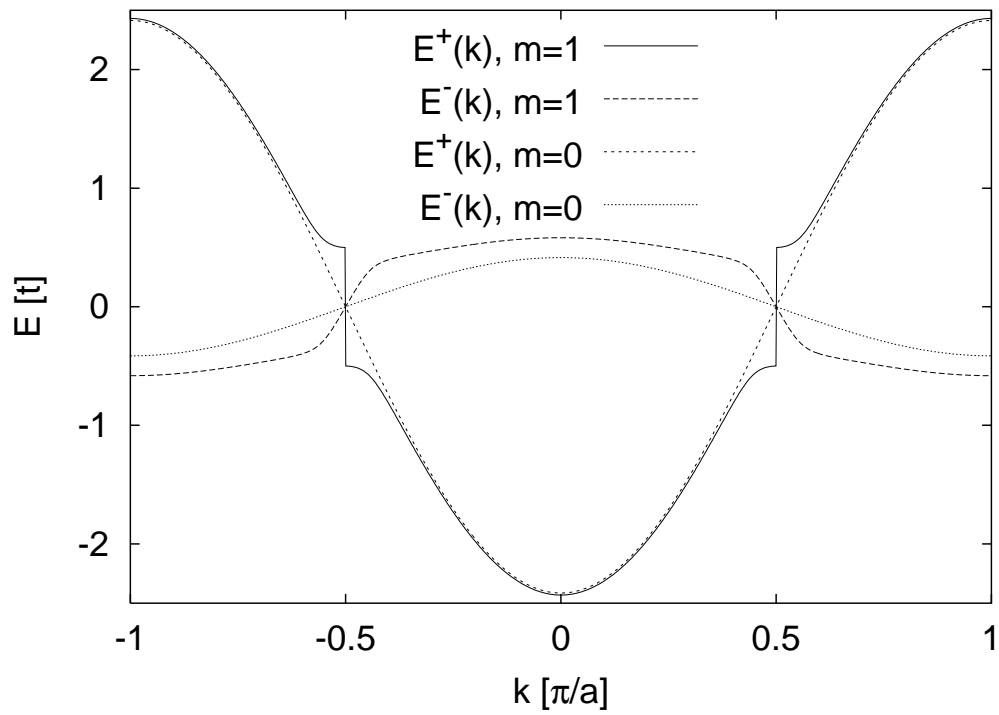


Figure C.2: Band structure of the one-dimensional symmetric periodic Anderson model with nearest-neighbor hybridization in the antiferromagnetic phase, $U^f = 0.5$, and $V = 0.5$.

Bibliography

- [AB59] Y. Aharonov and D. Bohm, *Significance of electromagnetic potentials in the quantum theory*, Phys. Rev. **115** (1959), 485. 7
- [AGI91] B. L. Altshuler, Y. Gefen, and Y. Imry, *Persistent differences between canonical and grand canonical averages in mesoscopic ensembles: Large paramagnetic orbital susceptibilities*, Phys. Rev. Lett. **66** (1991), 88. 11
- [AM76] Neil W. Ashcroft and N. David Mermin, *Solid state physics*, Saunders College Publishing, New York, 1976. 43
- [AR98] A. Aviram and M. A. Ratner (eds.), *Molecular electronics: Science and technology*, New York Academy of Sciences, New York, 1998. 8
- [BBG00] C. D. Batista, J. Bonča, and J. E. Gubernatis, *Ferromagnetism in the two-dimensional periodic Anderson model*, Phys. Rev. B **63** (2000), 184428. 54
- [BCB98] Robert J. Bursill, Christopher Castleton, and William Barford, *Optimal parameterisation of the Pariser-Parr-Pople model for benzene and biphenyl*, Chemical Physics Letters **294** (1998), 307. 79, 96
- [BG98] J. Bonča and J. E. Gubernatis, *Effects of doping on spin correlations in the periodic Anderson model*, Phys. Rev. B **58** (1998), 6992. 56
- [BIA84] M. Büttiker, Y. Imry, and M. Ya. Azbel, *Quantum oscillations in one-dimensional normal-metal rings*, Phys. Rev. A **30** (1984), 1982. 11
- [BIL83] M. Büttiker, Y. Imry, and R. Landauer, *Josephson behavior in small normal one-dimensional rings*, Phys. Lett. **96A** (1983), 365. 7, 11, 27
- [Blo70] F. Bloch, *Josephson effect in a superconducting ring*, Phys. Rev. B **2** (1970), 109. 11, 27
- [Blü03] Nils Blümer, *Mott-Hubbard metal-insulator transition and optical conductivity in high dimensions*, Berichte aus der Physik, Shaker, Herzogenrath, 2003. 44
- [BY61] N. Byers and C. N. Yang, *Theoretical considerations concerning quantized magnetic flux in superconducting cylinders*, Phys. Rev. Lett. **7** (1961), 46. 11, 27

- [CB02] C. W. M. Castleton and W. Barford, *Screening and quantitative π -model description of the optical spectra and polarizations of phenyl based oligomers*, Journal of Chemical Physics **117** (2002), 3570. 79, 96
- [CP94] Tapash Chakraborty and Pekka Pietiläinen, *Electron-electron interaction and the persistent current in a quantum ring*, Phys. Rev. B **50** (1994), 8460. 28
- [CWB⁺91] V. Chandrasekhar, R. A. Webb, M. J. Brady, M. B. Ketchen, W. J. Gallagher, and A. Kleinsasser, *Magnetic response of a single, isolated gold loop*, Phys. Rev. Lett. **67** (1991), 3578. 11
- [CZP95] H. Castella, X. Zotos, and P. Prelovsek, *Integrability and ideal conductance at finite temperatures*, Phys. Rev. Lett. **74** (1995), 972. 47
- [Dai64] B. P. Dailey, *Chemical shifts, ring currents + magnetic anisotropy in aromatic hydrocarbons*, J. Chem. Phys. **41** (1964), 2304. 97
- [DM01] C. D. Dimitrakopoulos and D. J. Mascaró, *Organic thin-film transistors: A review of recent advances*, IBM J. Res. & Dev. **45** (2001), 11. 8
- [DWL68] Hyp J. Dauben, Jr. James Dennis Wilson, and John L. Laity, *Diamagnetic susceptibility exaltation as a criterion of aromaticity*, J. Am. Chem. Soc. **90** (1968), 811. 10, 97
- [DWL69] Hyp J. Dauben, Jr. J. Dennis Wilson, and John L. Laity, *Diamagnetic susceptibility exaltation in hydrocarbons*, J. Am. Chem. Soc. **91** (1969), 1991. 10, 97
- [EJ61] J. A. Elvidge and L. M. Jackman, J. Chem. Soc. (1961), 859. 9
- [FLI⁺01] A. Fuhrer, S. Lüscher, T. Ihn, T. Heinzl, K. Ensslin, W. Wegscheider, and M. Bichler, *Energy spectra of quantum rings*, Nature **413** (2001), 822. 11, 12, 13
- [Fly74] W. H. Flygare, *Magnetic interactions in molecules and an analysis of molecular electronic charge distribution from magnetic parameters*, Chem. Rev. **74** (1974), 653. 10
- [FMS⁺91] R. M. Fye, M. J. Martins, D. J. Scalapino, J. Wagner, and W. Hanke, *Drude weight, optical conductivity, and flux properties of one-dimensional Hubbard rings*, Phys. Rev. B **44** (1991), 6909. 68, 70, 79, 99
- [FP64] A. F. Ferguson and J. A. Pople, *Molecular orbital theory of diamagnetism. 5. Anisotropy of some aromatic hydrocarbon molecules*, J. Chem. Phys. **42** (1964), 1560. 97
- [GI84] Yuval Gefen and Yoseph Imry, *Quantum oscillations and the Aharonov-Bohm effect for parallel resistors*, Phys. Rev. Lett. **52** (1984), 129. 11

- [GKKR96] Antoine Georges, Gabriel Kotliar, Werner Krauth, and Marcelo J. Rozenberg, *Dynamical mean-field theory of strongly correlated fermion systems and the limit of infinite dimension*, Rev. Mod. Phys. **68** (1996), 13. 124
- [GM01] J. A. N. F. Gomes and R. B. Mallion, *Aromaticity and ring currents*, Chem. Rev. **101** (2001), 1349. 8, 9
- [GN96] M. Guerrero and R. M. Noack, *Phase diagram of the one-dimensional Anderson lattice*, Phys. Rev. B **53** (1996), 3707. 121, 124
- [GS95] Thierry Giamarchi and B. Sriram Shastry, *Persistent currents in a one-dimensional ring for a disordered Hubbard model*, Phys. Rev. B **51** (1995), 10915. 42
- [Gut63] M. C. Gutzwiller, *Effect of correlation on the ferromagnetism of transition metals*, Phys. Rev. Lett. **10** (1963), 159. 13
- [Har01] Darald J. Hartfield, *Matrix theory and applications with MATLAB*, CRC Press LLC, Boca Raton, 2001. 84
- [HB00] K. Held and R. Bulla, *Mott transition of the f-electron system in the periodic Anderson model with nearest neighbor hybridization*, Eur. Phys. J. B **17** (2000), 7. 57
- [HHSM00] K. Held, Carey Huscroft, R. T. Scalettar, and A. K. McMahan, *Similarities between the Hubbard and periodic Anderson models at finite temperatures*, Phys. Rev. Lett. **85** (2000), 373. 57
- [Hil75] B. P. Hillebrand, *A generalization of Krasnoselski's theorem on the real line*, Math. Mag. **48** (1975), 167. 76, 87
- [HJR99] Trygve Helgaker, Michal Jaszunski, and Kenneth Ruud, *Ab initio methods for the calculation of NMR shielding and indirect spin-spin coupling constants*, Chem. Rev. **99** (1999), 293. 10
- [HMS99] Carey Huscroft, A. K. McMahan, and R. T. Scalettar, *Magnetic and thermodynamic properties of the three-dimensional periodic Anderson Hamiltonian*, Phys. Rev. Lett. **82** (1999), 2342. 57
- [Hub63] J. Hubbard, *Electron correlations in narrow bands*, Proc. Roy. Soc. London A **276** (1963), 238. 13
- [Imr97] Yoseph Imry, *Introduction to mesoscopic physics*, Mesoscopic Physics and Nanotechnology, vol. 1, Oxford University Press, Oxford, 1997. 7
- [Kan03] C. L. Kane, *Telegraph noise and fractional statistics in the quantum Hall effect*, Phys. Rev. Lett. **90** (2003), 226802. 12
- [KEH99] S. Kirchner, H. G. Evertz, and W. Hanke, *Transport properties of one-dimensional Hubbard models*, Phys. Rev. B **59** (1999), 1825. 68, 70

- [KFBH03] U. F. Keyser, C. Fühner, S. Borck, and R. J. Haug, *Kondo effect in a few-electron quantum ring*, Phys. Rev. Lett. **90** (2003), 196601. 12
- [KKM] P. Koskinen, M. Koskinen, and M. Manninen, *Low-energy spectrum and finite temperature properties of quantum rings*, Eur. Phys. J. B **28**, 483. 36
- [Koh64] W. Kohn, *Theory of the insulating state*, Phys. Rev. **133** (1964), A171. 45, 47
- [Lai01] Dong Lai, *Matter in strong magnetic fields*, Rev. Mod. Phys. **73** (2001), 629. 37
- [Laz00] P. Lazzeretti, *Ring currents*, Progress in Nuclear Magnetic Resonance Spectroscopy **36** (2000), 1. 8, 9
- [LDDB90] L. P. Lévy, G. Dolan, J. Dunsmuir, and H. Bouchat, *Magnetization of mesoscopic copper rings: Evidence for persistent currents*, Phys. Rev. Lett. **64** (1990), 2074. 11
- [Lév00] Laurent-Patrick Lévy, *Magnetism and superconductivity*, Texts and Monographs in Physics, Springer, Berlin, 2000. 28, 37
- [LGB90] Daniel Loss, Paul Goldbart, and A. V. Balatsky, *Berry's phase and persistent charge and spin currents in textured mesoscopic rings*, Phys. Rev. Lett. **65** (1990), 1655. 12
- [LLG⁺00] A. Lorke, R. J. Luyken, A. O. Govorov, J. P. Kotthaus, J. M. Garcia, and P. M. Petroff, *Spectroscopy of nanoscopic semiconductor rings*, Phys. Rev. Lett. **84** (2000), 2223. 12
- [Lue99] Heiko Lueken, *Magnetochemie*, Teubner, Leipzig, 1999. 97
- [Mah90] Gerald D. Mahan, *Many-particle physics*, 2. ed., Plenum, New York, 1990. 48
- [MGS94] Vladimir I. Minkin, Mikhail N. Glukhovtsev, and Boris Ya Simkin, *Aromaticity and antiaromaticity: Electronic and structural aspects*, John Wiley and Sons, 1994. 10
- [MHK⁺98] A. F. Morpurgo, J. P. Heida, T. M. Klapwijk, B. J. van Wees, and G. Borghs, *Ensemble average spectrum of Aharonov-Bohm conductance oscillations: Evidence for spin-orbit-induced Berry's phase*, Phys. Rev. Lett. **80** (1998), 1050. 12
- [MW93] B. Möller and P. Wölfle, *Magnetic order in the periodic Anderson model*, Phys. Rev. B **48** (1993), 10320. 121

- [NPHC96] K. Niemelä, P. Pietiläinen, P. Hyvönen, and T. Chakraborty, *Fractional oscillations of electronic states in a quantum ring*, Europhys. Lett. **36** (1996), 533. 12
- [Ohn64] K. Ohno, Theor. Chim. Acta **2** (1964), 219. 79
- [PA02] N. M. R. Peres and M. A. N. Araújo, *Magnetic and superconducting instabilities in the periodic Anderson model*, J. Phys.: Condens. Matter **14** (2002), 5575. 49
- [Pau36] Linus Pauling, *The diamagnetic anisotropy of aromatic molecules*, J. Chem. Phys. **4** (1936), 673. 9
- [PBB95] M. C. Petty, M. R. Bryce, and D. Bloor (eds.), *Introduction to molecular electronics*, Oxford Univ. Press, New York, 1995. 8
- [Pop56] J. A. Pople, *Proton magnetic resonance of hydrocarbons*, J. Chem. Phys. **24** (1956), 1111. 9
- [Pop64] ———, *Molecular orbital theory of diamagnetism. 4. Anisotropic properties of benzene*, J. Chem. Phys. **41** (1964), 2559. 97
- [PPG⁺02] Jiwoong Park, Abhay N. Pasupathy, Jonas I. Goldsmith, Connie Chang, Yuval Yaish, Jason R. Petta, Marie Rinkoski, James P. Sethna, Hector D. Abrunas, Paul L. McEuen, and Daniel C. Ralph, *Coulomb blockade and the Kondo effect in single-atom transistors*, Nature **417** (2002), 722. 8
- [REH92] A. M. Reynolds, D. M. Edwards, and A. C. Hewson, *The Gutzwiller approach to magnetic instabilities in heavy-fermion systems*, J. Phys.: Condens. Matter **4** (1992), 7589. 121
- [Ris92] Peter S. Riseborough, *Theory of the dynamic magnetic response of $Ce_3Bi_4Pt_3$: A heavy-fermion semiconductor*, Phys. Rev. B **45** (1992), 13984. 121
- [RZM⁺97] M. A. Reed, C. Zhou, C. J. Muller, T. P. Burgin, and J. M. Tour, *Conductance of a molecular junction*, Science **278** (1997), 252. 8, 9
- [SMS91] C. A. Stafford, A. J. Millis, and B. S. Shastry, *Finite-size effects on the optical conductivity of a half-filled Hubbard ring*, Phys. Rev. B **43** (1991), 13660. 68, 70, 79, 99
- [SR95] Manfred Sigrist and T. M. Rice, *Unusual paramagnetic phenomena in granular high-temperature superconductors—A consequence of d-wave pairing?*, Rev. Mod. Phys **67** (1995), 503. 74, 80
- [TCC⁺87] G. Timp, A. M. Chang, J. E. Cunningham, T. Y. Chang, P. Mankiewich, R. Behringer, and R. E. Howard, *Observation of the Aharonov-Bohm effect for $\omega_c\tau > 1$* , Phys. Rev. Lett. **58** (1987), 2814. 11

- [TI96] W.-C. Tan and J. C. Inkson, *Landau quantization and the Aharonov-Bohm effect in a two-dimensional ring*, Phys. Rev. B **53** (1996), 6947. 30
- [Tia94] Guang-Shan Tian, *Antiferromagnetic order in the periodic Anderson model at half filling: A rigorous result*, Phys. Rev. B **50** (1994), 6246. 121
- [TK00] C. C. Tsuei and J. R. Kirtley, *Pairing symmetry in cuprate superconductors*, Rev. Mod. Phys. **72** (2000), 969. 74
- [Tom99] K. A. Tomilin, *Fine-structure constant and dimension analysis*, Eur. J. Phys. **20** (1999), L39. 109
- [TSU97] Hirokazu Tsunetsugu, Manfred Sigrist, and Kazuo Ueda, *The ground-state phase diagram of the one-dimensional Kondo lattice model*, Rev. Mod. Phys. **69** (1997), 809. 52
- [UTS92] Kazuo Ueda, Hirokazu Tsunetsugu, and Manfred Sigrist, *Singlet ground state of the periodic Anderson model at half filling: A rigorous result*, 1992, p. 1030. 121
- [VCS⁺95] M. Vekić, J. W. Cannon, D. J. Scalapino, R. T. Scalettar, and R. L. Sugar, *Competition between antiferromagnetic order and spin-liquid behavior in the two-dimensional periodic Anderson model at half-filling*, Phys. Rev. Lett. **74** (1995), 2367. 57
- [vD93] P. G. J. van Dongen, *Stark korrelierte Elektronen im Festkörper*, IFF Ferienkurs: Magnetismus von Festkörpern und Grenzflächen **24** (1993), 20. 121
- [vDMHZ01] P. G. J. van Dongen, Kingshuk Majumdar, Carey Huscroft, and Fu-Chen Zhang, *Quantum critical point in a periodic Anderson model*, Phys. Rev. B **64** (2001), 195123. 50, 57
- [VKDM03] S. Viefers, P. Koskinen, P. Singha Deo, and M. Manninen, *Quantum rings for beginners: Energy spectra and persistent currents*, arXiv:cond-mat/0310064 (2003). 14
- [VPL02] M. Di Ventura, S. T. Pantelides, and N. D. Lang, *Current-induced forces in molecular wires*, Phys. Rev. Lett. **88** (2002), 046801. 8
- [vRSMD⁺96] P. von Ragué Schleyer, C. Maerker, A. Dransfeld, H. Jiao, and N. J. R. van Eikema Hommes, *Nucleus-independent chemical shifts: A simple and efficient aromaticity probe*, J. Am. Chem. Soc. **118** (1996), 6317. 10
- [Wal92] Wolfgang Walter, *Analysis 1*, 3. ed., Springer, Berlin, 1992. 75

- [WAT⁺02] R. V. Williams, J. R. Armantrout, B. Twamley, R. H. Mitchell, T. R. Ward, and S. Bandyopadhyay, *A theoretical and experimental scale of aromaticity. the first nucleus-independent chemical shifts (NICS) study of the dimethyldihydropyrene nucleus*, J. Am. Chem. Soc. **124** (2002), 13495. 10
- [WSH⁺00] R. J. Warburton, C. Schäfflein, D. Haft, F. Bickel, A. Lorke, K. Karrai, J. M. Garcia, W. Schoenfeld, and P. M. Petroff, *Optical emission from a charge-tunable quantum ring*, Nature **405** (2000), 926. 12
- [WW92] S. A. Washburn and Webb, *Quantum transport in small disordered samples from the diffusive to the ballistic regime*, Rep. Prog. Phys. **55** (1992), 1311. 7
- [WWUL85] R. A. Webb, S. Washburn, C. P. Umbach, and R. B. Laibowitz, *Observation of h/e Aharonov-Bohm oscillations in normal metal rings*, Phys. Rev. Lett. **54** (1985), 2696. 11
- [ŽB03] R. Žitko and J. Bonča, *Microscopic mechanisms of dephasing due to electron-electron interactions*, Phys. Rev. B **68** (2003), 085313. 8, 44
- [ZP03] X. Zotos and P. Prelovšek, *Transport in one dimensional quantum systems*, arXiv:cond-mat/0304630v2 (2003). 42

Acknowledgments

First, I would very much like to thank Prof. Dr. [REDACTED], who was my advisor and gave me guidance throughout the years. Without his support and encouragement this thesis would not have been reality. It was a pleasure working in his research group. The same gratitude applies to Prof. Dr. [REDACTED], who, in company with Prof. Dr. [REDACTED], guided me around and through the occasional obstacles at various stages of my thesis.

I would like to thank Prof. Dr. [REDACTED] for agreeing to be on my thesis committee and reviewing my thesis.

A special thanks for useful discussions goes to PD Dr. [REDACTED], Dr. [REDACTED], and Dr. [REDACTED].

I am indebted to several colleagues on the first floor, namely to [REDACTED] who was always available to discuss the shallows of generic and object-oriented programming, [REDACTED], [REDACTED], Dr. [REDACTED], [REDACTED], [REDACTED], and Dr. [REDACTED] for the advice and innumerable discussions on physical, mathematical, and computational issues. I am also very grateful to Prof. Dr. [REDACTED] for providing the first floor with a fully automated coffee machine. It has been a pleasure to work surrounded by the people of his research group and to take part in the occasional events.

I gratefully acknowledge the help of Mrs. [REDACTED] concerning administrative issues.

I would like to express a special thank you to [REDACTED], [REDACTED], [REDACTED], [REDACTED], [REDACTED], [REDACTED], [REDACTED], [REDACTED], [REDACTED], [REDACTED], [REDACTED], and [REDACTED] for spending large parts of my spare time with me and thus refueling me for the writing of this thesis.

Last but not least, I would like to extend my gratitude to my parents, my brother Dr. [REDACTED] and my sister-in-law [REDACTED] for their constant commitment and support in every respect that I received during the course of my education and during the writing of this thesis.

Curriculum Vitae



Personal Details

Nationality: Markus Himmerich
German
Date of birth: ██████████
Address: ██████████
██████████

Academic Background

01.2001 – 03.2004 PhD student in physics at the Johannes Gutenberg University of Mainz
Supervisor: Prof. Dr. ██████████

10.1995 – 12.2000 Student in physics at the University of Mainz
12.12.2000 **Degree:** Diplom
Title of the thesis: *Instabilität im zweidimensionalen Elektronengas mit anziehender Wechselwirkung* (Instability in the two-dimensional electron gas with attractive interaction)
Supervisor: Prof. Dr. ██████████

08.1998 – 04.1999 Socrates exchange student in physics at the University of Bristol/UK
Research project: *Vibrating Sample Magnetometer*
Supervisor: ██████████, PhD

26.09.1997 Vordiplom

Education

1986 – 1995 Priv. Gymn. der Zisterzienserabtei Marienstatt
Major courses: Mathematics, Physics, English

Work Experience

02.1998 – 04.1998 Student trainee at Bayer AG in Leverkusen
Project: Simulation of the spinning process of synthetical threads
Supervisor: Dr. ██████████ and Dr. ██████████

- 09.1997 – 10.1997 Assistant at the GeoForschungsZentrum Potsdam (GFZ)
Project: Development of software for calculating the earth's magnetic field from satellite data
Supervisor: Prof. Dr. ██████████
- 07.1995 – 09.1995 Research placement at the GFZ with focus on Electromagnetic Deep Sounding
Projects: Field measurements in Ireland, setup and maintenance of measuring devices, analysis of data from the earth's magnetic field
Supervisor: Prof. Dr. ██████████

Honors and Awards

- 03.2001 – 03.2004 Scholarship from e-fellows.net
04.1998 – 12.2000 Scholarship from the German National Academic Foundation
31.03.1995 Participation in the "Jugend forscht" state competition in Ludwigshafen (won a research internship at the GFZ Potsdam)
10.02.1995 Participation in the "Jugend forscht" regional competition in Lahnstein with software for calculating electronic circuits (won first prize)

Publications and Talks

- 24.09.2001 Markus Himmerich and Martin Letz: *Electron gas with a strong pairing interaction: Three-particle correlations and the Thouless instability*, Physical Review B, Vol. 64, 144519
27.03.2001 Talk at the spring meeting of the German National Physical Society in Hamburg: *Low-density extension for the electron gas with attractive interaction*